

Search for a scalar or pseudoscalar dilepton resonance produced in association with a massive vector boson or top quark-antiquark pair in multilepton events at $\sqrt{s}=13$ TeV

A. Tumasyan *et al.*^{*}
(CMS Collaboration)



(Received 16 February 2024; accepted 24 May 2024; published 24 July 2024)

A search for beyond the standard model spin-0 bosons, ϕ , that decay into pairs of electrons, muons, or tau leptons is presented. The search targets the associated production of such bosons with a W or Z gauge boson, or a top quark-antiquark pair, and uses events with three or four charged leptons, including hadronically decaying tau leptons. The proton-proton collision data set used in the analysis was collected at the LHC from 2016 to 2018 at a center-of-mass energy of 13 TeV, and corresponds to an integrated luminosity of 138 fb^{-1} . The observations are consistent with the predictions from standard model processes. Upper limits are placed on the product of cross sections and branching fractions of such new particles over the mass range of 15 to 350 GeV with scalar, pseudoscalar, or Higgs-boson-like couplings, as well as on the product of coupling parameters and branching fractions. Several model-dependent exclusion limits are also presented. For a Higgs-boson-like ϕ model, limits are set on the mixing angle of the Higgs boson with the ϕ boson. For the associated production of a ϕ boson with a top quark-antiquark pair, limits are set on the coupling to top quarks. Finally, limits are set for the first time on a fermiophilic dilaton-like model with scalar couplings and a fermiophilic axion-like model with pseudoscalar couplings.

DOI: 10.1103/PhysRevD.110.012013

I. INTRODUCTION

A search for a beyond-the-standard-model spin-0 boson, ϕ , is presented, where the ϕ is produced in association with a W boson, a Z boson, or a top quark-antiquark pair ($t\bar{t}$), and decays into pairs of electrons, muons, or tau leptons. The search uses events containing three or four charged leptons in the final state, selected from proton-proton (pp) collision data collected by the CMS experiment at the CERN LHC at $\sqrt{s}=13$ TeV from 2016–2018, and corresponding to an integrated luminosity of 138 fb^{-1} . The analysis includes the leptonic and hadronic decays of tau leptons and targets events for which the two leptons from the ϕ decay form a localized excess in the dilepton mass spectrum.

This search targets possible new physics at the LHC that could underlie electroweak symmetry breaking. Motivated by many extensions [1–4] of the standard model (SM) that include additional spin-0 particles beyond the single Higgs boson (H), a minimal extension of the SM is considered that consists of a single neutral spin-0 boson, ϕ [5,6].

The effective Lagrangian relevant for this work is detailed in Ref. [7]. For the production of ϕ bosons with an SM W or Z boson, denoted $W\phi$ and $Z\phi$, respectively, two coupling structures are considered. First, a scenario is considered in which the ϕ mixes with the SM H (H-like), yielding a coupling proportional to $\sin\theta$, where θ is the mixing angle, resulting in an interaction of the form,

$$\mathcal{L} \subset -2 \sin\theta \frac{\phi_H}{v} \left(m_W^2 W^{+\mu} W_\mu^- + \frac{1}{2} m_Z^2 Z^\mu Z_\mu \right), \quad (1)$$

where $v \simeq 246$ GeV is the Higgs field vacuum expectation value and ϕ_H denotes the ϕ boson in the H-like scenario. Currently, there is an indirect bound on $\sin^2\theta$ of approximately 0.1 [8].

Second, effective operators are considered that couple a scalar (S) or pseudoscalar (PS) ϕ boson to the $SU(2)_L$ field strength tensors $F_{\mu\nu}^a$ and $\tilde{F}_{\mu\nu}^a = \frac{1}{2} \epsilon^{\mu\nu\rho\sigma} F_{\rho\sigma}^a$, where a denotes the $SU(2)_L$ triplet index. The operators take the form,

$$\mathcal{L} \subset \frac{1}{\Lambda_S} \phi_S F^{a\mu\nu} F_{\mu\nu}^a + \frac{1}{\Lambda_{PS}} \phi_{PS} F^{a\mu\nu} \tilde{F}_{\mu\nu}^a, \quad (2)$$

where Λ_S and Λ_{PS} are the mass scales of the effective interactions, and ϕ_S and ϕ_{PS} denote the ϕ boson under the S or PS hypotheses, respectively. The production of ϕ bosons

^{*}Full author list given at the end of the article.

Published by the American Physical Society under the terms of the [Creative Commons Attribution 4.0 International license](#). Further distribution of this work must maintain attribution to the author(s) and the published article's title, journal citation, and DOI. Funded by SCOAP³.

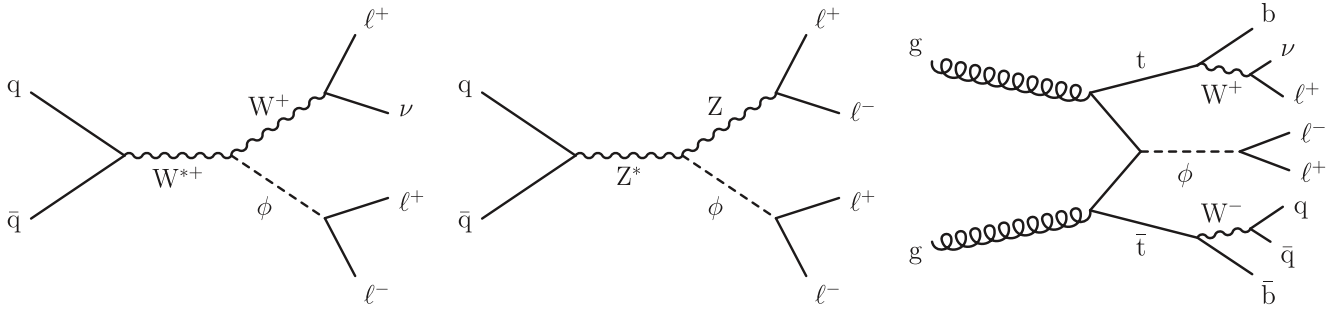


FIG. 1. Example production and decay processes of $W\phi$, $Z\phi$, and $t\bar{t}\phi$ signals with multilepton final states, where ℓ stands for electron, muon, or tau lepton. Only leptonic decays of W and Z bosons are considered for $W\phi$ and $Z\phi$ signals, while for the $t\bar{t}\phi$ signal, W bosons from top quark decay can also decay hadronically.

in association with SM Higgs bosons or photons is not considered within the scope of this work.

For the coupling of ϕ to fermions, flavor-conserving S or PS interactions of the following form are considered:

$$\mathcal{L} \subset -\frac{g_{\psi S}}{\sqrt{2}} \phi_S \bar{\psi} \psi - \frac{g_{\psi PS}}{\sqrt{2}} \phi_{PS} \bar{\psi} i\gamma_5 \psi, \quad (3)$$

where $g_{\psi S}$ and $g_{\psi PS}$ are dimensionless couplings to a given fermion field, ψ . These terms describe the associated production of the ϕ with $t\bar{t}$ ($t\bar{t}\phi$). Probing the $t\bar{t}\phi$ production mode is particularly motivated if the couplings are proportional to the fermion masses [5,6]. This is the case in the H-like coupling scenario where a scalar coupling between the ϕ_H and fermions would be $g_{\psi S} = \sqrt{2} \sin \theta m_\psi / v$.

The three production modes, $W\phi$, $Z\phi$, and $t\bar{t}\phi$, populate a large, complementary multilepton signature space, and are collectively referred to as $X\phi$. For all production modes, only decays of ϕ bosons to electron, muon, or tau lepton pairs are considered, as described by the couplings in Eq. (3). The ϕ decays are assumed to conserve lepton number and electric charge, $\phi \rightarrow \ell^+ \ell^-$, where $\ell = e, \mu$, or τ , and are taken to occur at the production vertex. As this search targets multilepton signatures, the W and Z bosons in $W\phi$ and $Z\phi$ signal models are required to decay leptonically, whereas one of the W bosons in the $t\bar{t}\phi$ signal model may decay hadronically. The $W\phi$ signal provides a signature with three leptons in the final state, primarily populating phase space regions with significant momentum imbalance due to the undetected neutrino from the W decay, low hadronic activity, and no heavy-flavored jets. The $t\bar{t}\phi$ signal can yield three- or four-lepton signatures, depending on the decay mode of the $t\bar{t}$ system, and populates the phase space with similarly large momentum imbalance, but with b jets and high hadronic activity. The $Z\phi$ signal produces a four-lepton signature with low hadronic activity and no heavy-flavored jets, as well as no neutrinos in the final state. A complete decay chain example is $t\bar{t}\phi \rightarrow (bW^+) (\bar{b}W^-) (\ell^+ \ell^-) \rightarrow (b\ell^+ \nu) (\bar{b}q\bar{q}) (\ell^+ \ell^-)$, where b is the SM bottom quark, q represents quarks of the first

and second generations, and ℓ (ν) represents the SM charged leptons (neutrinos).

Figure 1 illustrates possible production and decay processes of $W\phi$, $Z\phi$, and $t\bar{t}\phi$ that result in three- or four-lepton final states. This search targets ϕ masses between 15–350 GeV, excluding masses between 75–108 GeV for the $\phi \rightarrow ee/\mu\mu$ signal scenarios because of high SM Z boson background contributions. Decays of ϕ to gauge boson (top quark) pairs are no longer negligible when the ϕ boson mass is above twice that of the associated gauge bosons (top quarks) in each of the $X\phi$ signals. To facilitate comparisons of results across the signal phase space under consideration, an upper ϕ mass value of 350 GeV, slightly higher than twice the top quark mass, is chosen uniformly for all three $X\phi$ signals. For ϕ masses below the associated gauge boson (top quark) mass, the ϕ boson may also arise from a three-body decay of an on-shell gauge boson (top quark). The width of the ϕ boson is taken to be negligible in all signal models.

The search results are presented in terms of model-independent exclusions along with several model-dependent interpretations. For the model-independent results, $(3 + 3 + 2)3 = 24$ separate production and decay modes are probed separately in terms of the product of the production cross section and leptonic branching fraction $\mathcal{B}(\phi \rightarrow \ell\ell)$: three coupling structures (S, PS, and H) each for the $W\phi$ and $Z\phi$ production modes, two coupling structures (S and PS) for the $t\bar{t}\phi$ production mode, and three decay modes for the ϕ (ee , $\mu\mu$, and $\tau\tau$). The model-dependent results are obtained from a subset of the experimental channels. First, direct bounds are set on models in which ϕ is a fermiophilic dilaton-like [9–12] or a fermiophilic axion-like [13–16] state, with couplings $g_{\psi S}$ and $g_{\psi PS}$ proportional to fermion masses. Only the $t\bar{t}\phi$ production mode is considered in these cases, as fermiophilic particles do not couple to vector bosons. Next, assuming an H-like ϕ production scenario, the $W\phi$, $Z\phi$, or $t\bar{t}\phi$ events are considered to be produced through mixing between the ϕ and SM Higgs boson, and constraints are set on the product of $\sin^2 \theta$ and $\mathcal{B}(\phi \rightarrow \ell\ell)$. Under the additional assumption that the ϕ has the same branching fractions as the SM Higgs boson [6,17,18],

constraints are set on $\sin^2 \theta$ directly. All results presented in the paper, with accompanying material for reinterpretation, are provided in the HEPDATA record for this analysis [19]. For the model-independent bounds, additional representation is provided in terms of the product of the production coupling constant squared and $\mathcal{B}(\phi \rightarrow \ell\ell)$, along with overlaid results from the ee , $\mu\mu$, and $\tau\tau$ decay channels for easier comparison.

Spin-0 states produced in association with SM gauge bosons or top quark pairs and decaying into SM gauge bosons or fermions have been previously searched for by the LEP, Tevatron, and LHC experiments [20–36]. In comparison, this analysis constitutes a direct and model-independent search at the LHC for a dilepton resonance of any flavor produced in association with a W or a Z gauge boson, or a top quark pair. In the context of the $X\phi$ signals described above, the CMS Collaboration has previously probed the $t\bar{t}\phi$ scenario with ϕ decays into dielectron or dimuon pairs with the combined 2016–2018 data set at $\sqrt{s} = 13$ TeV [37]. The current analysis also considers a $t\bar{t}\phi \rightarrow \tau\tau$ signal and achieves increased sensitivity for the $t\bar{t}\phi \rightarrow ee/\mu\mu$ signal over the entire mass range using improved event selection and analysis techniques.

This paper is organized as follows. The CMS detector is briefly described in Sec. II, followed by the summary of data and simulation samples in Sec. III. Section IV covers event reconstruction, while Sec. V covers event selection and background estimation. Systematic uncertainties are discussed in Sec. VI and results in Sec. VII. The analysis is summarized in Sec. VIII.

II. THE CMS DETECTOR

The central feature of the CMS apparatus is a superconducting solenoid of 6 m internal diameter, providing a magnetic field of 3.8 T. Within the solenoid volume are a silicon pixel and strip tracker, a lead tungstate crystal electromagnetic calorimeter (ECAL), and a brass and scintillator hadron calorimeter (HCAL), each composed of a barrel and two end cap sections. Forward calorimeters extend the pseudorapidity (η) coverage provided by the barrel and end cap detectors. Muons are measured in gas-ionization detectors embedded in the steel flux-return yoke outside the solenoid. A more detailed description of the CMS detector, together with a definition of the coordinate system used and the relevant kinematic variables, can be found in Refs. [38,39].

Events of interest are selected using a two-tiered trigger system. The first level is composed of custom hardware processors, and uses information from the calorimeters and muon detectors to select events at a rate of around 100 kHz within a fixed latency of about 4 μ s [40]. The second level, known as the high-level trigger, consists of a farm of processors running a version of the full event reconstruction

software optimized for fast processing, and reduces the event rate to around 1 kHz before data storage [41].

III. DATA SAMPLES AND EVENT SIMULATION

This analysis probes a data set that was collected in pp collisions at $\sqrt{s} = 13$ TeV and corresponds to an integrated luminosity of 138 fb^{-1} , with 36.3, 41.5, and 59.8 fb^{-1} recorded in the years 2016, 2017, and 2018, respectively [42–44]. The data presented here were collected using a combination of isolated single-electron (-muon) triggers with corresponding transverse momentum, p_T , thresholds of 27 (24), 32 (27), and 32 (24) GeV in these three years.

The rates of signal and SM background processes that give rise to isolated and prompt leptons are estimated from Monte Carlo (MC) simulations, which incorporate detailed detector and pp collision properties. The $Z\gamma$, WZ , $t\bar{t}V$, and triboson (VVV) backgrounds, where V denotes a W or Z boson, are generated using MadGraph5_amc@NLO [45] at next-to-leading order (NLO) accuracy in perturbative quantum chromodynamics (QCD). Version 2.2.2 (2.4.2) of MadGraph5_amc@NLO is used for all background samples for 2016 (2017–2018) data. The $Z\gamma$ background includes all diagrams contributing to $pp \rightarrow \ell\ell\gamma$, with photons from both initial- and final-state radiation, and with a Lorentz-invariant mass requirement of $m(\ell^+\ell^-) > 10$ GeV. The ZZ background contribution produced from quark-antiquark annihilation is generated using POWHEG 2.0 [46–48] at NLO, whereas the contribution from gluon-gluon fusion is generated at leading order (LO) using MCFM 7.0.1 [49]. The SM processes involving Higgs boson production are generated using POWHEG 2.0, MadGraph5_amc@NLO, and JHUGEN 7.0.11 [50–53] at NLO, with a Higgs boson mass of 125 GeV. Processes with a single top quark and a Z boson or with four top quarks are simulated using MadGraph5_amc@NLO at NLO in QCD. Other small contributions from processes involving a single top quark and an electroweak boson or Higgs boson, two top quarks and two bosons, or three top quarks are simulated using MadGraph5_amc@NLO at LO in QCD. Simulated event samples for the Drell–Yan (DY) and $t\bar{t}$ processes, which are used for systematic uncertainty studies, are generated at NLO with MadGraph5_amc@NLO and POWHEG 2.0, respectively.

The $X\phi$ signal event generation and production cross section determination are performed at LO accuracy using MadGraph5_amc@NLO 2.6.0 for $t\bar{t}\phi$ and 2.6.5 for $W\phi$ and $Z\phi$. The $t\bar{t}\phi$ signal samples are generated with inclusive decays of the $t\bar{t}$ system, while the $W\phi$ and $Z\phi$ signal samples are generated with leptonically decaying W and Z bosons, $W \rightarrow \ell\nu$ and $Z \rightarrow \ell\ell$, respectively. The samples satisfy an invariant mass requirement of $m(\ell^+\ell^-) > 5$ GeV and an angular separation requirement $\Delta R(\ell^+\ell^-) > 0.05$ for the

Z decay products, where $\Delta R \equiv [(\Delta\eta)^2 + (\Delta\varphi)^2]^{1/2}$, η is the pseudorapidity and φ is the azimuthal angle [38].

The NNPDF3.0 LO or NLO parton distribution function (PDF) sets [54] are used for all background and signal samples for 2016 data, with a perturbative order matching that of the matrix element calculations. The NNPDF3.1 next-to-NLO PDF set [55] is used for all 2017–2018 samples. To perform the parton showering, fragmentation, and hadronization of the matrix-element-level events, PYTHIA [56] is used in all samples, with the event tune CUETP8M1 [57] (CP5 [58]) in 2016 (2017–2018). PYTHIA version 8.226 (8.230) is used for all background and signal samples for 2016 (2017–2018) data. The MLM [59] or FxFx [60] jet matching schemes are used for MadGraph5_amc@NLO samples at LO or NLO, respectively. The simulation of the response of the CMS detector to incoming particles is performed using the Geant4 toolkit [61]. Additional p_T interactions from the same or nearby bunch crossings (pileup) are simulated with PYTHIA and incorporated in the MC samples.

IV. EVENT RECONSTRUCTION

In each event, the primary vertex (PV) is taken to be the vertex corresponding to the hardest scattering in the bunch crossing, evaluated using tracking information alone, as described in Section 9.4.1 of Ref. [62]. The full event information is then used by a particle-flow (PF) algorithm [63], which aims to reconstruct and identify each individual particle (photon, electron, muon, charged hadron, neutral hadron) with an optimized combination of information from the various elements of the CMS detector.

Electrons are reconstructed by geometrically matching charged-particle tracks from the tracking system with energy clusters deposited in the ECAL [64]. The energy of electrons is determined from a combination of the electron momentum at the primary interaction vertex as determined by the tracker, the energy of the corresponding ECAL cluster, and the energy sum of all bremsstrahlung photons spatially compatible with originating from the electron track. The momentum resolution for electrons with $p_T \approx 45$ GeV from $Z \rightarrow ee$ decays ranges from 1.6% to 5.0%. It is generally better in the barrel region of the ECAL ($|\eta| < 1.479$) than in the end caps, and also depends on the bremsstrahlung energy emitted by the electron as it traverses the material in front of the ECAL [64,65]. To suppress undesired electrons originating from photon conversions in detector material and from the misidentification of hadrons, the electron candidates are required to satisfy shower shape and track quality requirements, using the medium cut-based criteria described in Ref. [64]. Electrons used in this analysis are required to also satisfy $p_T > 10$ GeV and $|\eta| < 2.4$.

Muons are reconstructed from compatible tracks in the inner tracker and the muon detectors [66]. The energy of muons is obtained from the curvature of the corresponding

track. Additional track fit and matching quality criteria suppress the misidentification of hadronic showers that penetrate the calorimeters and reach the muon system. The matching of muon system tracks to those measured in the silicon tracker results in a relative p_T resolution of 1% in the barrel and 3% in the end caps for muons with p_T up to 100 GeV, and of better than 7% in the barrel for muons with p_T up to 1 TeV [66]. Muons used in this analysis must lie within the muon system acceptance, $|\eta| < 2.4$, and are required to have $p_T > 10$ GeV.

Hadronically decaying tau lepton (τ_h) candidates are reconstructed from jets, using the hadrons-plus-strips algorithm [67], which combines one or three tracks with a strip of energy deposits in the calorimeter. The energy deposits capture photons from neutral pion decay and electrons, and vary in size in η and φ as a function of p_T of the photon or electron candidate. Reconstructed τ_h candidates must satisfy $|\eta| < 2.3$ and $p_T > 20$ GeV, where p_T refers to the visible momentum of the tau lepton.

Jets are clustered from PF candidates using the anti- k_T algorithm [68] with a distance parameter of 0.4, as implemented in the FastJet package [69]. The jet momentum is given by the vector sum of all particle momenta in the jet. Pileup interactions can contribute extra tracks and calorimetric energy depositions, increasing the apparent jet momentum. To mitigate this effect, tracks identified to be originating from pileup vertices are discarded, and an offset correction is applied to correct for remaining contributions. Jet energy corrections are derived from simulation studies so that the average measured energy of jets becomes identical to that of particle-level jets. *In situ* measurements of the momentum balance in dijet, photon + jet, $Z +$ jet, and multijet events are used to determine any residual differences between the jet energy scale in data and in simulation, and appropriate corrections are made [70]. Additional selection criteria are applied to each jet to remove jets potentially dominated by instrumental effects or reconstruction failures. The minimum p_T threshold for the jets selected in this analysis is 30 GeV, and the central axis of the jet is also required to be inside the muon system acceptance, $|\eta| < 2.4$. The selected jets must lie outside a cone defined by $\Delta R = 0.4$ relative to a selected muon, electron, or τ_h candidate, as defined later in this section.

The missing transverse momentum \vec{p}_T^{miss} is defined as the negative vector p_T sum of all the PF candidates in an event, and its magnitude is denoted as p_T^{miss} [71]. The pileup per particle identification algorithm [72] is applied to reduce the pileup dependence of the \vec{p}_T^{miss} observable. The \vec{p}_T^{miss} is computed using the PF candidates weighted by their probability to originate from the PV, and is modified to account for corrections to the energy scale of the reconstructed jets in the event [73].

Leptons produced from the decays of H and massive vector bosons (either directly or via a leptonically decaying

tau lepton) are referred to as prompt leptons, and are often indistinguishable in momentum and isolation from those produced in signal events. Thus, the SM processes giving rise to three or more isolated leptons, such as WZ , ZZ , $t\bar{t}V$, VVV , and H boson production, are referred to as the prompt backgrounds in this analysis. On the other hand, reducible backgrounds are defined as those from SM processes in which the jets are misidentified as leptons, or where the leptons originate from heavy-quark decays. Leptons from such sources are referred to as misidentified leptons, and SM background processes with such leptons are collectively labeled as “MisID” backgrounds. Some examples of such backgrounds are $Z + \text{jets}$ or $t\bar{t} + \text{jets}$ production, in which the prompt leptons are accompanied by leptons that are within or near jets, hadrons that traverse the HCAL and reach the muon detectors, or hadronic showers with large electromagnetic energy fractions.

The reducible backgrounds are significantly suppressed by applying stringent requirements on the lepton isolation and displacement. For electron and muon candidates, the relative isolation is defined as the scalar p_T sum of photon and hadron PF objects within a cone of fixed ΔR around the lepton, divided by the lepton p_T . For electrons, the relative isolation is required to be less than $0.0478 + 0.506 \text{ GeV}/p_T$ in the barrel section of the ECAL ($|\eta| < 1.479$) and less than $0.0658 + 0.963 \text{ GeV}/p_T$ in the end cap section ($|\eta| > 1.479$), with $\Delta R = 0.3$ [64]. The relative isolation for muons is required to be less than 0.15 with $\Delta R = 0.4$ [66]. The isolation quantities are also corrected for contributions from particles originating from pileup vertices [64,66]. In addition to the isolation requirement, electrons in the barrel must satisfy $|d_z| < 0.1 \text{ cm}$ and $|d_{xy}| < 0.05 \text{ cm}$, and in the end cap $|d_z| < 0.2 \text{ cm}$ and $|d_{xy}| < 0.1 \text{ cm}$, where d_z and d_{xy} are the longitudinal and transverse impact parameters of electrons with respect to the PV, respectively. Similarly, muons must satisfy $|d_z| < 0.1 \text{ cm}$ and $|d_{xy}| < 0.05 \text{ cm}$. For both electrons and muons, the three-dimensional impact parameter significance (SIP3D) is defined as the absolute value of the impact parameter divided by its uncertainty [74]. It is tuned to account for changes in detector and pileup conditions, and must be less than 10, 12, and 9 in 2016, 2017, and 2018 data, respectively. All selected electrons within a cone of $\Delta R < 0.05$ centered on a selected muon are discarded in order to reduce the inclusion of nonprompt electrons originating from muon bremsstrahlung.

For τ_h leptons, the DEEPTAU [75] algorithm is used to distinguish genuine τ_h lepton decays from jets originating from the hadronization of quarks or gluons, as well as from electrons or muons. Information from all individual reconstructed particles near the τ_h candidate axis is combined with properties of the τ_h candidate and of the event. The very tight working point of the jet discriminator of the DEEPTAU algorithm is used to suppress misidentified

contributions from jets, with an identification efficiency of about 50% depending on the visible p_T and η of the τ_h candidate. Similarly, the loose working points of the DEEPTAU electron and muon discriminators are used to suppress such misidentified contributions, with identification efficiencies of about 95% and 99.9%, respectively. These result in misidentification probabilities of about 0.5% for jets and electrons, and 0.05% for muons, as measured in events enriched in $DY + \text{jets}$ and $W + \text{jets}$ processes. In addition to this multivariate requirement, τ_h candidates are required to satisfy $|d_z| < 0.2 \text{ cm}$. All selected τ_h candidates within a cone of $\Delta R < 0.5$ of a selected electron or muon are also discarded to suppress contributions from electrons or muons misidentified as taus.

Reconstructed jets originating from b hadrons are identified using the medium working point of the DEEPCSV b tagging algorithm [74]. To suppress contributions due to misidentified leptons originating from heavy-flavor jet decays, a b tag veto is applied, where lepton candidates are discarded if any b -tagged jet with a less stringent selection ($p_T > 10 \text{ GeV}$, $|\eta| < 2.5$) is found within a cone of $\Delta R < 0.4$ centered on the candidate. Selection criteria including requirements on d_{xy} , d_z , SIP3D, and b -tag veto are collectively referred to as the lepton displacement veto.

These reconstruction and selection requirements result in typical efficiencies of 40–85% for electrons, 65–90% for muons, and 30–50% for τ_h leptons, depending on the lepton p_T and η , as evaluated for prompt leptons originating from W and Z boson decays. Similarly, the b tagging working point achieves an identification efficiency of 60–75% for b quark jets depending on jet p_T and η , and a misidentification probability of about 10 (1)% for c quark (light-quark and gluon) jets, respectively, as evaluated in events enriched in $t\bar{t}$ and multijet processes.

V. EVENT SELECTION AND BACKGROUND ESTIMATION

In this analysis, events with three or more leptons satisfying the selection criteria given in Sec. IV are considered. Among these leptons, events must contain at least one muon with $p_T > 26(29) \text{ GeV}$ in 2016 and 2018 (2017) or at least one electron with $p_T > 30(35) \text{ GeV}$ in 2016 (2017–2018). The analysis thresholds are set 3 GeV (2 GeV) higher than electron (muon) trigger thresholds.

All events are categorized in seven distinct final states (channels) based on the number of light leptons ($L = e, \mu$) and τ_h (T) candidates. These seven channels are mutually exclusive, and are defined as (i) 1L2T, with exactly one light lepton and exactly two τ_h candidates; (ii) 1L3T, with exactly one light lepton and three or more τ_h candidates; (iii) 2L1T, with exactly two light leptons and exactly one τ_h candidates; (iv) 2L2T, with exactly two light leptons and two or more τ_h candidates; (v) 3L, with exactly three light leptons and no τ_h

TABLE I. A summary of control regions for the SM processes ZZ , $Z\gamma$, WZ , and $t\bar{t}Z$, and for the misidentified lepton backgrounds (MisID e/μ and MisID τ). The p_T^{miss} , M_T , 3L minimum lepton transverse momentum p_{T3} , M_ℓ , and S_T quantities are given in units of GeV. The 3L OnZ CR is further split into 3L MisID e/μ CR, 3L WZ CR, and 3L $t\bar{t}Z$ CR. The terminology is described in Sec. V.

CR name	OSSF n	M_{OSSF}	N_b	p_T^{miss}	M_T	p_{T3}	Other selections
4L ZZ	OSSF2	Double-OnZ	0
3L $Z\gamma$	OSSF1	BelowZ	0	$76 < M_\ell < 106$
3L OnZ	OSSF1	OnZ	...	<125	<150
3L WZ	OSSF1	OnZ	0	<125	50–150	>20	...
3L $t\bar{t}Z$	OSSF1	OnZ	≥ 1	<125	<150	>20	$N_j \geq 3, S_T > 350$
3L MisID e/μ	OSSF1	OnZ	0	<100	<50
2L1T MisID τ	OSSF1	OnZ	...	<100

candidates; (vi) 3L1T, with exactly three light leptons and one or more τ_h candidates; and (vii) 4L, with four or more light leptons and any number of τ_h candidates.

In the 4L channel, only the leading four light leptons in p_T are used in the subsequent analysis. Likewise, in the 3L1T, 2L2T, and 1L3T channels, only the leading one, two, and three τ_h candidates are used, respectively.

The main SM backgrounds are constrained using dedicated control regions (CRs), as described in detail in Secs. VA and VB and summarized in Table I. Lepton and jet multiplicity categorization, transverse momenta, and invariant mass variables are used to define CRs enriched in specific SM background processes or MisID backgrounds. The CRs are then excluded from the analysis phase space. The remaining events are grouped in different signal regions (SR) to increase signal sensitivity across the

probed dilepton mass spectra. The SRs are described in detail in Sec. VC.

In order to suppress contributions due to low-mass quarkonium resonances, cascade decays of heavy-flavor hadrons, and low- ΔR final-state radiation events are discarded if $M_{\min} < 12$ GeV or $\Delta R_{\min} < 0.2$, where M_{\min} and ΔR_{\min} are defined as the minimum Lorentz-invariant mass and minimum ΔR of all lepton pairs in the event, irrespective of lepton charge and flavor. This requirement is applied to all CR and SR events. A binned representation of the CRs and SRs illustrating the expected background composition is given in Fig. 2, where the normalizations of the background samples in the CRs are as described in Secs. VA and VB.

The multiplicity of jets (b jets) satisfying the selection criteria stated in Sec. IV is denoted as N_j (N_b). The L_T and

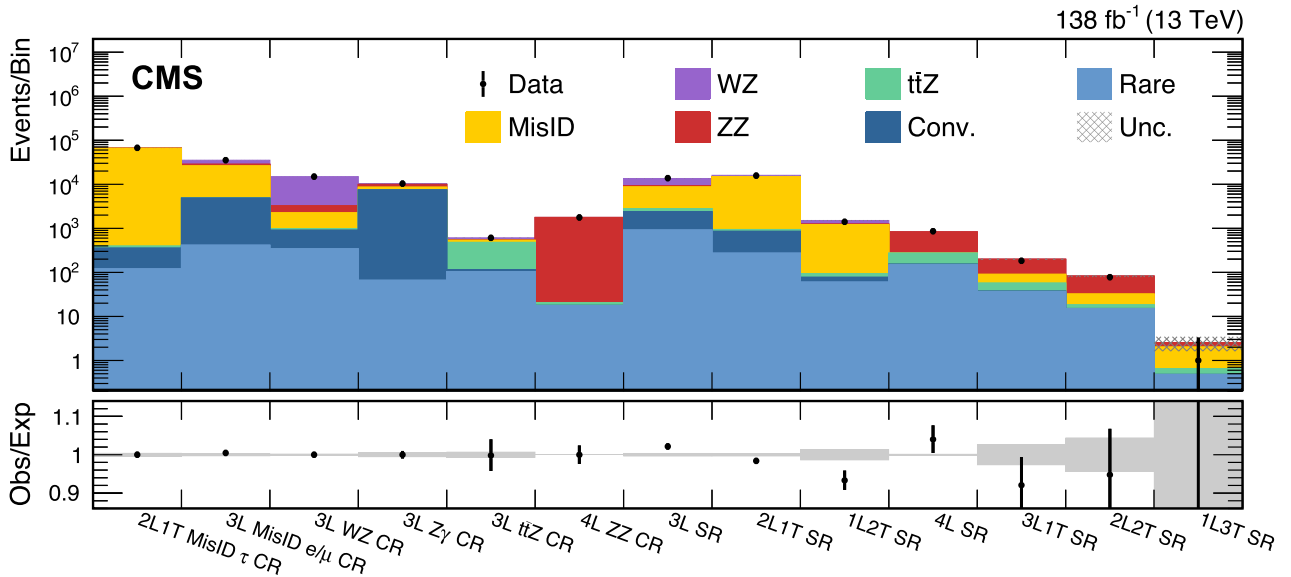


FIG. 2. Binned representation of the control and signal regions for the combined multilepton event selection and the combined 2016–2018 data set. The CR bins follow their definitions as given in Table I, and the SR bins correspond to the channels as defined by the lepton flavor composition. The normalizations of the background samples in the CRs are described in Secs. VA and VB. All three (four) lepton events are required to have $Q_\ell = 1(0)$, and those satisfying any of the CR requirements are removed from the SR bins. All subsequent selections given in Tables II and III are based on events given in the SR bins. The lower panel shows the ratio of observed events to the total expected SM background prediction (Obs/Exp), and the gray band represents the statistical uncertainties in the background prediction.

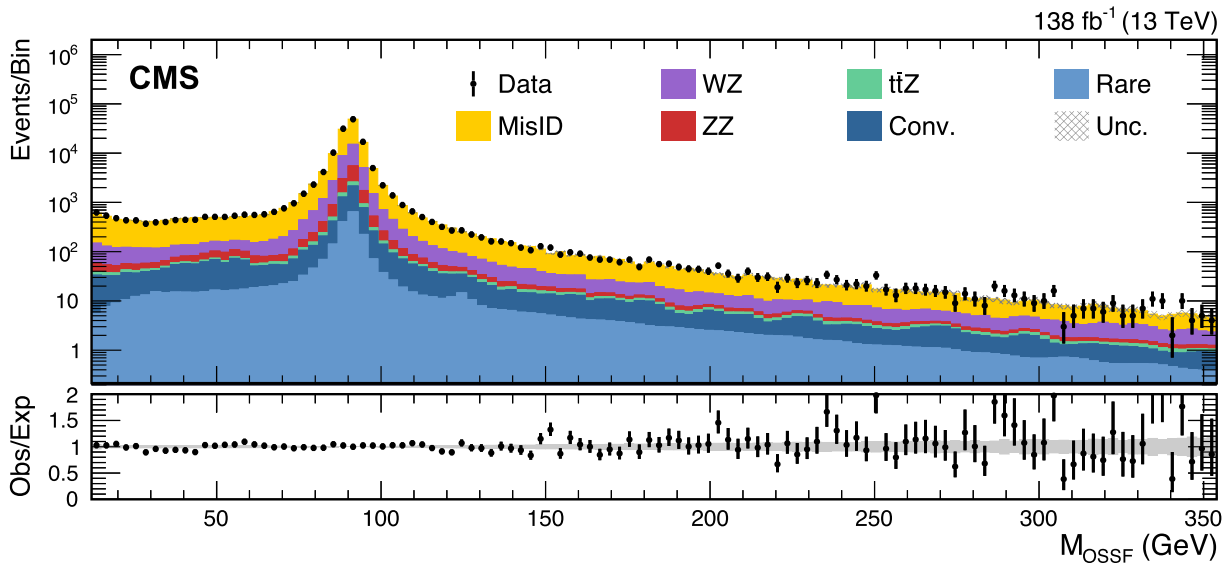


FIG. 3. The M_{OSSF} spectrum for the combined 2L1T, 2L2T, 3L, 3L1T, and 4L event selection (excluding the $Z\gamma$ CR) and the combined 2016–2018 data set. All three (four) lepton events are required to have $Q_\ell = 1(0)$. The lower panel shows the ratio of observed events to the total expected SM background prediction (Obs/Exp), and the gray band represents the statistical uncertainties in the background prediction.

H_T variables are defined as the scalar p_T sum of all charged leptons (e , μ , τ_h) and jets in an event, respectively. The invariant mass of all leptons in a given event is defined as M_ℓ , and the absolute value of the charge sum of all leptons as Q_ℓ . For the L_T , M_ℓ , and Q_ℓ calculations, only the charged leptons used to define the channel are used. The variable S_T is defined as the scalar sum of L_T , H_T , and p_T^{miss} .

The number of distinct opposite-sign same-flavor lepton pairs in an event is denoted as OSSF n , where n is the number of OSSF pairs. Some examples of the OSSF1 events are $e^+e^-e^+$ in 3L, $\mu^+\mu^-\tau_h^+$ in 2L1T, $e^+e^-e^+\mu^-$ in 4L. Only 4L and 2L2T events can be categorized as OSSF2, for example, $e^+e^-\mu^+\mu^-$ in 4L and $\mu^+\mu^-\tau_h^+\tau_h^-$ in 2L2T. OSSF0 events are all those with no opposite-sign same-flavor pairs, for example, $e^+e^+\mu^+$ or $e^+e^+e^+$ in 3L.

To identify an event likely to contain a Z boson, M_{OSSF} is defined to be the invariant mass of the OSSF dielectron or dimuon pair that is closest to 91 GeV, and an event with $76 < M_{\text{OSSF}} < 106$ GeV is labeled as OnZ. The OSSF1 or OSSF2 events that are not OnZ are labeled as OffZ, and if an OffZ event has $M_{\text{OSSF}} < 76$ GeV, it is classified as BelowZ. The minimum lepton p_T in 3-lepton events is referred to as p_{T3} . The transverse mass for a single lepton i is defined as $M_T^i = (2p_T^{\text{miss}} p_T^i [1 - \cos(\vec{p}_T^{\text{miss}}, \vec{p}_T^i)])^{1/2}$, where p_T^i is the p_T of lepton i . In 3L OSSF1 events, the lepton that is not used in the M_{OSSF} pair is used in the calculation of M_T . In the 3L events with two nondistinct OSSF pairs (such as in $e^+e^-e^+$ or $\mu^+\mu^-\mu^+$), the events are classified as OnZ if either pair satisfies $76 < M_{\text{OSSF}} < 106$ GeV. Also in such events, the assignment of which leptons form the OSSF pair and which is used in the M_T calculation is made

simultaneously so that the event is OnZ, and M_T is in the range 50–150 GeV. If such a choice is not kinematically possible, building an OnZ candidate is prioritized. Similarly, in 4L OSSF2 events with four electrons or muons, M_{OSSF} is chosen to give the maximum number of distinct OSSF OnZ pairs, and such events are labeled as Single- or Double-OnZ, depending on whether they have one or two distinct OnZ OSSF pairs. The M_{OSSF} spectrum for the combined 2L1T, 2L2T, 3L, 3L1T, and 4L event selection (excluding the $Z\gamma$ CR) is illustrated in Fig. 3.

A. Prompt-lepton backgrounds

The prompt-lepton backgrounds arise from processes in which all reconstructed leptons originate from decays of SM bosons. These backgrounds are irreducible, and their contributions are estimated with simulated event samples, which have been normalized and validated using data in dedicated CRs for each of the major WZ , ZZ , $t\bar{Z}$, and $Z\gamma$ processes, as summarized in Table I. The normalizations for these processes are typically found to be within 20% of the NLO theoretical cross sections, and are applied together with the associated uncertainties to the corresponding background estimates in the SRs. These uncertainties include both statistical and systematic contributions, and take into account the contributions of events from other processes. The measurements for the diboson processes are largely independent of one another because of the high purity of the corresponding CRs. Since these backgrounds make significant contributions to the $t\bar{Z}$ enriched CR, the normalization for this process is measured after the corresponding corrections have been obtained for the other backgrounds.

The $ZZ \rightarrow 4\ell$ and $WZ \rightarrow 3\ell\nu$ processes are the primary prompt-background processes in the channels with four and three leptons, respectively. The $qq \rightarrow ZZ$ and $gg \rightarrow ZZ$ processes are considered collectively as the ZZ background. The 4L ZZ CR require two OSSF lepton pairs with invariant masses consistent with the Z boson mass. While the 3L WZ CR requires one OnZ lepton pair and M_T consistent with the W mass. The 4L ZZ CR has a purity greater than 99%, whereas that of the 3L WZ CR is greater than 75%. In both CRs, events with b -tagged jets are vetoed, and in the 3L WZ CR, the minimum lepton p_T cut is raised to 20 GeV, and p_T^{miss} is required to be less than 125 GeV to suppress contributions from other background processes. Relative uncertainties of 3–5% are observed in the normalizations across the three data-taking periods for these processes. The ZZ and WZ simulation samples are reweighted as functions of the jet multiplicity as well as the visible diboson p_T to match the simulated distributions to those of the data in these CRs, where the visible diboson p_T is defined as the vector p_T sum of the charged leptons in the event. This reweighting accounts for missing higher-order QCD and electroweak corrections, and yields an improved description of leptonic and hadronic quantities of interest in this analysis.

Production of $t\bar{t}Z$ is a major prompt SM background process for all channels with $N_b \geq 1$. A $t\bar{t}Z$ enriched CR is created by selecting 3L events similarly to the 3L WZ CR, but with inverted requirement of at least one b -tagged jet, and with additional requirements of at least 3 jets and S_T greater than 350 GeV. The purity of the 3L $t\bar{t}Z$ CR selection is about 60%, and relative uncertainties of 15–25% are measured in the normalizations across the three data-taking periods.

A smaller background contribution arises from initial- or final-state radiation photons that convert asymmetrically such that only one of the resultant leptons is reconstructed in the detector. The DY process with an additional photon is the dominant source of such backgrounds, collectively referred to as the conversion background. The cross section of this process is normalized in a dedicated 3L $Z\gamma$ CR, where the mass of the three-lepton system is required to be within the Z mass window, (91 ± 15) GeV, and events with b -tagged jets are vetoed. This CR targets $Z \rightarrow \ell\ell + \gamma$ events, where, for example, the photon converts in the detector and the energy of one of the four leptons is too low to satisfy the lepton selection criteria. Relative uncertainties of about 10% are obtained in the normalizations across the three data-taking periods, where the quoted value also includes a lepton-flavor-dependent component because the fractions of internal and external conversions vary as a function of the electron multiplicity in the events.

Other SM processes that are not normalized in a dedicated CR in data are estimated from simulation samples and normalized to their theoretical cross sections. These processes consist of triboson, Higgs boson, and other

rare SM contributions, and are collectively referred to as “rare” backgrounds.

B. Misidentified-lepton backgrounds

The misidentified-lepton backgrounds are estimated from data using three- or four-dimensional implementations of a matrix method [76], where the dimensionality corresponds to the lepton multiplicity in the targeted SRs. For a given SR, the matrix method involves extrapolating the misidentified-lepton contributions from a set of sideband regions into the SR event-by-event using lepton “misidentification” and “prompt” rates.

The sideband regions include all the lepton selection criteria described in Sec. IV, with the exception of the isolation requirements, which are relaxed. We refer to the requirements in the SRs and sideband regions as “tight” and “loose”, respectively. Specifically, for the loose requirement, the relative isolation must be less than 1.0 for electrons and muons, and τ_h candidates are required to pass a looser working point of the DEEPTAU algorithm jet discriminator. Accounting for the possible combinations, for a given SR with 3 or 4 leptons, the matrix method uses 7 or 15 nonoverlapping sideband regions, respectively. The sideband regions are mutually exclusive to the SRs by construction.

The misidentification rates are defined as the probabilities that misidentified leptons pass the tight selection, given that they satisfy the loose selection. Because of the isolation requirements used in the single-lepton triggers, background contributions with up to 2 (3) simultaneously misidentified leptons in 3 (4) lepton events can be predicted by this method. The fraction of signal events where all lepton candidates are misidentified leptons is found to be negligible in simulation. The $DY + \text{jets}$ and $t\bar{t} + \text{jets}$ processes are the dominant SM contributions to the total misidentified-lepton background in multilepton events. Misidentification rates are derived in dedicated CRs in data and used in the matrix method in SRs. Data-based misidentification rate measurements in $DY + \text{jets}$ events are performed using a variant of the “tag-and-probe” method [77] in three-lepton CR events. In the 3L MisID and 2L1T MisID CRs, the OnZ leptons are taken as the tag leptons, and the additional lepton is taken as the misidentified-lepton probe, e.g., $e\mu\mu$ and $\mu\mu\mu$ events are used to measure the muon misidentification rates, while $e\tau_h\tau_h$ and $\mu\tau_h\tau_h$ events are used to measure the τ_h misidentification rates. In all data-based misidentification rate measurements, contributions due to prompt probe leptons are estimated and subtracted using MC simulation. Misidentification rates in $t\bar{t} + \text{jets}$ events may differ by up to 50% from those in $DY + \text{jets}$ events for a given lepton flavor, because of different gluon, light quark, and heavy quark compositions, as well as different event kinematic properties. As it is impractical to create a high purity $t\bar{t} + \text{jets}$ enriched selection of events with

well-defined misidentified-lepton probes in data, dedicated $t\bar{t} + \text{jets}$ misidentification rates for all lepton flavors are obtained in simulated samples instead, using object and event selections compatible with the SR selections. These simulation-based rates are verified in dedicated data CRs enriched in $t\bar{t} + \text{jets}$ contributions with a misidentified lepton, where one lepton is required to fail the three-dimensional impact parameter significance requirement or the b tag veto described in Sec. IV.

The lepton misidentification rates are measured as functions of various kinematic features of leptons and the hadronic properties of events that affect the lepton isolation. All misidentification rates are parametrized as functions of the lepton p_T and $|\eta|$. For tau leptons, the misidentification rates are measured separately for one- and three-prong reconstructed τ_h candidates. The misidentification rate for each lepton flavor is corrected as a function of the recoil of the event, as well as the multiplicity of tracks originating from the PV and the jet multiplicity. The recoil is defined as a projection along the lepton p_T axis of the vector sum of the p_T of all other leptons, jets, and p_T^{miss} in the event. The associated corrections significantly improve the modeling of misidentified-lepton backgrounds in DY + jets events, in which the misidentified lepton often originates from a jet recoiling against the leptonically decaying Z boson system. The final misidentification rates for all lepton flavors are obtained from a weighted average of the DY- and $t\bar{t}$ -based measurements. The weights are evaluated according to the expected DY- $t\bar{t}$ composition of the MisID background, as obtained from simulated samples in each SR category and for each b -tagged jet multiplicity. Half of the difference between the rates derived from DY- and $t\bar{t}$ -based measurements is assigned as a systematic uncertainty to account for inaccurate modeling of the expected background composition. Typical electron and muon misidentification rates,

relative to the loose selection, are in the range 5–30%, whereas those of τ_h objects are found to be in the range 1–15%.

Similarly, the prompt rates are defined as the probability for prompt and isolated leptons to pass the tight criteria given that they pass the loose criteria. Within the matrix method, they constitute a correction, and account for the contribution to the lepton sidebands from prompt leptons that fail the tight selection criteria. In data, the prompt rates for electrons, muons, and τ_h leptons are measured using the tag-and-probe method in DY-enriched ee , $\mu\mu$, and $e\tau_h/\mu\tau_h$ dilepton events, respectively, as functions of the lepton p_T and $|\eta|$, and are found to be in the range 50–95%. In simulation, the prompt rates are similarly measured in DY and $t\bar{t}$ MC samples, using reconstructed leptons kinematically matched to generator-level prompt leptons ($\Delta R < 0.2$). The final prompt rates for all lepton flavors are taken from the DY-enriched data measurements. The differences between the prompt rates derived from DY and $t\bar{t}$ MC samples are studied to assess their dependence on hadronic activity, and the impact of such systematic uncertainty contributions on the misidentified-lepton background estimate is found to be negligible.

C. Signal regions

The signals in the $X\phi \rightarrow ee/\mu\mu$ scenarios are expected to produce narrow enhancements in reconstructed opposite-sign dielectron and dimuon mass (M_{ee} and $M_{\mu\mu}$) spectra, whereas wider enhancements are obtained in the $X\phi \rightarrow \tau\tau$ scenarios because of undetected neutrinos originating from decays of tau leptons. A set of reconstructed dilepton invariant mass variables with additional selection criteria discriminates the $X\phi$ signal from the SM backgrounds, where the binning scheme and range of these variables are chosen to maximize sensitivity according to the expected signal shapes and SM backgrounds. These are summarized

TABLE II. Low- and high-mass signal region selections for $X\phi \rightarrow ee/\mu\mu$ signals. Events satisfying the control region requirements are vetoed throughout, and only those with a reconstructed ϕ candidate are retained using the specified dilepton mass variable. The S_T , p_{T3} , and M_ℓ requirements are specified in units of GeV. The two entries in the labels, channels, and dilepton mass variables are provided for the $X\phi \rightarrow ee$ and $X\phi \rightarrow \mu\mu$ signal scenarios, as appropriate.

Label	Channels	Q_ℓ	OSSF n	M_{OSSF}	N_b	S_T	p_{T3}	M_ℓ	Dilepton mass
$W\phi(ee/\mu\mu)$ SR1Low	3L($ee\mu/e\mu\mu$)	1	1	OffZ	0	<76, >106	$M_{ee}/M_{\mu\mu}$
$W\phi(ee/\mu\mu)$ SR2Low	3L($eee/\mu\mu\mu$)	1	1	OffZ	0	<76, >106	$M_{ee}^{\min}/M_{\mu\mu}^{\min}$
$W\phi(ee/\mu\mu)$ SR1High	3L($ee\mu/e\mu\mu$)	1	1	OffZ	0	>200	>15	>150	$M_{ee}/M_{\mu\mu}$
$W\phi(ee/\mu\mu)$ SR2High	3L($eee/\mu\mu\mu$)	1	1	OffZ	0	>200	>15	>150	$M_{ee}^{\max}/M_{\mu\mu}^{\max}$
$Z\phi(ee/\mu\mu)$ SRLow	4L + 3L1T + 2L2T	0	≥ 1	Not double-OnZ	0	$M_{ee}^{\min}/M_{\mu\mu}^{\min}$
$Z\phi(ee/\mu\mu)$ SRHigh	4L + 3L1T + 2L2T	0	≥ 1	Not double-OnZ	0	>200	...	>150	$M_{ee}^{\max}/M_{\mu\mu}^{\max}$
$t\bar{t}\phi(ee/\mu\mu)$ SR1Low	3L($ee\mu/e\mu\mu$)	1	1	OffZ	≥ 1	>350	...	>100	$M_{ee}/M_{\mu\mu}$
$t\bar{t}\phi(ee/\mu\mu)$ SR2Low	3L($eee/\mu\mu\mu$)	1	1	OffZ	≥ 1	>350	...	>100	$M_{ee}^{\min}/M_{\mu\mu}^{\min}$
$t\bar{t}\phi(ee/\mu\mu)$ SR1High	3L($ee\mu/e\mu\mu$)	1	1	OffZ	≥ 1	>400	>15	>100	$M_{ee}/M_{\mu\mu}$
$t\bar{t}\phi(ee/\mu\mu)$ SR2High	3L($eee/\mu\mu\mu$)	1	1	OffZ	≥ 1	>400	>15	>100	$M_{ee}^{\max}/M_{\mu\mu}^{\max}$
$t\bar{t}\phi(ee/\mu\mu)$ SR3Low	4L + 3L1T + 2L2T	0	≥ 1	OffZ	...	>350	$M_{ee}^{\min}/M_{\mu\mu}^{\min}$
$t\bar{t}\phi(ee/\mu\mu)$ SR3High	4L + 3L1T + 2L2T	0	≥ 1	OffZ	...	>400	$M_{ee}^{\max}/M_{\mu\mu}^{\max}$

TABLE III. Signal selections for $X\phi \rightarrow \tau\tau$ signals. Events satisfying the control region requirements are vetoed throughout, and only those with a reconstructed ϕ candidate are retained using the specified dilepton mass variable. The S_T , p_{T3} , and M_ℓ requirements are specified in units of GeV.

Label	Channels	Q_ℓ	OSSFn	M_{OSSF}	N_b	S_T	N_j	p_{T3}	M_ℓ	Dilepton mass
$W\phi(\tau\tau)$ SR1	3L	1	0	...	0	>200	...	>15	>150	$M_{e\mu}^{\min}$
$W\phi(\tau\tau)$ SR2	2L1T + 1L2T	1	0	...	0	>200	...	>30	>150	$M_{\ell\tau}^{\min}$
$W\phi(\tau\tau)$ SR3	1L2T	1	1	...	0	>200	...	>30	>150	$M_{\tau\tau}^{\min}$
$Z\phi(\tau\tau)$ SR1	4L + 2L2T	0	1	...	0	>200	$M_{e\mu}^{\min}$
$Z\phi(\tau\tau)$ SR2	3L1T	0	1	...	0	>200	$M_{\ell\tau}^{\min}$
$Z\phi(\tau\tau)$ SR2	2L2T	0	0	...	0	>200	$M_{\ell\tau}^{\min}$
$Z\phi(\tau\tau)$ SR3	2L2T	0	2	...	0	>200	$M_{\tau\tau}^{\min}$
$t\bar{t}\phi(\tau\tau)$ SR1	3L	1	0	...	0	>400	>1	>15	>100	$M_{e\mu}^{\min}$
$t\bar{t}\phi(\tau\tau)$ SR2	2L1T + 1L2T	1	0	...	0	>400	>1	>30	>100	$M_{\ell\tau}^{\min}$
$t\bar{t}\phi(\tau\tau)$ SR3	1L2T	1	1	...	0	>400	>1	>30	>100	$M_{\tau\tau}^{\min}$
$t\bar{t}\phi(\tau\tau)$ SR4	3L	1	1	OffZ	>0	>400	>1	>15	>100	$M_{e\mu}^{\min}$
$t\bar{t}\phi(\tau\tau)$ SR4	3L	1	0	...	>0	>400	>1	>15	>100	$M_{e\mu}^{\min}$
$t\bar{t}\phi(\tau\tau)$ SR5	2L1T + 1L2T	1	0	...	>0	>400	>1	>30	>100	$M_{\ell\tau}^{\min}$
$t\bar{t}\phi(\tau\tau)$ SR6	1L2T	1	1	...	>0	>400	>1	>30	>100	$M_{\tau\tau}^{\min}$
$t\bar{t}\phi(\tau\tau)$ SR7	3L1T	0	1	OffZ	...	>400	$M_{\ell\tau/\tau\tau}^{\min}$
$t\bar{t}\phi(\tau\tau)$ SR7	3L1T	0	0	>400	$M_{\ell\tau/\tau\tau}^{\min}$
$t\bar{t}\phi(\tau\tau)$ SR7	2L2T	0	2	OffZ	...	>400	$M_{\ell\tau/\tau\tau}^{\min}$
$t\bar{t}\phi(\tau\tau)$ SR7	2L2T	0	< 2	>400	$M_{\ell\tau/\tau\tau}^{\min}$
$t\bar{t}\phi(\tau\tau)$ SR7	1L3T	0	1	>400	$M_{\ell\tau/\tau\tau}^{\min}$

in Tables II and III for the $X\phi \rightarrow ee/\mu\mu$ narrow resonance search and the $X\phi \rightarrow \tau\tau$ wide resonance search, respectively.

For the $X\phi \rightarrow ee/\mu\mu$ signal scenarios, M_{ee} and $M_{\mu\mu}$ are utilized. The SM-background-enriched mass window around the Z boson mass is excluded, dividing the mass spectra into two mass regions. The SRs containing events with a ϕ mass below or above the Z boson mass window are referred to as the low- or high-mass region, respectively. The low (high) dilepton mass range spans 12–76 (106–366) GeV. In events with more than one opposite sign ee pair, such as $e^+e^+e^-$, masses are defined for two possible pairings of e^- and e^+ . The lower of the two ϕ masses is referred to as M_{ee}^{\min} and the higher one is referred to as M_{ee}^{\max} . Dimuon decay scenarios are handled similarly, where $M_{\mu\mu}^{\min}$ ($M_{\mu\mu}^{\max}$) is the minimum (maximum) opposite-sign $\mu\mu$ invariant mass per event. On the other hand, for the $X\phi \rightarrow \tau\tau$ signal, where tau can subsequently decay to e or μ , a different categorization based on three new mass variables is adopted because of the absence of a narrow resonance in DY background, where the full mass range above 12 GeV, including the Z boson mass region, is used. These variables correspond to the minimum invariant mass among all $\tau_h\tau_h$ pairs ($M_{\tau\tau}^{\min}$), $e\mu$ pairs ($M_{e\mu}^{\min}$), and $e\tau_h$ or $\mu\tau_h$ pairs ($M_{\ell\tau}^{\min}$), as well as the minimum of $M_{\tau\tau}^{\min}$ and $M_{\ell\tau}^{\min}$ ($M_{\ell\tau/\tau\tau}^{\min}$). For all three decay modes of ϕ , the targeted mass ranges for reconstructed dilepton masses are taken to be wider than the probed ϕ mass range (15–350 GeV) to

minimize loss of signal acceptance due to detector resolution effects.

To increase signal sensitivity, further selections consisting of requirements on lepton and jet multiplicities, total lepton charge, minimum lepton p_T , and the combined invariant mass of all leptons in the event (M_ℓ) are used. For the $X\phi \rightarrow ee/\mu\mu$ samples with high mass, requiring larger S_T , p_{T3} , and M_ℓ suppresses the MisID background and increases sensitivity. For the $X\phi \rightarrow \tau\tau$ signals, because of significant contributions from misidentified tau lepton candidates, a minimum p_T threshold of 30 GeV is applied to the τ_h candidates in all 3-lepton channels. In various signal regions, minimum S_T requirements are applied as an approximate measure of the effective mass of all particles produced in the targeted final state. Signal events with $t\bar{t}$ pairs are distinguished from others based on N_b . Specifically, the $Z\phi$ and $W\phi$ SRs include only events with $N_b = 0$, while most $t\bar{t}\phi$ SRs require $N_b \geq 1$. For the $t\bar{t}\phi$ signal in the 4L channel, no requirement is imposed on N_b selection because of the high- S_T requirement and the already low total background expectation. Furthermore, all SRs are required to have a total absolute charge consistent with the probed signal scenario, i.e., $Q_\ell = 0(1)$ for all 4(3) lepton events. In SRs with significant background contributions, events with a single ϕ candidate are considered separately from those with more than one candidate, to mitigate the effects of dilepton mispairings in the resolution of the reconstructed ϕ mass.

In order to improve the ϕ selection efficiency in channels with multiple candidates, certain signal-specific kinematic features are used to help correctly identify the ϕ decay products. In the $W\phi(ee/\mu\mu)$ SR2 channels with ambiguity in OSSF pair construction, the lepton with M_T closest to the W boson mass in the (81 ± 30) GeV mass window is selected first, and the other two leptons are taken to reconstruct the ϕ mass. If no W candidate in the specified M_T window is found, or if one is found but the remaining two leptons are not of opposite charge, then the dilepton pair with the minimum or maximum mass is used. Similarly, in the $t\bar{t}\phi(ee/\mu\mu)$ SR2 channels, the lepton with minimum M_T is identified first, and the remaining two leptons are labeled as the ϕ decay products, provided they form an opposite-sign pair. In the 4L channel of the $Z\phi(ee/\mu\mu)$ SR with OSSF2, the Z candidate is identified using the M_{OSSF} variable and a mass window of (91 ± 15) GeV, and the other two leptons are taken as ϕ decay products. These ϕ selection algorithms were evaluated using simulations and found to correctly identify the ϕ decay products in more than 70% of events with multiple ϕ candidates.

In each $X\phi(ee/\mu\mu)$ SR, 1(5) GeV-wide dilepton mass bins are used to probe the targeted phase space for low (high) ϕ masses. These bin widths are chosen to be consistent with the narrow-width assumption for the ϕ boson as well as the detector resolution effects on the M_{ee} and $M_{\mu\mu}$ spectra over the probed mass range. The $X\phi \rightarrow ee/\mu\mu$ signal mass hypotheses that are closer to the dilepton mass bin boundaries than to the bin centers are probed with a modified binning scheme, where the mass bin boundaries are shifted by half the value of the bin widths. A smoothing procedure is separately applied to the prompt and MisID background contributions in these SRs, using a nonparametric kernel density estimation method with a Gaussian kernel [78]. A fixed-width kernel is used except within 10% from each edge in the mass spectra, where the kernel size is reduced significantly to prevent artificial shaping of the expected background distributions. The smoothing procedure mitigates the impact of statistical fluctuations in the expected background spectra and ensures a stable signal sensitivity across the probed mass bins. No additional uncertainties have been added for the smoothing procedure since different choices of kernel widths yield differences within the existing uncertainties. No smoothing procedure is applied to $X\phi(\tau\tau)$ SRs, as these mass spectra are binned using wider bins with variable widths ranging 5–60 GeV to achieve smoothly behaving expected background distributions.

To summarize all mass spectra listed above, 6 low-mass and 6 high-mass M_{ee} and $M_{\mu\mu}$ spectra are probed for each of the $X\phi \rightarrow ee/\mu\mu$ signals, and 13 dilepton mass spectra are probed for the $X\phi \rightarrow \tau\tau$ signals. This results in a total of 37 mass spectra covering all dilepton decay modes.

VI. SYSTEMATIC UNCERTAINTIES

All background and signal estimates have uncertainties because of the finite number of events in simulated samples or data sidebands. These statistical uncertainties are typically less important, but are nonetheless propagated to the results.

Systematic uncertainties arise from the corrections applied to the background and signal simulations. These include corrections for the efficiencies of the electron and muon triggers, electron charge misidentification probability, lepton reconstruction, identification and isolation, and lepton displacement veto selection, as well as the lepton energy scale and resolution modeling, b tagging efficiency, pileup modeling, and energy scale corrections for jets and p_T^{miss} .

Each of the uncertainty sources is studied for the main SM backgrounds (WZ , ZZ , $t\bar{t}Z$, and $Z\gamma$) and various signal samples covering all probed ϕ mass hypotheses in the different production modes. The impact of each source is evaluated by varying the corresponding correction factor up and down within one standard deviation of its associated uncertainty. The resulting variations in the mass spectra are then used to define an envelope of the impact from each source of systematic uncertainty. The uncertainties that only affect the overall normalization of the expected backgrounds play a less important role in the resonant search, particularly in the $X\phi \rightarrow ee/\mu\mu$ signal scenarios. Such uncertainties are collectively labeled as “flat” in the discussion below.

Uncertainties in the lepton trigger and selection efficiencies are largely mass independent, and are in the 1–15% range, depending on the lepton flavor, p_T , and η . Uncertainties affecting the lepton energies, which account for any mismodeling of the overall energy scale and resolution in simulated samples, are evaluated for the background and signal processes and are taken to be correlated. These uncertainty sources affect only the normalization of the background distributions. However, for the signal, they are the most important uncertainties, as they affect the mean and width of the reconstructed signal mass distributions. A maximum shift of 0.5 (0.1)% is observed in the mean of the reconstructed resonant ϕ mass distribution for dielectron (dimuon) decays. The width of the resonant signal changes by around 2% for low ϕ masses and up to 6% for the largest ϕ mass scenarios, for both electrons and muons. The correction and uncertainty in the electron charge misidentification rate, obtained in a dedicated DY-enriched dielectron selection of data events, are found to have a negligible impact. Uncertainties in the signal acceptance, as well as the acceptance and cross section of the dominant SM backgrounds, due to the choices of factorization and renormalization scales [79] and PDFs [54,55] are found to be negligible.

The uncertainty in the integrated luminosity is partially correlated between data-taking years. The integrated luminosities of the 2016, 2017, and 2018 data-taking periods have uncorrelated uncertainties ranging from 1.2–2.5% [42–44], and a correlated uncertainty of 1.6%. The pileup modeling correction has an associated uncertainty of 3% in the normalization of the dilepton mass distributions, evaluated by varying the total inelastic p_T cross section used in the correction procedure up and down by 5% [80,81].

Dedicated uncertainties are considered for the modeling of primary SM backgrounds, including WZ , ZZ , $t\bar{t}Z$, and $Z\gamma$ processes, which were normalized to data in dedicated CRs. The relative uncertainties in the normalizations for WZ , $Z\gamma$, $t\bar{t}Z$, and ZZ backgrounds are 3–5%, 10%, 15–25%, and 4–5%, respectively, in all three years of data collection. The diboson p_T correction typically has a flat 1–5 (4–9)% effect on the WZ (ZZ) background, while the jet multiplicity reweighting has an effect up to 10 (3–30)%. For the rare background processes, a 50% systematic uncertainty is assigned to the theoretical cross section estimates to cover any higher-order effects and PDF uncertainties.

The uncertainty in the misidentified lepton background estimation, which is obtained from data via the matrix

method, is dominated by the uncertainties in the lepton misidentification rates. The relative statistical uncertainties in the measurement of the misidentification rates are the dominant source of uncertainty, and are typically in the 10–30% range. As the τ_h (e and μ) misidentification rates are extrapolated from low p_T to $p_T > 80(50)$ GeV, these uncertainties are doubled, and a 60% relative uncertainty for such high- p_T leptons is assigned. In summary, the lepton misidentification rates have typical relative uncertainties of 10%, 30%, and 60% in the low- p_T (10–20 GeV for light leptons and 10–30 GeV for τ_h), medium- p_T (20–50 GeV for light leptons and 30–80 GeV for τ_h), and high- p_T (> 50 GeV for light leptons and > 80 GeV for τ_h) regions, respectively. These uncertainties in the total misidentified lepton background correspond to the contribution of 20–50%. The uncertainties are uncorrelated across lepton flavors, the three p_T regions, and the three data-taking periods. In addition, process-dependent uncertainties in the lepton misidentification rates are considered as a separate source of uncertainty. These are estimated by comparing the misidentification rates observed in the DY- and $t\bar{t}$ -enriched samples, and are typically in the range 5–25%, correlated across the data-taking periods.

The uncertainty sources, the affected processes, the resulting uncertainties in the yields of those processes,

TABLE IV. Sources, magnitudes, impacts, and correlation properties of systematic uncertainties in the signal regions. Magnitude refers to the relative change in the underlying uncertainty source, whereas impact quantifies the resultant relative change in the signal and background yields passing the event selection. Uncertainty sources marked as “Yes” under the Correlation column are correlated across the 3 years of data collection, and those marked with an asterisk in the Impact column are mass dependent.

Uncertainty source	Magnitude	Type	Processes	Impact	Correlation
Statistical	1–100%	Per event	All MC samples	1–100%	No
Integrated luminosity	1.2–2.5%	Per event	Conversion/Rare/Signal	1.2–2.5%	Yes
Pileup	5%	Per event	All MC samples	< 5%	Yes
Trigger efficiency	1–4%	Per lepton	All MC samples	< 2%	No
Electron reco., ID and iso. efficiency	1–5%	Per lepton	All MC samples	1–3%	No
Muon reco., ID and iso. efficiency	1–5%	Per lepton	All MC samples	1–3%	No
Tau lepton reco., ID and iso. efficiency	5–15%	Per lepton	All MC samples	5–25%*	No
Electron energy scale and resolution	< 2%	Per lepton	All MC samples	< 10%*	Yes
Muon energy scale and resolution	2%	Per lepton	All MC samples	< 10%*	No
Tau lepton energy scale	< 10%	Per lepton	All MC samples	< 5%*	No
Lepton displacement veto efficiency	1–2%	Per lepton	All MC samples	3–5%	No
b tagging efficiency	1–10%	Per jet	All MC samples	1–5%	No
Jet energy scale	1–10%	Per jet	All MC samples	< 10%	No
Unclustered energy scale	1–25%	Per event	All MC samples	< 3%	No
Electron charge misidentification	30%	Per lepton	All MC samples	< 1%	No
WZ normalization	3–5%	Per event	WZ	3–5%	No
ZZ normalization	4–5%	Per event	ZZ	4–5%	No
$t\bar{t}Z$ normalization	15–25%	Per event	$t\bar{t}Z$	15–25%	No
Conversion normalization	10–50%	Per event	$Z\gamma$ /Conversion	10–50%	No
Rare normalization	50%	Per event	Rare	50%	No
Prompt and misidentification rates	20–60%	Per lepton	MisID	20–50%*	No
DY- $t\bar{t}$ process dependence	5–25%	Per lepton	MisID	5–25%	Yes
Diboson jet multiplicity modeling	< 30%	Per event	WZ/ZZ	< 30%	No
Diboson p_T modeling	< 30%	Per event	WZ/ZZ	1–10%	No

and the correlations across the data-taking periods are summarized in Table IV. The overall uncertainties in the total expected backgrounds are largely dominated by those affecting the WZ , ZZ , $t\bar{t}Z$, and MisID processes.

VII. RESULTS

A. Model-independent results

In total, 37 dilepton mass spectra are probed, corresponding to the 12 $X\phi \rightarrow ee$, 12 $X\phi \rightarrow \mu\mu$, and 13 $X\phi \rightarrow \tau\tau$ SRs defined in Sec. VC; these are illustrated in Figs. 4–10, respectively. To test each given $X\phi$ production, decay, and mass scenario, a subset of these SRs is used, resulting in $(3+3+2)3 = 24$ model-independent bounds on $X\phi$ signal hypotheses, as shown in Figs. 11–14. For example, considering a $W\phi \rightarrow ee$ signal scenario with S, PS, or H-like couplings at a ϕ mass of 50 GeV, the M_{ee} and M_{ee}^{\min} distributions in the mass range of 12–76 GeV are used in the 3L($ee\mu$) and 3L(eee) channels, respectively. Similarly, for a $t\bar{t}\phi \rightarrow \mu\mu$ signal scenario with S or PS couplings at a ϕ mass of 200 GeV, the $M_{\mu\mu}$, $M_{\mu\mu}^{\max}$, and $M_{\mu\mu}^{\min}$ distributions in the mass range of 106–366 GeV are used in the 3L($e\mu\mu$), 3L(eee), and 4L + 3L1T + 2L2T channels, respectively. In the case of a $Z\phi \rightarrow \tau\tau$ signal with S, PS, or H-like couplings of any ϕ mass, $M_{e\mu}^{\min}$ and $M_{\tau\tau}^{\min}$ distributions are used in 4L + 2L2T and 2L2T (OSSF1) channels, whereas $M_{\ell\tau}^{\min}$ distributions are used in both 3L1T and 2L2T (OSSFO) channels. In all cases involving contributions from more than one channel, all channels are considered in combination, including correlations between systematic uncertainties, as described in Sec. VI.

No statistically significant deviation from the SM expectations is observed in any of the probed mass distributions. The largest local deviation is observed in the high mass $Z\phi \rightarrow ee$ search, corresponding to the $Z\phi(ee)$ SRHigh mass spectrum in Fig. 4, where an excess at a ϕ mass of 156 GeV corresponding to 2.9 standard deviations is observed, without considering the look-elsewhere effect (LEE) [82]. The corresponding global significance, obtained taking into account LEE in an M_{ee} range of 106–366 GeV, is 1.4 standard deviations.

Upper limits at 95% confidence level (CL) are set on the product of the production cross sections and branching fractions, $\sigma(X\phi)\mathcal{B}(\phi \rightarrow \ell\ell)$, using a modified frequentist approach based on the CL_s criterion [83,84] in the asymptotic approximation [85,86]. For each signal hypothesis, a binned maximum-likelihood fit is performed to discriminate between the potential signal and the SM background processes. The systematic uncertainties and their correlations, described in Sec. VI, are incorporated in the likelihood as nuisance parameters with log-normal probability density functions. The statistical uncertainties in the signal and background estimates are modeled with gamma functions. The expected and observed upper

limits on the probed signals are provided in Figs. 11–14. The $Z\phi \rightarrow ee/\mu\mu$ sensitivity is driven by the 4L channel, while the $W\phi \rightarrow ee/\mu\mu$ and $t\bar{t}\phi \rightarrow ee/\mu\mu$ sensitivities are driven by the 3L channels with 0b jets and 1 or more b jets, respectively. For the $X\phi \rightarrow \tau\tau$ signals, the sensitivity at high ϕ mass is driven by the channels with at least two τ_h s.

For all $X\phi$ signals, the expected upper limits are the most stringent for signals with the dimuon decay modes, with the dielectron modes less stringent by as much as a factor of two for low ϕ mass hypotheses because of the lower electron reconstruction and selection efficiencies. For high ϕ masses, the expected constraints are comparable for all signals with any coupling scenario with dielectron or dimuon coupling scenario. Similarly, constraints on the $\tau\tau$ decay modes are less stringent than those on the light lepton decay modes throughout, limited by the τ lepton energy resolution, the reconstruction and identification efficiencies, and the higher SM background contributions in these final states, especially for ϕ masses below 40 GeV.

For the $W\phi$ signal, there are three coupling scenarios, among which the pseudoscalar coupling for a 15 GeV $\phi \rightarrow \mu\mu$ results in the most stringent limit of about 10 fb. For scalar and H-like couplings at the same mass and decay mode, the $\sigma\mathcal{B}$ values above 20 and 100 fb are excluded, respectively. For $\phi \rightarrow ee$, the limits are about two times less stringent, and for $\phi \rightarrow \tau\tau$, the upper limits are in the range 150–250 fb at a ϕ mass of 40 GeV. For a ϕ mass of 350 GeV, the upper limits are in the range 0.8–2.0 fb across all couplings with dielectron and dimuon decay modes, whereas for $\tau\tau$ decays, the limits are around 8 fb.

The observed constraints on the $Z\phi$ signal are similar for the dielectron and dimuon decay modes, where values of the $\sigma\mathcal{B}$ are excluded above 20–30, 20–30, and 50–60 fb at a ϕ mass of 15 GeV for scalar, pseudoscalar, and H-like couplings, respectively; for the $Z\phi \rightarrow \tau\tau$ signal at a mass hypothesis of 40 GeV, the upper limits for the same couplings are about 300, 200, and 800 fb. For a ϕ mass of 350 GeV, these constraints are about 1 (10) fb for all coupling scenarios of dielectron and dimuon (of $\tau\tau$) decays.

For the $t\bar{t}\phi \rightarrow \mu\mu/ee$ signal, values of the $\sigma\mathcal{B}$ above 4–7 and 1.5–2.5 fb are excluded for the ϕ mass of 15 GeV for the scalar and pseudoscalar coupling scenarios, respectively. For a 350 GeV ϕ boson, these constraints for both decay modes and coupling scenarios are about 0.6 fb. For the $t\bar{t}\phi \rightarrow \tau\tau$ signal and the scalar (pseudoscalar) coupling scenario, the upper limit on the $\sigma\mathcal{B}$ varies from 200 (80) fb for a ϕ mass of 40 GeV to 5 fb for a mass of 350 GeV.

For all $X\phi$ signal scenarios, the differences in the low-mass exclusion limits of scalar, pseudoscalar, and H-like signals result from different Lorentz structures of the interactions, which affect the signal acceptance.

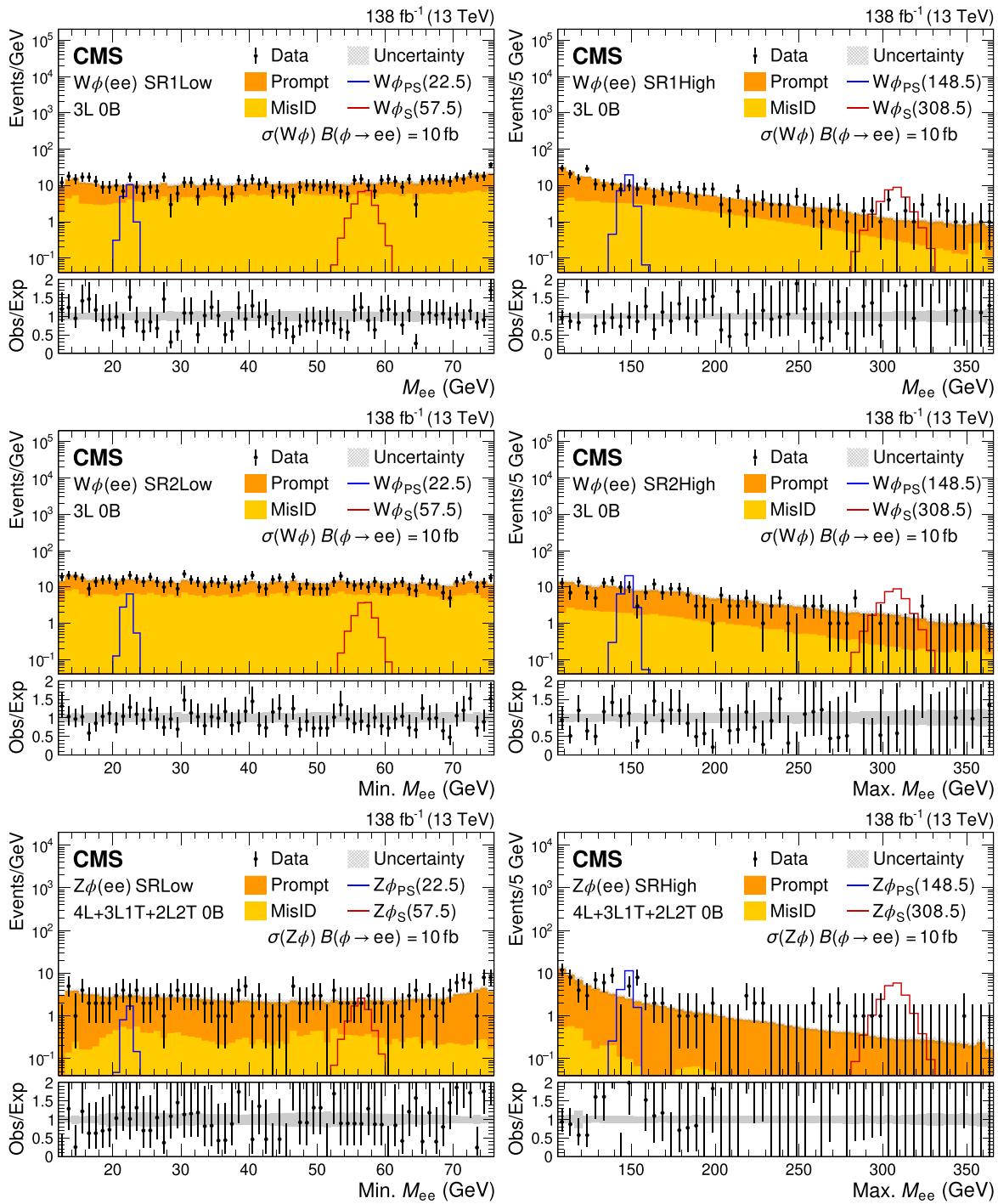


FIG. 4. Dilepton mass spectra for the $W\phi(ee)$ SR1 (upper), SR2 (middle), and for the $Z\phi(ee)$ SR (lower) event selections for the combined 2016–2018 data set. The low (high) mass spectra are shown on the left (right). The lower panel shows the ratio of observed events to the total expected SM background prediction (Obs/Exp), and the gray band represents the sum of statistical and systematic uncertainties in the background prediction. The expected background distributions and the uncertainties are shown after the data are fit under the background-only hypothesis. For illustration, two example signal hypotheses for the production and decay of a scalar and a pseudoscalar ϕ boson are shown, and their masses (in units of GeV) are indicated in the legend. The signals are normalized to the product of the cross section and branching fraction of 10 fb.

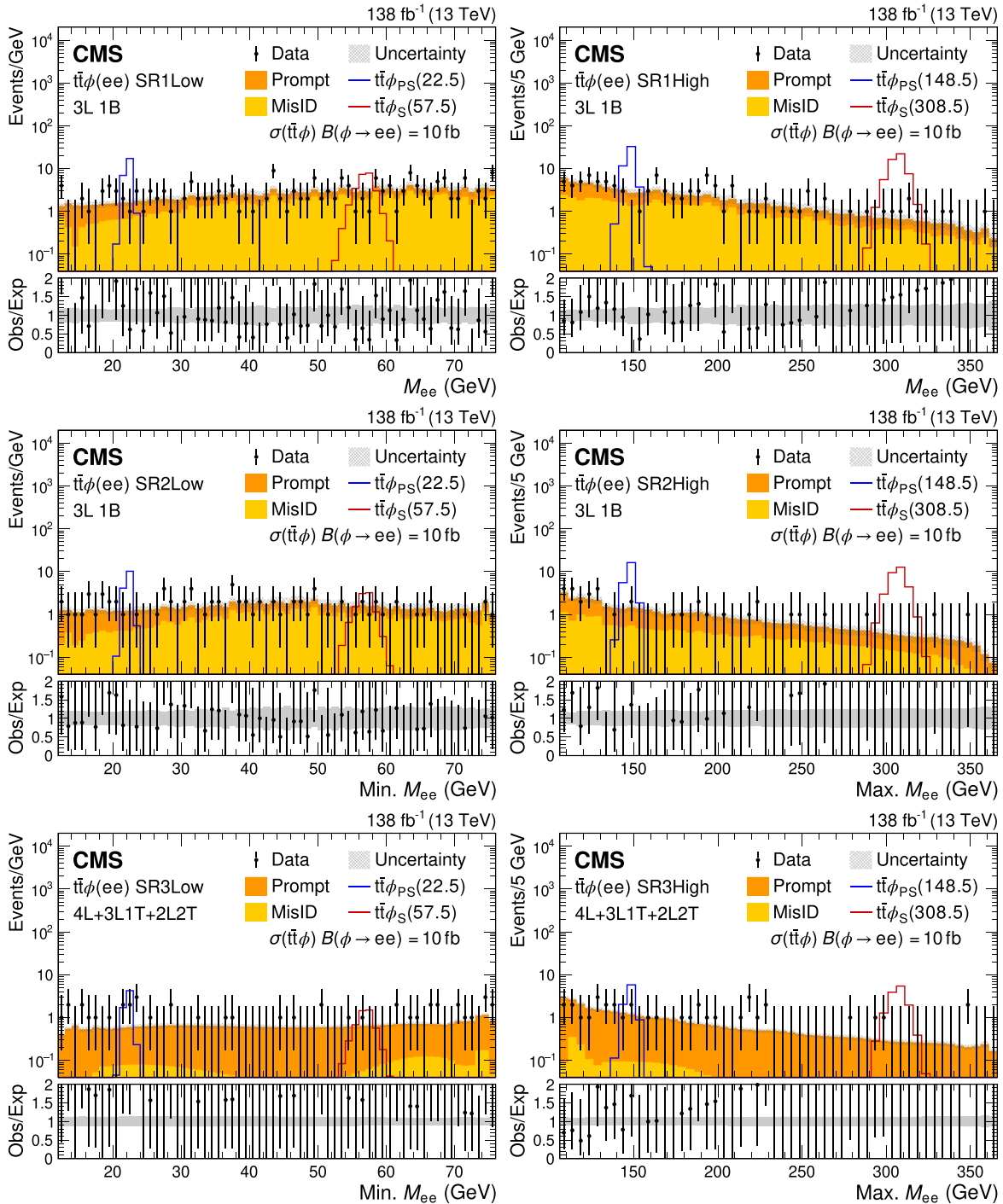


FIG. 5. Dilepton mass spectra for the $t\bar{t}\phi(ee)$ SR1 (upper), SR2 (middle), and SR3 (lower) event selections for the combined 2016–2018 data set. The low (high) mass spectra are shown on the left (right). The lower panel shows the ratio of observed events to the total expected SM background prediction (Obs/Exp), and the gray band represents the sum of statistical and systematic uncertainties in the background prediction. The expected background distributions and the uncertainties are shown after the data are fit under the background-only hypothesis. For illustration, two example signal hypotheses for the production and decay of a scalar and a pseudoscalar ϕ boson are shown, and their masses (in units of GeV) are indicated in the legend. The signals are normalized to the product of the cross section and branching fraction of 10 fb.

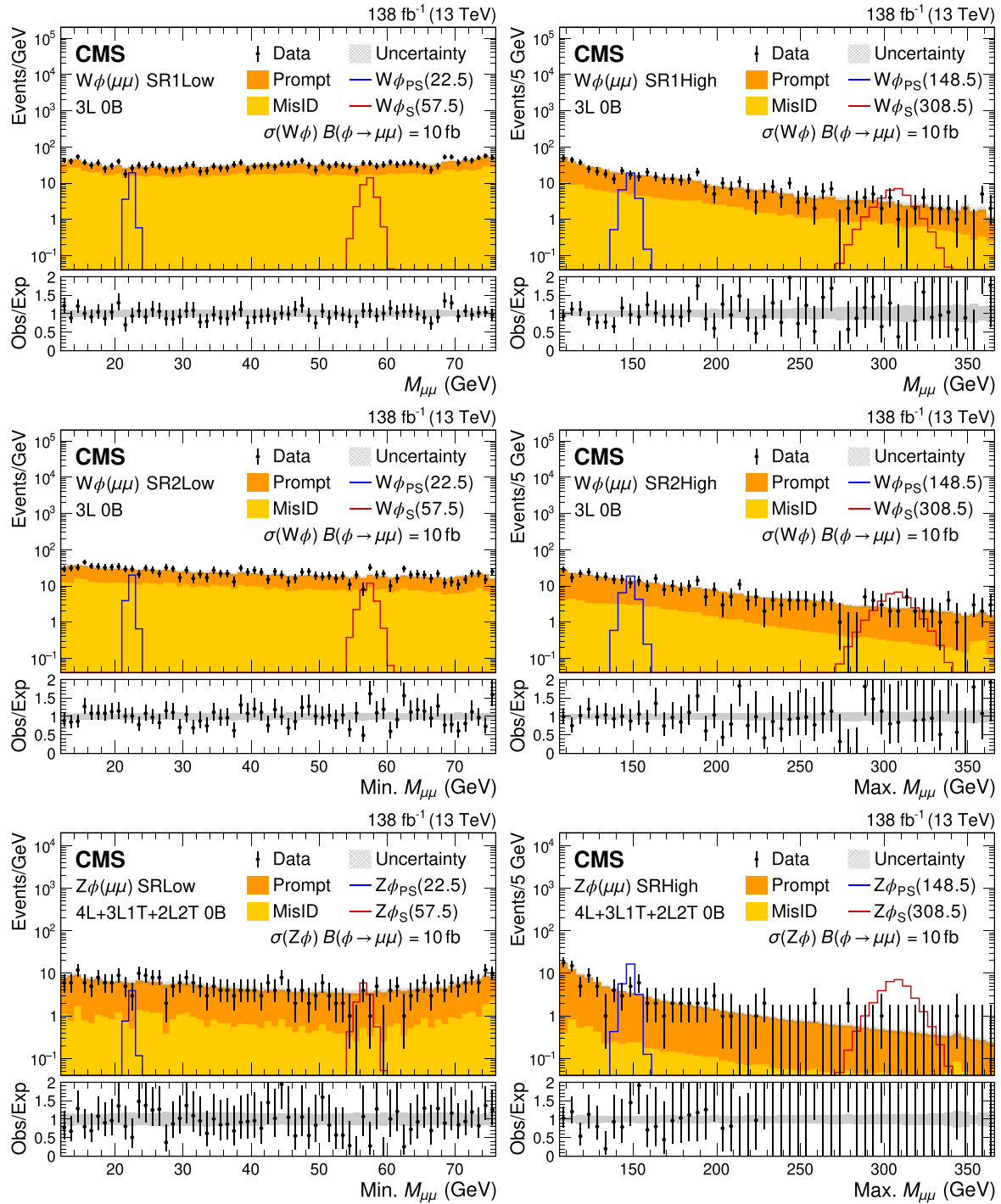


FIG. 6. Dilepton mass spectra for the $W\phi(\mu\mu)$ SR1 (upper), SR2 (middle), and $Z\phi(\mu\mu)$ SR (lower) event selections for the combined 2016–2018 data set. The low (high) mass spectra are shown on the left (right). The lower panel shows the ratio of observed events to the total expected SM background prediction (Obs/Exp), and the gray band represents the sum of statistical and systematic uncertainties in the background prediction. The expected background distributions and the uncertainties are shown after the data are fit under the background-only hypothesis. For illustration, two example signal hypotheses for the production and decay of a scalar and a pseudoscalar ϕ boson are shown, and their masses (in units of GeV) are indicated in the legend. The signals are normalized to the product of the cross section and branching fraction of 10 fb.

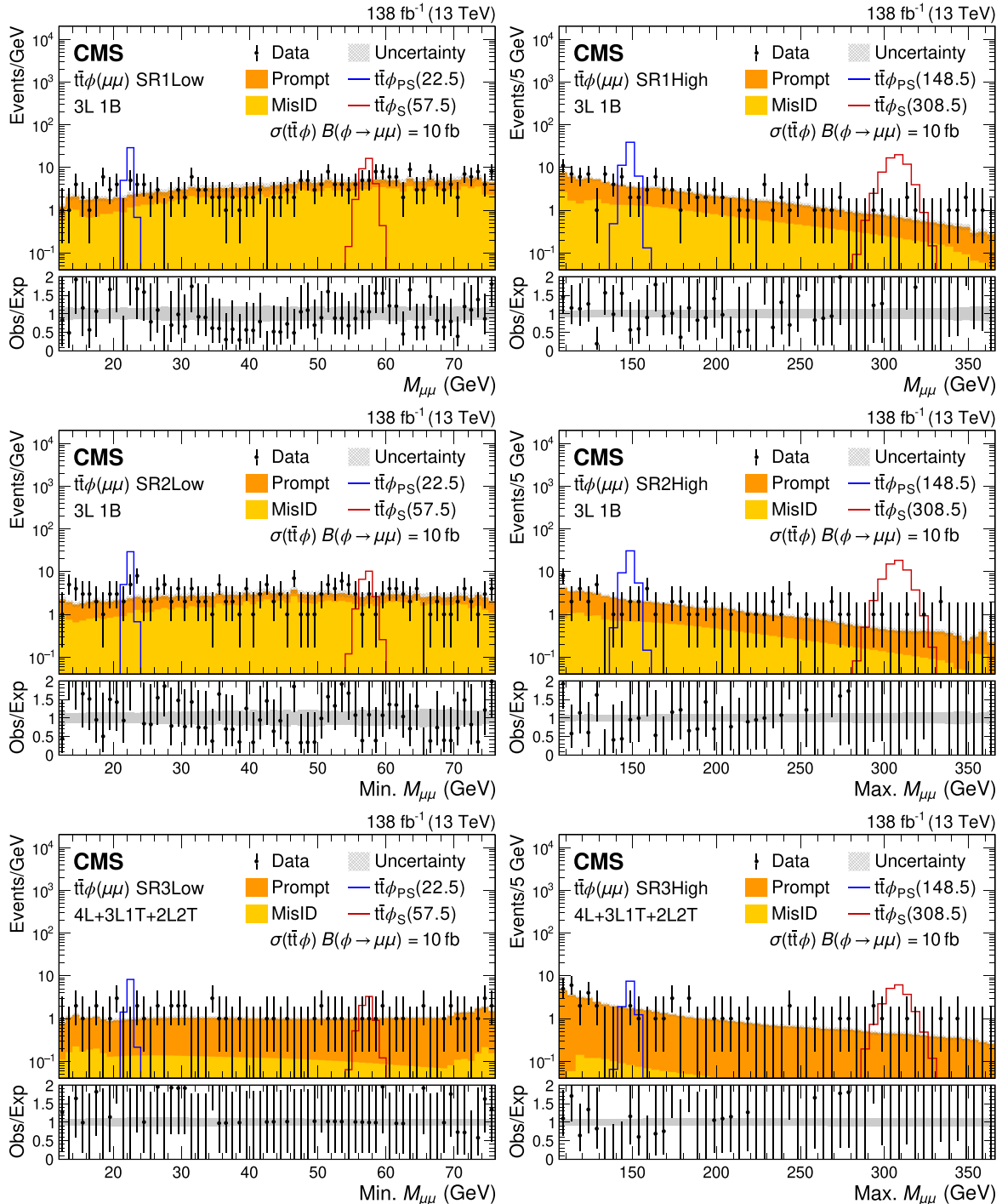


FIG. 7. Dilepton mass spectra for the $t\bar{t}\phi(\mu\mu)$ SR1 (upper), SR2 (middle), and SR3 (lower) event selections for the combined 2016–2018 data set. The low (high) mass spectra are shown on the left (right). The lower panel shows the ratio of observed events to the total expected SM background prediction (Obs/Exp), and the gray band represents the sum of statistical and systematic uncertainties in the background prediction. The expected background distributions and the uncertainties are shown after the data are fit under the background-only hypothesis. For illustration, two example signal hypotheses for the production and decay of a scalar and a pseudoscalar ϕ boson are shown, and their masses (in units of GeV) are indicated in the legend. The signals are normalized to the product of the cross section and branching fraction of 10 fb.

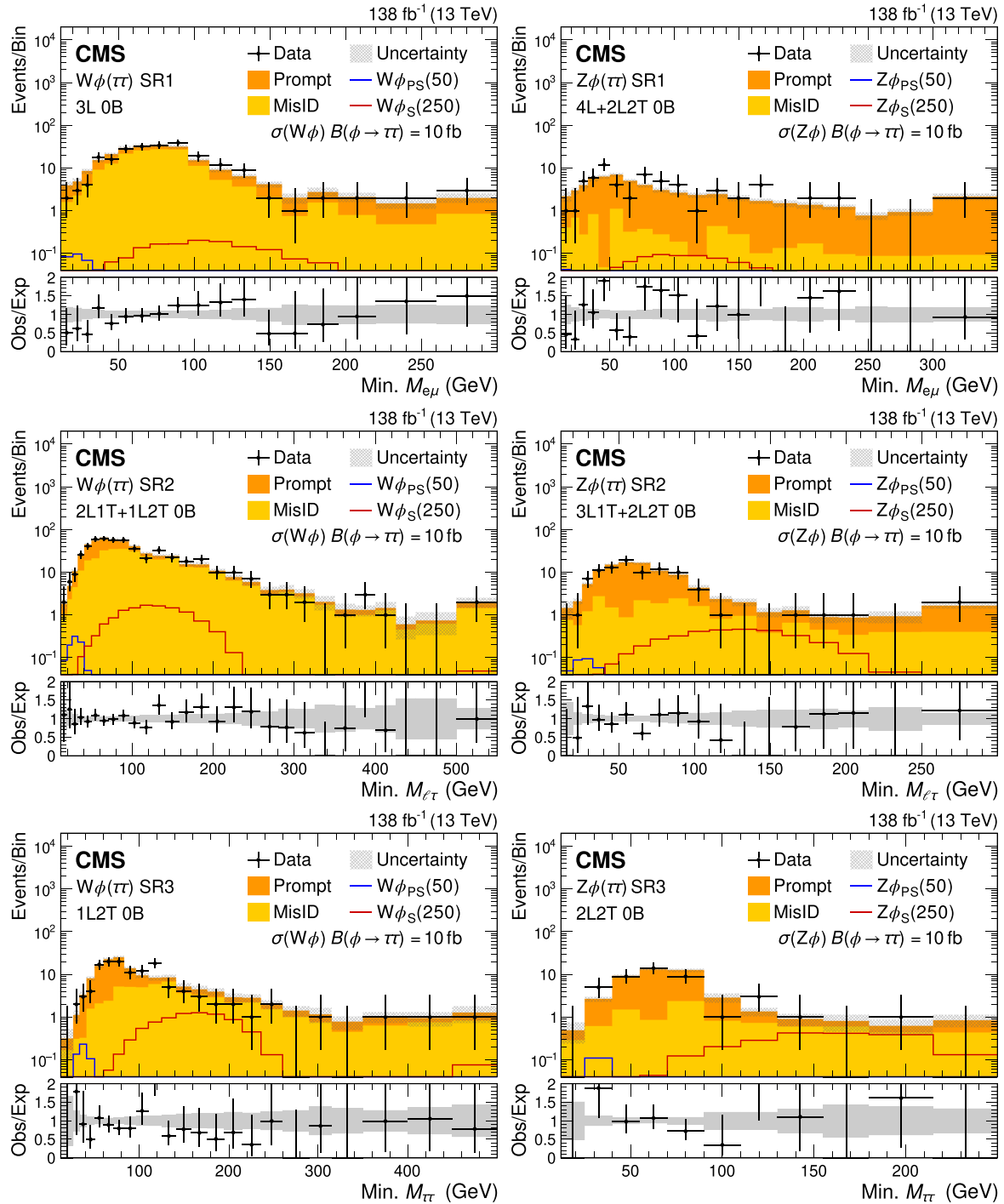


FIG. 8. Dilepton mass spectra for the $W\phi(\tau\tau)$ SR (left) and $Z\phi(\tau\tau)$ SR (right) event selections for the combined 2016–2018 data set. The lower panel shows the ratio of observed events to the total expected SM background prediction (Obs/Exp), and the gray band represents the sum of statistical and systematic uncertainties in the background prediction. The rightmost bins contain the overflow events in each distribution. The expected background distributions and the uncertainties are shown after the data are fit under the background-only hypothesis. For illustration, two example signal hypotheses for the production and decay of a scalar and a pseudoscalar ϕ boson are shown, and their masses (in units of GeV) are indicated in the legend. The signals are normalized to the product of the cross section and branching fraction of 10 fb.

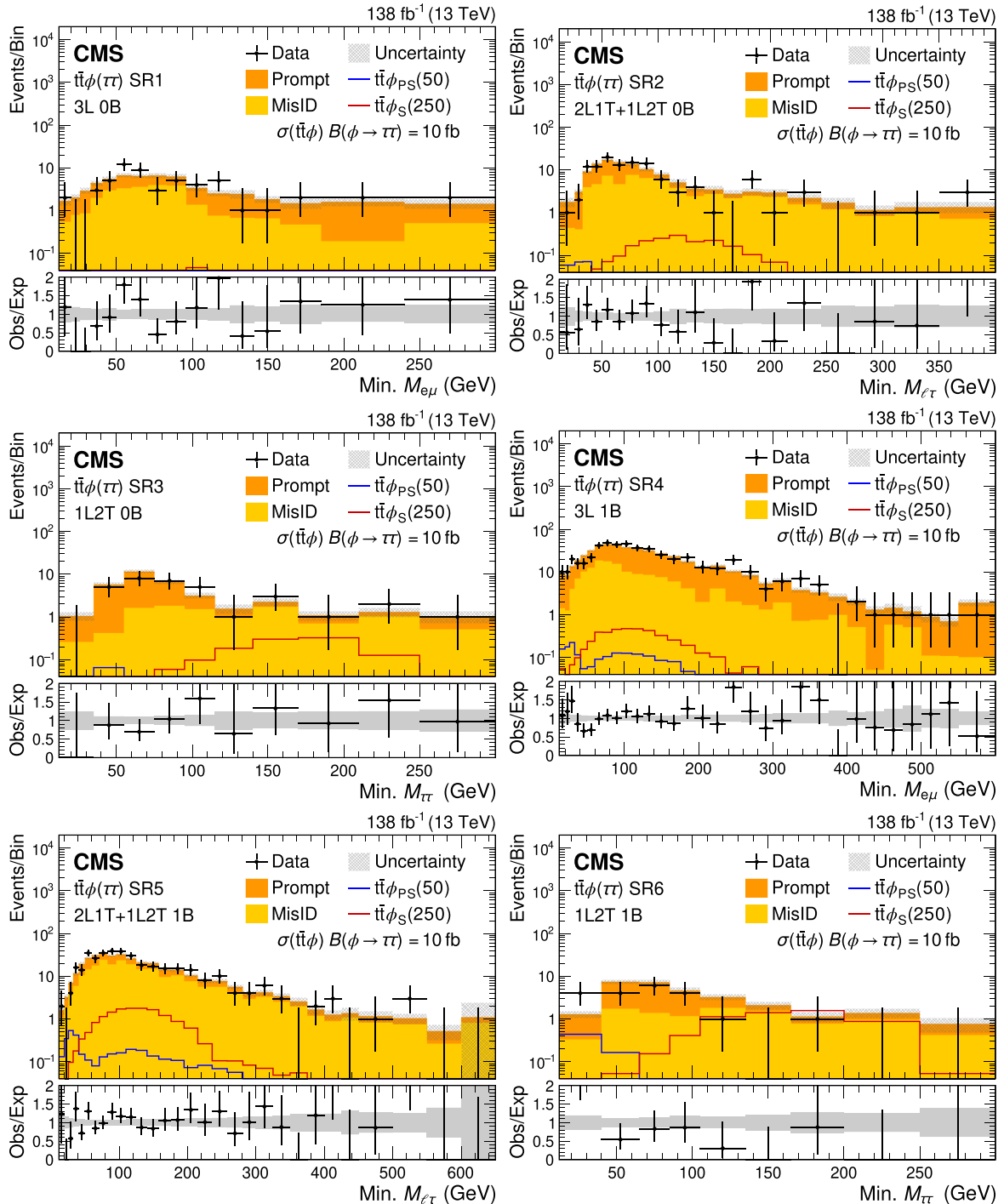


FIG. 9. Dilepton mass spectra for the $t\bar{t}\phi(\tau\tau)$ SR1-6 event selections for the combined 2016–2018 data set. The lower panel shows the ratio of observed events to the total expected SM background prediction (Obs/Exp), and the gray band represents the sum of statistical and systematic uncertainties in the background prediction. The rightmost bins contain the overflow events in each distribution. The expected background distributions and the uncertainties are shown after the data are fit under the background-only hypothesis. For illustration, two example signal hypotheses for the production and decay of a scalar and a pseudoscalar ϕ boson are shown, and their masses (in units of GeV) are indicated in the legend. The signals are normalized to the product of the cross section and branching fraction of 10 fb.

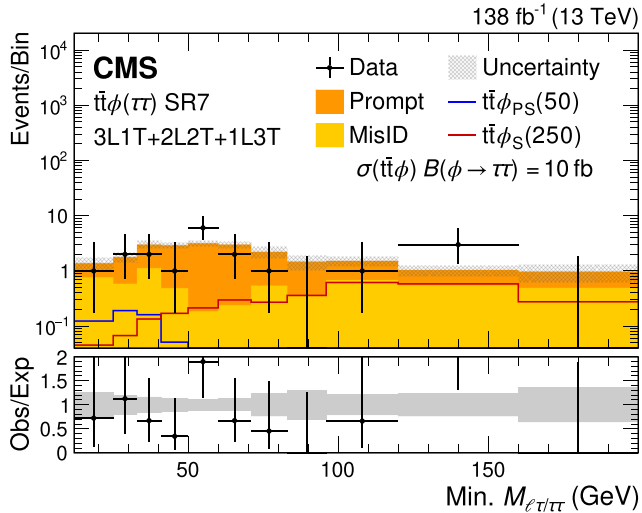


FIG. 10. Dilepton mass spectra for the $t\bar{t}\phi(\tau\tau)$ SR7 event selection for the combined 2016–2018 data set. The lower panel shows the ratio of observed events to the total expected SM background prediction (Obs/Exp), and the gray band represents the sum of statistical and systematic uncertainties in the background prediction. The rightmost bins contain the overflow events in each distribution. The expected background distributions and the uncertainties are shown after the data are fit under the background-only hypothesis. For illustration, two example signal hypotheses for the production and decay of a scalar and a pseudoscalar ϕ boson are shown, and their masses (in units of GeV) are indicated in the legend. The signals are normalized to the product of the cross section and branching fraction of 10 fb.

The exclusions are also reinterpreted as upper limits on the coupling parameters, and are provided in digital format in the HEPDATA record [19]. For the $W\phi$ and $Z\phi$ signal scenarios with scalar and pseudoscalar couplings, limits on the product of the inverse square mass scale and branching fraction to leptons, $(1/\Lambda_S)^2 \mathcal{B}(\phi \rightarrow \ell\ell)$ and $(1/\Lambda_{PS})^2 \mathcal{B}(\phi \rightarrow \ell\ell)$, are derived. For the associated production of ϕ bosons with top quark pairs, the limits on the product of the coupling to top quarks and the branching fraction to leptons, $g_{ts}^2 \mathcal{B}(\phi \rightarrow \ell\ell)$ and $g_{t\bar{t}}^2 \mathcal{B}(\phi \rightarrow \ell\ell)$, are derived for a scalar and pseudoscalar ϕ , respectively.

B. Model-dependent results

Several model-dependent exclusions are also presented. These are obtained from a weighted combination of non-overlapping SRs, as summarized in Table V, that target multiple decay modes, production modes, or both, relevant for the signal model under consideration.

First, the $t\bar{t}\phi$ mode is interpreted in the context of fermiophilic dilaton-like scalar boson and fermiophilic axion-like pseudoscalar boson signal models. These ϕ couplings are proportional to the fermion mass in both production and decay, so the $\mu\mu$ and $\tau\tau$ channels are

combined to probe the coupling to top quarks for each of these scenarios. The combined 95% CL exclusions are shown in Fig. 15.

For the H-like production scenario, the constraints from the $W\phi$, $Z\phi$, and $t\bar{t}\phi$ production modes are combined and labeled as the $X\phi$ combination. Upper limits at 95% CL are derived on the product of the mixing angle, $\sin^2 \theta$, and the branching fractions to lepton pairs. For ϕ bosons decaying to electrons or muons, the most stringent expected limit is obtained by combining all $W\phi$ and $Z\phi$ signal regions with $t\bar{t}\phi$ signal regions SR1 and SR2, which cover 3L events with one or more b jets and are independent of the $W\phi$ and $Z\phi$ signal regions. The combined $X\phi$ signal model limits on the product of the mixing angle and the branching fractions are shown in Fig. 16. For a ϕ mass of 125 GeV, the $X\phi$ combination excludes $\sin^2 \theta \mathcal{B}(\phi \rightarrow ee)$ above 2.7×10^{-3} and $\sin^2 \theta \mathcal{B}(\phi \rightarrow \mu\mu)$ above 1.5×10^{-3} . No combination is performed under the H-like production scenario for ϕ bosons decaying to tau leptons, as the most stringent expected limits over most of the mass range result from the $t\bar{t}\phi$ signal regions alone, and therefore are proportional to the upper limits obtained for the scalar $t\bar{t}\phi \rightarrow \tau\tau$ signal scenario. These are also provided in digital format in the HEPDATA record [19].

Assuming further that the ϕ branching fractions, particularly $\mathcal{B}(\phi \rightarrow \mu\mu)$ and $\mathcal{B}(\phi \rightarrow \tau\tau)$, are equal to those of the SM Higgs boson as a function of mass, the independent $\mu\mu$ and $\tau\tau$ channels are combined to derive a combined exclusion on $\sin^2 \theta$ for an H-like ϕ model, as illustrated in Fig. 17. The $\mathcal{B}(\phi \rightarrow \mu\mu)$ and $\mathcal{B}(\phi \rightarrow \tau\tau)$ values as functions of mass are obtained using the HDECAY program v.6.61 [87,88]. This combination is dominated by the $\mu\mu$ mode for ϕ masses below 30 GeV, and by the $\tau\tau$ mode for higher ϕ masses. Values of $\sin^2 \theta \leq 1$ are excluded in the ϕ mass range 15–102 GeV. Although values of $\sin^2 \theta > 1$ are unphysical in this scenario, limits on $\sin^2 \theta$ treated as a free unconstrained parameter can be considered in more general interpretations, as presented in Fig. 17.

In all model-dependent signal scenarios where ϕ is allowed to decay into pairs of leptons of all three flavors, the $X\phi \rightarrow \tau\tau$ signal contributions in which both tau leptons decay leptonically into nonresonant ee and $\mu\mu$ pairs are not considered in the M_{ee} and $M_{\mu\mu}$ spectra. Such contributions are found to be negligible across the three model-dependent interpretations carried out in this analysis.

VIII. SUMMARY

A search for beyond-the-standard-model phenomena producing resonant dilepton signatures of any flavor in multilepton events has been performed using pp collision data collected with the CMS detector at $\sqrt{s} = 13$ TeV, corresponding to an integrated luminosity of 138 fb^{-1} .

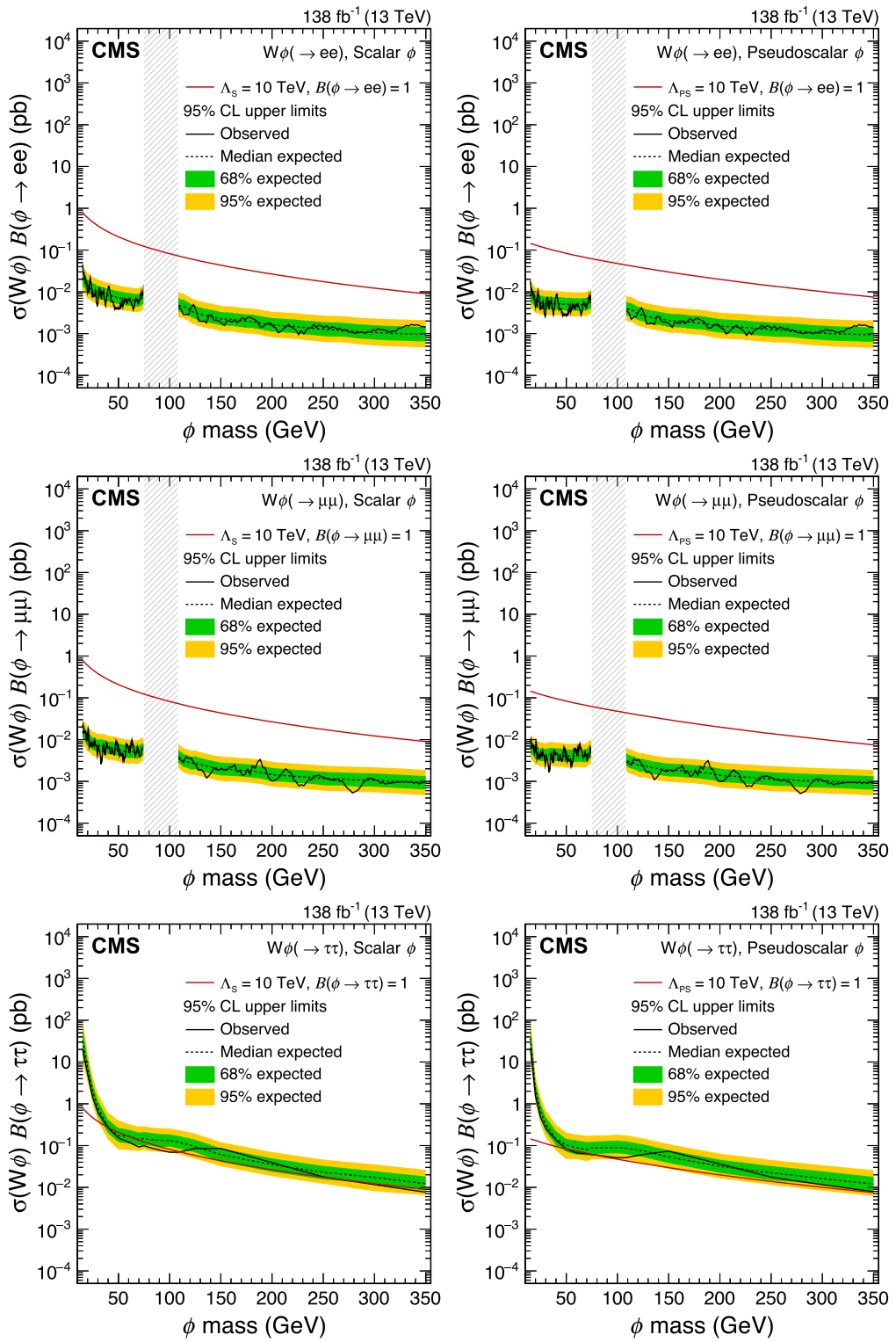


FIG. 11. The 95% confidence level upper limits on the product of the production cross section and branching fraction of the $W\phi$ signal in the ee (upper), $\mu\mu$ (middle), and $\tau\tau$ (lower) decay scenarios. The results for the scalar coupling are shown on the left and pseudoscalar on the right. The vertical gray band indicates the mass region not considered in the analysis. The red line is the theoretical prediction for the product of the production cross section and branching fraction of the $W\phi$ signal.

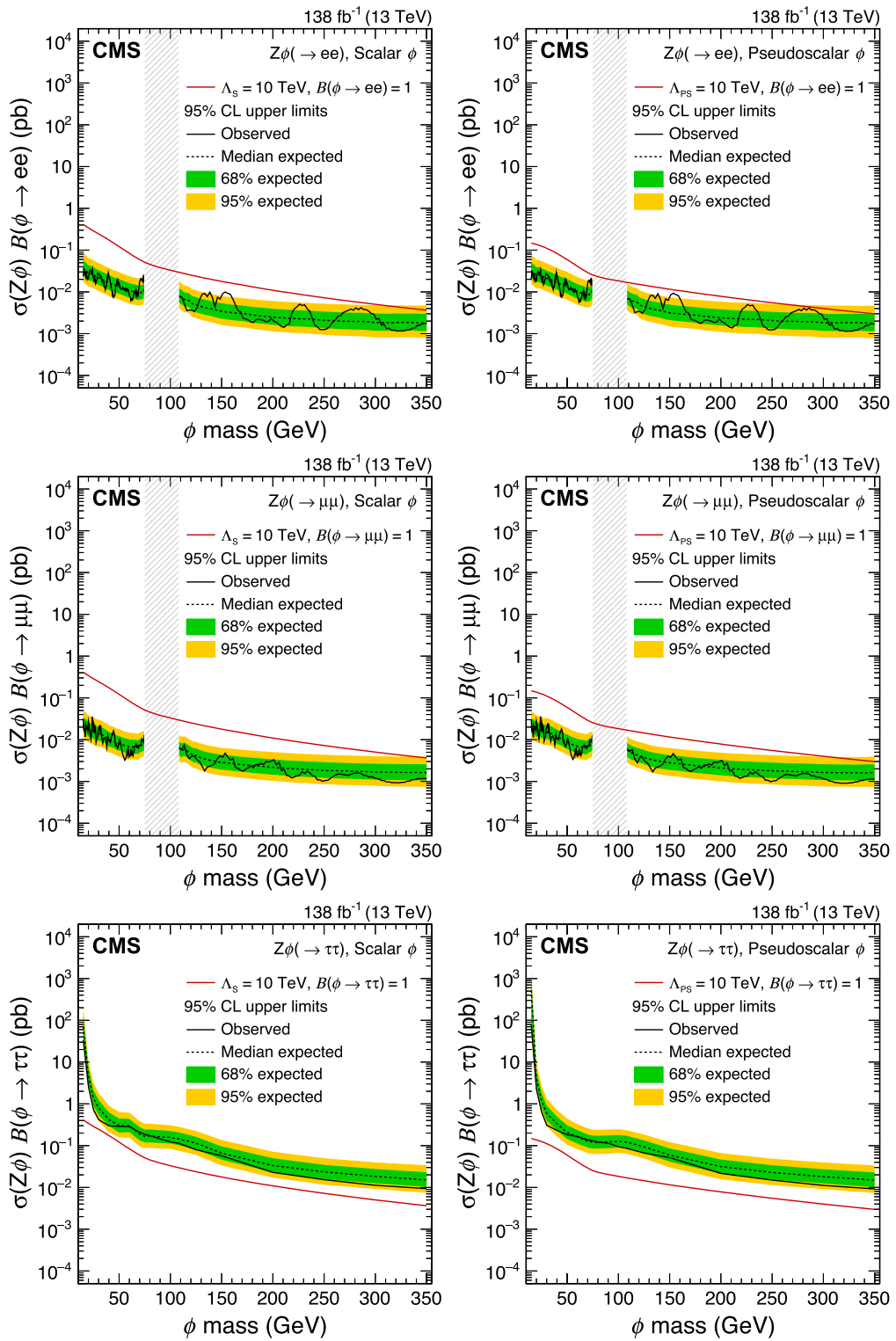


FIG. 12. The 95% confidence level upper limits on the product of the production cross section and branching fraction of the $Z\phi$ signal in the ee (upper), $\mu\mu$ (middle) and $\tau\tau$ (lower) decay scenarios. The results for the scalar coupling are shown on the left and pseudoscalar on the right. The vertical gray band indicates the mass region not considered in the analysis. The red line is the theoretical prediction for the product of the production cross section and branching fraction of the $Z\phi$ signal.

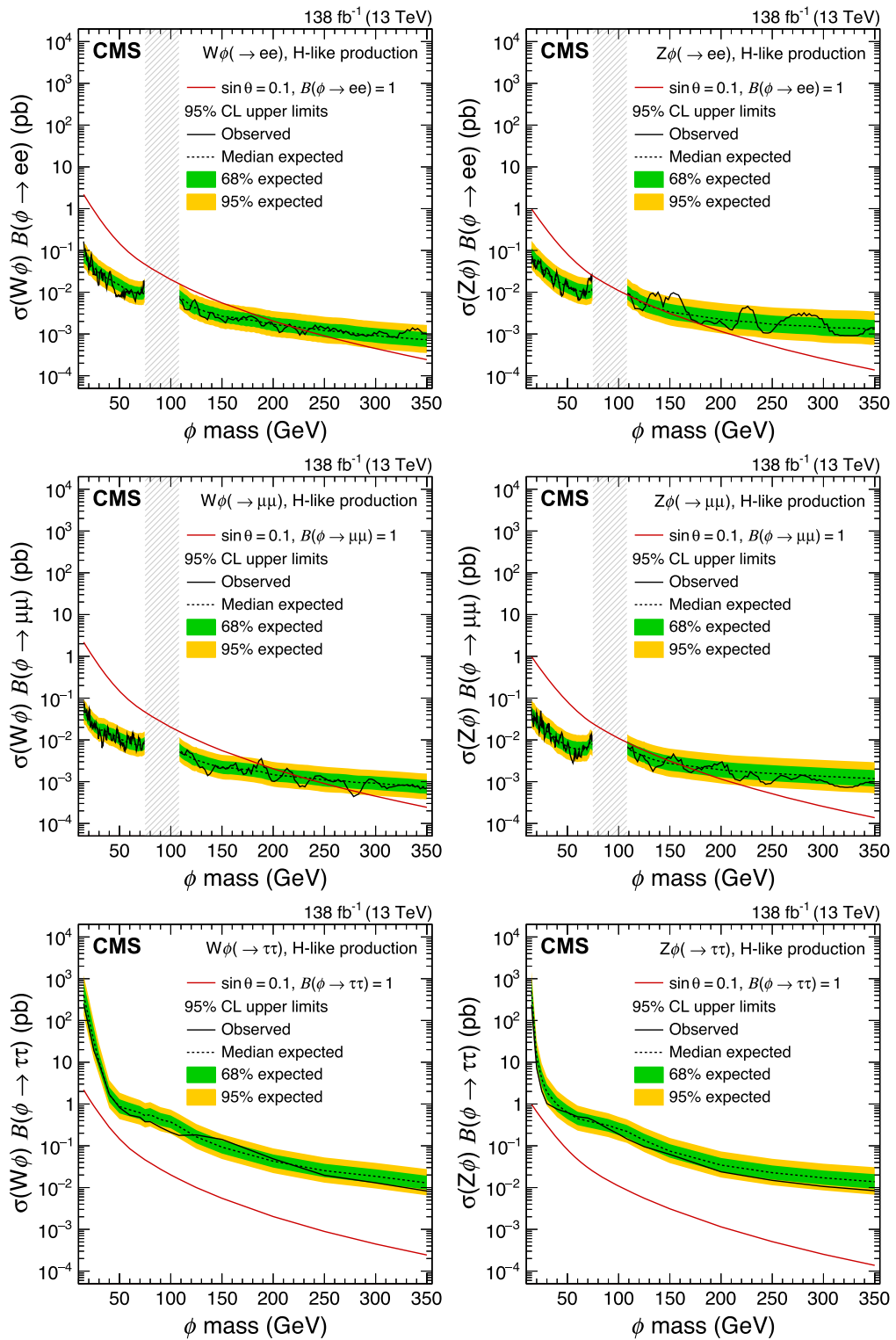


FIG. 13. The 95% confidence level upper limits on the product of the production cross section and branching fraction of the $W\phi$ signal on the left and the $Z\phi$ signal on the right with H-like couplings in the ee (upper), $\mu\mu$ (middle) and $\tau\tau$ (lower) decay scenarios. The vertical gray band indicates the mass region not considered in the analysis. The red line is the theoretical prediction for the product of the production cross section and branching fraction of the $W\phi$ and $Z\phi$ signals.

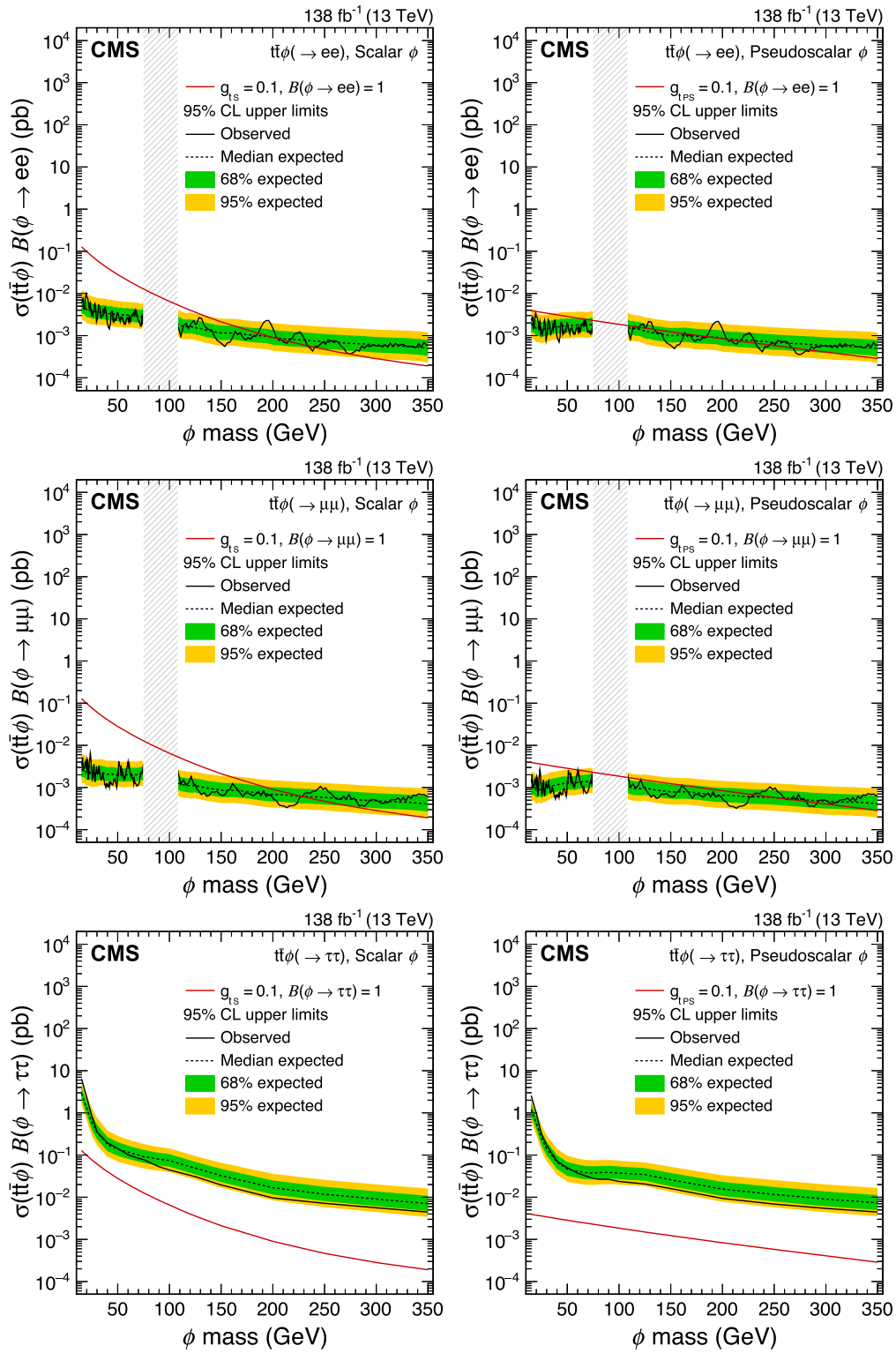


FIG. 14. The 95% confidence level upper limits on the product of the production cross section and branching fraction of the $t\bar{t}\phi$ signal in the ee (upper), $\mu\mu$ (middle) and $\tau\tau$ (lower) decay scenarios. The results for the scalar coupling are shown on the left and pseudoscalar on the right. The vertical gray band indicates the mass region not considered in the analysis. The red line is the theoretical prediction for the product of the production cross section and branching fraction of the $t\bar{t}\phi$ signal.

TABLE V. A summary of model-dependent scenarios, and the corresponding subsets of SRs combined in the interpretations.

Signal	Parameter	SRs used in combination
Fermiophilic dilaton-like ϕ production and decay $t\bar{t}\phi(\rightarrow \mu\mu, \rightarrow \tau\tau)$ combination	g_{ts}^2	For ϕ masses less than 30 GeV: $t\bar{t}\phi(\mu\mu)$ SR1-2 and $t\bar{t}\phi(\tau\tau)$ SR1-3, 5-7 For ϕ masses more than or equal to 30 GeV: $t\bar{t}\phi(\tau\tau)$ all SRs
Fermiophilic axion-like ϕ production and decay $t\bar{t}\phi(\rightarrow \mu\mu, \rightarrow \tau\tau)$ combination	g_{tpS}^2	For ϕ masses less than 30 GeV: $t\bar{t}\phi(\mu\mu)$ SR1-2 and $t\bar{t}\phi(\tau\tau)$ SR1-3, 5-7 For ϕ masses more than or equal to 30 GeV: $t\bar{t}\phi(\tau\tau)$ all SRs
H-like production $X\phi(\rightarrow ee)$ combination	$\sin^2 \theta \mathcal{B}(\phi \rightarrow ee)$	$W\phi(ee)/Z\phi(ee)$ all SRs, and $t\bar{t}\phi(ee)$ SR1-2
H-like production $X\phi(\rightarrow \mu\mu)$ combination	$\sin^2 \theta \mathcal{B}(\phi \rightarrow \mu\mu)$	$W\phi(\mu\mu)/Z\phi(\mu\mu)$ all SRs, and $t\bar{t}\phi(\mu\mu)$ SR1-2
H-like ϕ production and decay $X\phi(\rightarrow \mu\mu, \rightarrow \tau\tau)$ combination	$\sin^2 \theta$	For ϕ masses less than 30 GeV: $X\phi(\rightarrow \mu\mu)$ combination and $t\bar{t}\phi(\tau\tau)$ SR2-3 For ϕ masses more than or equal to 30 GeV: $t\bar{t}\phi(\tau\tau)$ all SRs

The results provide direct and model independent constraints on the allowed parameter space for new spin-0 particles, ϕ , with scalar, pseudoscalar, or H-like couplings. The ϕ bosons are assumed to be produced in association with a W or Z boson or a top quark-antiquark ($t\bar{t}$) pair, and decay into ee , $\mu\mu$, or $\tau\tau$ pairs. Constraints are calculated at 95% confidence level on the product of the production cross section and leptonic branching fraction of such bosons with masses in the range 15–350 GeV. No statistically significant excess is observed over the standard model background in the probed mass spectra. Over this mass range, the product of the cross section and branching fraction for the $\tau\tau$ (ee and $\mu\mu$) final states is excluded above 0.004–35, 0.004–80, and 0.008–250 pb (0.5–50, 0.5–30, and 1–200 fb) as a function of ϕ mass for scalar, pseudoscalar, and H-like bosons, respectively.

Several model-dependent interpretations have also been considered. The $t\bar{t}\phi$ mode provides the first direct bounds on the coupling of the ϕ boson to top quarks in the context of fermiophilic models. For a fermiophilic dilaton-like model with scalar couplings, the most stringent limit on the coupling is 0.63–0.66, obtained in the ϕ mass range 40–60 GeV. For a fermiophilic axion-like model with pseudoscalar couplings, the most stringent limit on the coupling is 1.59, obtained for a ϕ mass of 70 GeV. To constrain the Higgs- ϕ mixing angle, $\sin^2 \theta$, in the case where the ϕ is H-like, the independent $W\phi$, $Z\phi$, and $t\bar{t}\phi$ signal regions are combined. The observed (expected) upper limit on $\sin^2 \theta$ is 1.2 (1.9) for a ϕ mass of 125 GeV; the most stringent observed exclusion is obtained for a ϕ mass of 30 GeV, corresponding to an upper limit on $\sin^2 \theta$ of 0.59 (0.64).

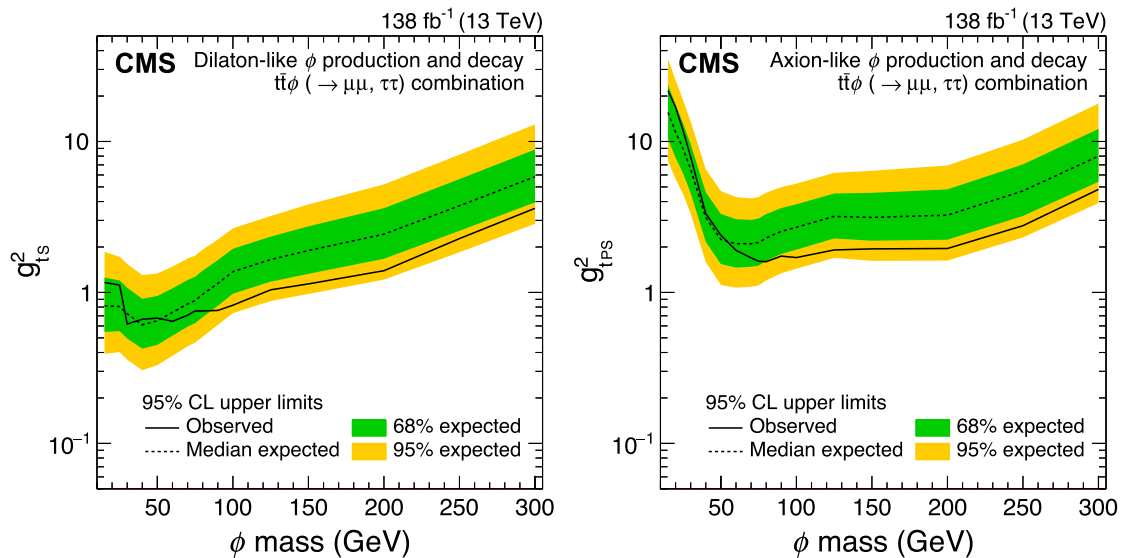


FIG. 15. The 95% confidence level upper limits on g_{ts}^2 and g_{tpS}^2 for the dilaton- and axion-like $t\bar{t}\phi$ signal model (left and right). Masses of the ϕ boson above 300 GeV are not probed for the dilaton- and axion-like signal models as the ϕ branching fraction into top quark-antiquark pairs becomes non-negligible.

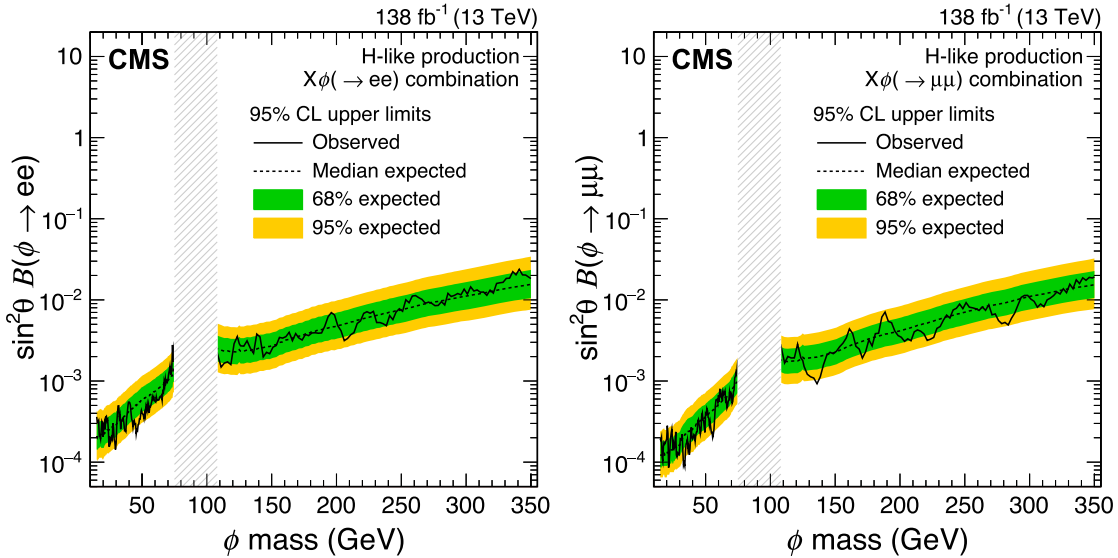


FIG. 16. The 95% confidence level upper limits on the product of $\sin^2 \theta$ and branching fraction for the H-like production of $X\phi \rightarrow ee$ and $X\phi \rightarrow \mu\mu$ (left and right). The vertical gray band indicates the mass region not considered in the analysis.

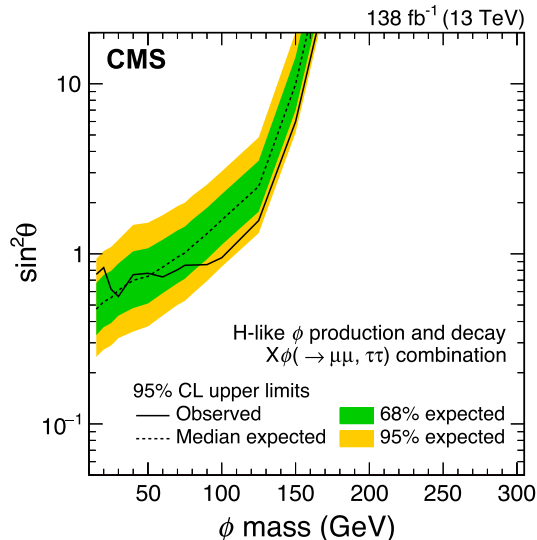


FIG. 17. The 95% confidence level upper limits on $\sin^2 \theta$ for the H-like production and decay of $X\phi$ signal model, where the ϕ boson has the same branching fractions to $\mu\mu$ and $\tau\tau$ as an SM Higgs boson with the same mass.

ACKNOWLEDGMENTS

We congratulate our colleagues in the CERN accelerator departments for the excellent performance of the LHC and thank the technical and administrative staffs at CERN and at other CMS institutes for their contributions to the success of the CMS effort. In addition, we gratefully acknowledge the computing centers and personnel of the Worldwide LHC Computing Grid and other centers for delivering so effectively the computing infrastructure essential to our analyses. Finally, we acknowledge the enduring support for

the construction and operation of the LHC, the CMS detector, and the supporting computing infrastructure provided by the following funding agencies: SC (Armenia), BMBWF and FWF (Austria); FNRS and FWO (Belgium); CNPq, CAPES, FAPERJ, FAPERGS, and FAPESP (Brazil); MES and BNSF (Bulgaria); CERN; CAS, MoST, and NSFC (China); MINCIENCIAS (Colombia); MSES and CSF (Croatia); RIF (Cyprus); SENESCYT (Ecuador); ERC PRG, RVTT3 and MoER TK202 (Estonia); Academy of Finland, MEC, and HIP (Finland); CEA and CNRS/IN2P3 (France); SRNSF (Georgia); BMBF, DFG, and HGF (Germany); GSRI (Greece); NKFIH (Hungary); DAE and DST (India); IPM (Iran); SFI (Ireland); INFN (Italy); MSIP and NRF (Republic of Korea); MES (Latvia); LMTLT (Lithuania); MOE and UM (Malaysia); BUAP, CINVESTAV, CONACYT, LNS, SEP, and UASLP-FAI (Mexico); MOS (Montenegro); MBIE (New Zealand); PAEC (Pakistan); MES and NSC (Poland); FCT (Portugal); MESTD (Serbia); MCIN/AEI and PCTI (Spain); MOSTR (Sri Lanka); Swiss Funding Agencies (Switzerland); MST (Taipei); MHESI and NSTDA (Thailand); TUBITAK and TENMAK (Turkey); NASU (Ukraine); STFC (United Kingdom); DOE and NSF (USA). Individuals have received support from the Marie-Curie program and the European Research Council and Horizon 2020 Grant, Contracts No. 675440, No. 724704, No. 752730, No. 758316, No. 765710, No. 824093, No. 101115353, and COST Action CA16108 (European Union); the Leventis Foundation; the Alfred P. Sloan Foundation; the Alexander von Humboldt Foundation; the Science Committee, Project No. 22rl-037 (Armenia); the Belgian Federal Science Policy Office; the Fonds pour la Formation à la

Recherche dans l'Industrie et dans l'Agriculture (FRIA—Belgium); the Agentschap voor Innovatie door Wetenschap en Technologie (IWT—Belgium); the F. R. S.-FNRS and FWO (Belgium) under the “Excellence of Science—EOS”—be.h project n. 30820817; the Beijing Municipal Science & Technology Commission, No. Z191100007219010 and Fundamental Research Funds for the Central Universities (China); the Ministry of Education, Youth and Sports (MEYS) of the Czech Republic; the Shota Rustaveli National Science Foundation, Grant No. FR-22-985 (Georgia); the Deutsche Forschungsgemeinschaft (DFG), under Germany's Excellence Strategy—EXC 2121 “Quantum Universe”—390833306, and under Project No. 400140256—GRK2497; the Hellenic Foundation for Research and Innovation (HFRI), Project No. 2288 (Greece); the Hungarian Academy of Sciences, the New National Excellence Program—ÚNKP, the NKFIH research Grants No. K 124845, No. K 124850, No. K 128713, No. K 128786, No. K 129058, No. K 131991, No. K 133046, No. K 138136, No. K 143460, No. K 143477, No. 2020-2.2.1-ED-2021-00181, and No. TKP2021-NKTA-64 (Hungary); the Council of Science and Industrial Research, India; ICSC—National

Research Center for High Performance Computing, Big Data and Quantum Computing, funded by the EU NexGeneration program (Italy); the Latvian Council of Science; the Ministry of Education and Science, Project No. 2022/WK/14, and the National Science Center, Contracts Opus No. 2021/41/B/ST2/01369 and No. 2021/43/B/ST2/01552 (Poland); the Fundação para a Ciência e a Tecnologia, Grant CEECIND/01334/2018 (Portugal); the National Priorities Research Program by Qatar National Research Fund; MCIN/AEI/10.13039/501100011033, ERDF “a way of making Europe”, and the Programa Estatal de Fomento de la Investigación Científica y Técnica de Excelencia María de Maeztu, Grant No. MDM-2017-0765 and Programa Severo Ochoa del Principado de Asturias (Spain); the Chulalongkorn Academic into Its 2nd Century Project Advancement Project, and the National Science, Research and Innovation Fund via the Program Management Unit for Human Resources & Institutional Development, Research and Innovation, Grant No. B37G660013 (Thailand); the Kavli Foundation; the Nvidia Corporation; the SuperMicro Corporation; the Welch Foundation, Contract No. C-1845; and the Weston Havens Foundation (USA).

-
- [1] G. Cacciapaglia, G. Ferretti, T. Flacke, and H. Serodio, Light scalars in composite Higgs models, *Front. Phys.* **7**, 22 (2019).
 - [2] U. Ellwanger, C. Hugonie, and A. M. Teixeira, The next-to-minimal supersymmetric standard model, *Phys. Rep.* **496**, 1 (2010).
 - [3] M. Maniatis, The next-to-minimal supersymmetric extension of the standard model reviewed, *Int. J. Mod. Phys. A* **25**, 3505 (2010).
 - [4] M. R. Buckley, D. Feld, and D. Goncalves, Scalar simplified models for dark matter, *Phys. Rev. D* **91**, 015017 (2015).
 - [5] M. Casolino, T. Farooque, A. Juste, T. Liu, and M. Spannowsky, Probing a light CP -odd scalar in di-top-associated production at the LHC, *Eur. Phys. J. C* **75**, 498 (2015).
 - [6] W.-F. Chang, T. Modak, and J. N. Ng, Signal for a light singlet scalar at the LHC, *Phys. Rev. D* **97**, 055020 (2018).
 - [7] P. Artoisenet *et al.*, A framework for Higgs characterisation, *J. High Energy Phys.* **11** (2013) 043.
 - [8] T. Ghosh, H.-K. Guo, T. Han, and H. Liu, Electroweak phase transition with an SU(2) dark sector, *J. High Energy Phys.* **07** (2021) 045.
 - [9] E. Gildener and S. Weinberg, Symmetry breaking and scalar bosons, *Phys. Rev. D* **13**, 3333 (1976).
 - [10] W. D. Goldberger, B. Grinstein, and W. Skiba, Distinguishing the Higgs boson from the dilaton at the Large Hadron Collider, *Phys. Rev. Lett.* **100**, 111802 (2008).
 - [11] A. Ahmed, A. Mariotti, and S. Najjari, A light dilaton at the LHC, *J. High Energy Phys.* **05** (2020) 093.
 - [12] V. Barger, M. Ishida, and W.-Y. Keung, Dilaton at the LHC, *Phys. Rev. D* **85**, 015024 (2012).
 - [13] H. Georgi, D. B. Kaplan, and L. Randall, Manifesting the invisible axion at low-energies, *Phys. Lett.* **169B**, 73 (1986).
 - [14] K. Mimasu and V. Sanz, ALPs at colliders, *J. High Energy Phys.* **06** (2015) 173.
 - [15] I. Brivio, M. B. Gavela, L. Merlo, K. Mimasu, J. M. No, R. del Rey, and V. Sanz, ALPs effective field theory and collider signatures, *Eur. Phys. J. C* **77**, 572 (2017).
 - [16] M. Bauer, M. Heiles, M. Neubert, and A. Thamm, Axion-like particles at future colliders, *Eur. Phys. J. C* **79**, 74 (2019).
 - [17] R. M. Schabinger and J. D. Wells, A minimal spontaneously broken hidden sector and its impact on Higgs boson physics at the large hadron collider, *Phys. Rev. D* **72**, 093007 (2005).
 - [18] V. Barger, P. Langacker, M. McCaskey, M. J. Ramsey-Musolf, and G. Shaughnessy, LHC phenomenology of an extended Standard Model with a real scalar singlet, *Phys. Rev. D* **77**, 035005 (2008).
 - [19] HEPData record for this analysis (2024), 10.17182/hepdata.132367.
 - [20] D. Buskulic *et al.* (ALEPH Collaboration), Search for a nonminimal Higgs boson produced in the reaction $e^+e^- \rightarrow hZ^*$, *Phys. Lett. B* **313**, 312 (1993).

- [21] M. Acciarri *et al.* (L3 Collaboration), Search for neutral Higgs boson production through the process $e^+e^- \rightarrow Z^*H^0$, *Phys. Lett. B* **385**, 454 (1996).
- [22] LEP working group for Higgs boson searches, ALEPH, DELPHI, L3 and OPAL Collaborations, Search for the standard model Higgs boson at LEP, *Phys. Lett. B* **565**, 61 (2003).
- [23] V. M. Abazov *et al.* (D0 Collaboration), Combined search for the Higgs boson with the D0 experiment, *Phys. Rev. D* **88**, 052011 (2013).
- [24] T. Aaltonen *et al.* (CDF Collaboration), Combination of searches for the Higgs boson using the full CDF data set, *Phys. Rev. D* **88**, 052013 (2013).
- [25] CDF and D0 Collaborations, Higgs boson studies at the Tevatron, *Phys. Rev. D* **88**, 052014 (2013).
- [26] CMS Collaboration, Search for the standard model Higgs boson produced in association with W and Z bosons in pp collisions at $\sqrt{s} = 7$ TeV, *J. High Energy Phys.* **11** (2012) 088.
- [27] ATLAS Collaboration, Measurement of the production cross section for a Higgs boson in association with a vector boson in the $H \rightarrow WW^* \rightarrow \ell\nu\ell\nu$ channel in pp collisions at $\sqrt{s} = 13$ TeV with the ATLAS detector, *Phys. Lett. B* **798**, 134949 (2019).
- [28] CMS Collaboration, Evidence for the 125 GeV Higgs boson decaying to a pair of τ leptons, *J. High Energy Phys.* **05** (2014) 104.
- [29] ATLAS Collaboration, Evidence for the Higgs-boson Yukawa coupling to tau leptons with the ATLAS detector, *J. High Energy Phys.* **04** (2015) 117.
- [30] CMS Collaboration, Search for the associated production of the Higgs boson with a top-quark pair, *J. High Energy Phys.* **09** (2014) 087; **10** (2014) 106(E).
- [31] ATLAS Collaboration, Search for new phenomena in events with same-charge leptons and b jets in pp collisions at $\sqrt{s} = 13$ TeV with the ATLAS detector, *J. High Energy Phys.* **12** (2018) 039.
- [32] CMS Collaboration, Evidence for Higgs boson decay to a pair of muons, *J. High Energy Phys.* **01** (2021) 148.
- [33] ATLAS Collaboration, A search for the dimuon decay of the standard model Higgs boson with the ATLAS detector, *Phys. Lett. B* **812**, 135980 (2021).
- [34] CMS Collaboration, Observation of Higgs boson decay to bottom quarks, *Phys. Rev. Lett.* **121**, 121801 (2018).
- [35] ATLAS Collaboration, Observation of $H \rightarrow b\bar{b}$ decays and VH production with the ATLAS detector, *Phys. Lett. B* **786**, 59 (2018).
- [36] ATLAS Collaboration, Search for a new pseudoscalar decaying into a pair of muons in events with a top-quark pair at $\sqrt{s} = 13$ TeV with the ATLAS detector, *Phys. Rev. D* **108**, 092007 (2023).
- [37] CMS Collaboration, Search for physics beyond the standard model in multilepton final states in proton-proton collisions at $\sqrt{s} = 13$ TeV, *J. High Energy Phys.* **03** (2020) 051.
- [38] CMS Collaboration, The CMS experiment at the CERN LHC, *J. Instrum.* **3**, S08004 (2008).
- [39] CMS Collaboration, Development of the CMS detector for the CERN LHC Run 3, *J. Instrum.* **19**, P05064 (2024).
- [40] CMS Collaboration, Performance of the CMS level-1 trigger in proton-proton collisions at $\sqrt{s} = 13$ TeV, *J. Instrum.* **15**, P10017 (2020).
- [41] CMS Collaboration, The CMS trigger system, *J. Instrum.* **12**, P01020 (2017).
- [42] CMS Collaboration, Precision luminosity measurement in proton-proton collisions at $\sqrt{s} = 13$ TeV in 2015 and 2016 at CMS, *Eur. Phys. J. C* **81**, 800 (2021).
- [43] CMS Collaboration, CMS luminosity measurement for the 2017 data-taking period at $\sqrt{s} = 13$ TeV, CMS Physics Analysis Summary CMS-PAS-LUM-17-004, 2018, <http://cds.cern.ch/record/2621960>.
- [44] CMS Collaboration, CMS luminosity measurement for the 2018 data-taking period at $\sqrt{s} = 13$ TeV, CMS Physics Analysis Summary CMS-PAS-LUM-18-002, 2019, <http://cds.cern.ch/record/2676164>.
- [45] J. Alwall, R. Frederix, S. Frixione, V. Hirschi, F. Maltoni, O. Mattelaer, H. S. Shao, T. Stelzer, P. Torrielli, and M. Zaro, The automated computation of tree-level and next-to-leading order differential cross sections, and their matching to parton shower simulations, *J. High Energy Phys.* **07** (2014) 079.
- [46] P. Nason, A new method for combining NLO QCD with shower Monte Carlo algorithms, *J. High Energy Phys.* **11** (2004) 040.
- [47] S. Frixione, P. Nason, and C. Oleari, Matching NLO QCD computations with parton shower simulations: The POWHEG method, *J. High Energy Phys.* **11** (2007) 070.
- [48] S. Alioli, P. Nason, C. Oleari, and E. Re, A general framework for implementing NLO calculations in shower Monte Carlo programs: The POWHEG BOX, *J. High Energy Phys.* **06** (2010) 043.
- [49] J. M. Campbell and R. K. Ellis, MCFM for the Tevatron and the LHC, *Nucl. Phys. B, Proc. Suppl.* **205–206**, 10 (2010).
- [50] Y. Gao, A. V. Gritsan, Z. Guo, K. Melnikov, M. Schulze, and N. V. Tran, Spin determination of single-produced resonances at hadron colliders, *Phys. Rev. D* **81**, 075022 (2010).
- [51] S. Bolognesi, Y. Gao, A. V. Gritsan, K. Melnikov, M. Schulze, N. V. Tran, and A. Whitbeck, On the spin and parity of a single-produced resonance at the LHC, *Phys. Rev. D* **86**, 095031 (2012).
- [52] I. Anderson, S. Bolognesi, F. Caola, Y. Gao, A. V. Gritsan, C. B. Martin, K. Melnikov, M. Schulze, N. V. Tran, A. Whitbeck, and Y. Zhou, Constraining anomalous HVV interactions at proton and lepton colliders, *Phys. Rev. D* **89**, 035007 (2014).
- [53] A. V. Gritsan, R. Röntsch, M. Schulze, and M. Xiao, Constraining anomalous Higgs boson couplings to the heavy flavor fermions using matrix element techniques, *Phys. Rev. D* **94**, 055023 (2016).
- [54] R. D. Ball *et al.* (NNPDF Collaboration), Parton distributions for the LHC Run II, *J. High Energy Phys.* **04** (2015) 040.
- [55] R. D. Ball *et al.* (NNPDF Collaboration), Parton distributions from high-precision collider data, *Eur. Phys. J. C* **77**, 663 (2017).
- [56] T. Sjöstrand, S. Ask, J. R. Christiansen, R. Corke, N. Desai, P. Ilten, S. Mrenna, S. Prestel, C. O. Rasmussen, and P. Z.

- Skands, An introduction to PYTHIA 8.2, *Comput. Phys. Commun.* **191**, 159 (2015).
- [57] CMS Collaboration, Event generator tunes obtained from underlying event and multiparton scattering measurements, *Eur. Phys. J. C* **76**, 155 (2016).
- [58] CMS Collaboration, Extraction and validation of a new set of CMS PYTHIA8 tunes from underlying-event measurements, *Eur. Phys. J. C* **80**, 4 (2020).
- [59] J. Alwall *et al.*, Comparative study of various algorithms for the merging of parton showers and matrix elements in hadronic collisions, *Eur. Phys. J. C* **53**, 473 (2008).
- [60] R. Frederix and S. Frixione, Merging meets matching in MC@NLO, *J. High Energy Phys.* **12** (2012) 061.
- [61] S. Agostinelli *et al.* (GEANT4 Collaboration), GEANT4—a simulation toolkit, *Nucl. Instrum. Methods Phys. Res., Sect. A* **506**, 250 (2003).
- [62] CMS Collaboration, Technical proposal for the Phase-II upgrade of the Compact Muon Solenoid, CMS Technical Proposal, Reports No. CERN-LHCC-2015-010, No. CMS-TDR-15-02, 2015, [10.17181/CERN.VU8I.D59J](https://cds.cern.ch/record/1017181/CERN.VU8I.D59J).
- [63] CMS Collaboration, Particle-flow reconstruction and global event description with the CMS detector, *J. Instrum.* **12**, P10003 (2017).
- [64] CMS Collaboration, Electron and photon reconstruction and identification with the CMS experiment at the CERN LHC, *J. Instrum.* **16**, P05014 (2021).
- [65] CMS Collaboration, ECAL 2016 refined calibration and Run2 summary plots, CMS Detector Performance Note, Report No. CMS-DP-2020-021, 2020, <http://cds.cern.ch/record/2717925>.
- [66] CMS Collaboration, Performance of the CMS muon detector and muon reconstruction with proton-proton collisions at $\sqrt{s} = 13$ TeV, *J. Instrum.* **13**, P06015 (2018).
- [67] CMS Collaboration, Performance of reconstruction and identification of τ leptons decaying to hadrons and ν_τ in pp collisions at $\sqrt{s} = 13$ TeV, *J. Instrum.* **13**, P10005 (2018).
- [68] M. Cacciari, G. P. Salam, and G. Soyez, The anti- k_T jet clustering algorithm, *J. High Energy Phys.* **04** (2008) 063.
- [69] M. Cacciari, G. P. Salam, and G. Soyez, FastJet user manual, *Eur. Phys. J. C* **72**, 1896 (2012).
- [70] CMS Collaboration, Jet energy scale and resolution in the CMS experiment in pp collisions at 8 TeV, *J. Instrum.* **12**, P02014 (2017).
- [71] CMS Collaboration, Performance of missing transverse momentum reconstruction in proton-proton collisions at $\sqrt{s} = 13$ TeV using the CMS detector, *J. Instrum.* **14**, P07004 (2019).
- [72] D. Bertolini, P. Harris, M. Low, and N. Tran, Pileup per particle identification, *J. High Energy Phys.* **10** (2014) 059.
- [73] CMS Collaboration, Pileup mitigation at CMS in 13 TeV data, *J. Instrum.* **15**, P09018 (2020).
- [74] CMS Collaboration, Identification of heavy-flavour jets with the CMS detector in pp collisions at 13 TeV, *J. Instrum.* **13**, P05011 (2018).
- [75] CMS Collaboration, Identification of hadronic tau lepton decays using a deep neural network, *J. Instrum.* **17**, P07023 (2022).
- [76] CMS Collaboration, Search for third-generation scalar leptoquarks in the $t\bar{t}$ channel in proton-proton collisions at $\sqrt{s} = 8$ TeV, *J. High Energy Phys.* **07** (2015) 042; **11** (2016) 56.
- [77] CMS Collaboration, Measurement of the inclusive W and Z production cross sections in pp collisions at $\sqrt{s} = 7$ TeV, *J. High Energy Phys.* **10** (2011) 132.
- [78] K. S. Cranmer, Kernel estimation in high-energy physics, *Comput. Phys. Commun.* **136**, 198 (2001).
- [79] M. Cacciari, S. Frixione, M. L. Mangano, P. Nason, and G. Ridolfi, The $t\bar{t}$ cross-section at 1.8 and 1.96 TeV: A study of the systematics due to parton densities and scale dependence, *J. High Energy Phys.* **04** (2004) 068.
- [80] CMS Collaboration, Measurement of the inelastic proton-proton cross section at $\sqrt{s} = 13$ TeV, *J. High Energy Phys.* **07** (2018) 161.
- [81] ATLAS Collaboration, Measurement of the inelastic proton-proton cross section at $\sqrt{s} = 13$ TeV with the ATLAS detector at the LHC, *Phys. Rev. Lett.* **117**, 182002 (2016).
- [82] E. Gross and O. Vitells, Trial factors for the look elsewhere effect in high energy physics, *Eur. Phys. J. C* **70**, 525 (2010).
- [83] T. Junk, Confidence level computation for combining searches with small statistics, *Nucl. Instrum. Methods Phys. Res., Sect. A* **434**, 435 (1999).
- [84] A. L. Read, Presentation of search results: The CL_s technique, *J. Phys. G* **28**, 2693 (2002).
- [85] G. Cowan, K. Cranmer, E. Gross, and O. Vitells, Asymptotic formulae for likelihood-based tests of new physics, *Eur. Phys. J. C* **71**, 1554 (2011); **73**, 2501(E) (2013).
- [86] ATLAS and CMS Collaborations, and LHC Higgs Combination Group, Procedure for the LHC Higgs boson search combination in Summer 2011, Technical Reports No. CMS-NOTE-2011-005, No. ATL-PHYS-PUB-2011-011, 2011, <http://cds.cern.ch/record/1379837>.
- [87] A. Djouadi, J. Kalinowski, and M. Spira, HDECAY: A program for Higgs boson decays in the standard model and its supersymmetric extension, *Comput. Phys. Commun.* **108**, 56 (1998).
- [88] A. Djouadi, J. Kalinowski, M. Muehlleitner, and M. Spira, HDECAY: Twenty++ years after, *Comput. Phys. Commun.* **238**, 214 (2019).

A. Tumasyan^{1,b}, W. Adam¹, J. W. Andrejkovic,² T. Bergauer¹, S. Chatterjee¹, K. Damanakis¹, M. Dragicevic¹, A. Escalante Del Valle¹, P. S. Hussain¹, M. Jeitler^{1,c}, N. Krammer¹, L. Lechner¹, D. Liko¹, I. Mikulec¹, P. Paulitsch¹, J. Schieck¹, R. Schöfbeck¹, D. Schwarz¹, M. Sonawane¹, S. Templ¹, W. Waltenberger¹, C.-E. Wulz¹, M. R. Darwish^{1,d}, T. Janssen¹, T. Kello^{3,e}, P. Van Mechelen¹, E. S. Bols¹, J. D'Hondt¹, A. De Moor¹, M. Delcourt¹, H. El Faham¹, S. Lowette¹, A. Morton¹, D. Müller¹, A. R. Sahasransu¹,

- S. Tavernier⁴ W. Van Doninck,⁴ S. Van Putte⁴ D. Vannerom⁴ B. Clerbaux⁵ S. Dansana⁵ G. De Lentdecker⁵
 L. Favart⁵ D. Hohov⁵ J. Jaramillo⁵ K. Lee⁵ M. Mahdavikhorrami⁵ I. Makarenko⁵ A. Malara⁵ S. Paredes⁵
 L. Pétré⁵ N. Postiau⁵ L. Thomas⁵ M. Vanden Bemden⁵ C. Vander Velde⁵ P. Vanlaer⁵ D. Dobur⁶ J. Knolle⁶
 L. Lambrecht⁶ G. Mestdach,⁶ C. Rendón,⁶ A. Samalan,⁶ K. Skovpen⁶ M. Tytgat⁶ N. Van Den Bossche⁶
 B. Vermassen,⁶ L. Wezenbeek⁶ A. Benecke⁷ G. Bruno⁷ F. Bury⁷ C. Caputo⁷ P. David⁷ C. Delaere⁷
 I. S. Donertas⁷ A. Giannanco⁷ K. Jaffel⁷ Sa. Jain⁷ V. Lemaitre,⁷ K. Mondal⁷ A. Taliercio⁷ T. T. Tran⁷
 P. Vischia⁷ S. Wertz⁷ G. A. Alves⁸ E. Coelho⁸ C. Hensel⁸ A. Moraes⁸ P. Rebello Teles⁸
 W. L. Aldá Júnior⁹ M. Alves Gallo Pereira⁹ M. Barroso Ferreira Filho⁹ H. Brandao Malbouisson⁹ W. Carvalho⁹
 J. Chinellato,^{9,f} E. M. Da Costa⁹ G. G. Da Silveira^{9,g} D. De Jesus Damiao⁹ V. Dos Santos Sousa⁹
 S. Fonseca De Souza⁹ J. Martins^{9,h} C. Mora Herrera⁹ K. Mota Amarilo⁹ L. Mundim⁹ H. Nogima⁹
 A. Santoro⁹ S. M. Silva Do Amaral⁹ A. Sznajder⁹ M. Thiel⁹ A. Vilela Pereira⁹ C. A. Bernardes^{10,g}
 L. Calligaris¹⁰ T. R. Fernandez Perez Tomei¹⁰ E. M. Gregores¹⁰ P. G. Mercadante¹⁰ S. F. Novaes¹⁰
 Sandra S. Padula¹⁰ A. Aleksandrov¹¹ G. Antchev¹¹ R. Hadjiiska¹¹ P. Iaydjiev¹¹ M. Misheva¹¹ M. Rodozov,¹¹
 M. Shopova¹¹ G. Sultanov¹¹ A. Dimitrov¹² T. Ivanov¹² L. Litov¹² B. Pavlov¹² P. Petkov¹² A. Petrov¹²
 E. Shumka¹² S. Keshri¹³ S. Thakur¹³ T. Cheng¹⁴ Q. Guo,¹⁴ T. Javaid^{14,i} M. Mittal¹⁴ L. Yuan¹⁴ G. Bauer,
 Z. Hu¹⁵ S. Lezki¹⁵ K. Yi^{15,j,k} G. M. Chen^{16,i} H. S. Chen^{16,i} M. Chen^{16,i} F. Iemmi¹⁶ C. H. Jiang,¹⁶
 A. Kapoor¹⁶ H. Liao¹⁶ Z.-A. Liu^{16,l} V. Milosevic¹⁶ F. Monti¹⁶ R. Sharma¹⁶ J. Tao¹⁶ J. Thomas-Wilsker¹⁶
 J. Wang¹⁶ H. Zhang¹⁶ J. Zhao¹⁶ A. Agapitos¹⁷ Y. Ban¹⁷ A. Carvalho Antunes De Oliveira¹⁷ A. Levin¹⁷,
 C. Li¹⁷ Q. Li¹⁷ X. Lyu,¹⁷ Y. Mao,¹⁷ S. J. Qian¹⁷ X. Sun¹⁷ D. Wang¹⁷ J. Xiao¹⁷ H. Yang,¹⁷ M. Lu¹⁸
 Z. You¹⁸ N. Lu¹⁹ X. Gao^{20,e} D. Leggat,²⁰ H. Okawa²⁰ Y. Zhang²⁰ Z. Lin²¹ C. Lu²¹ M. Xiao²¹ C. Avila²²
 D. A. Barbosa Trujillo,²² A. Cabrera²² C. Florez²² J. Fraga²² J. Mejia Guisao²³ F. Ramirez²³ M. Rodriguez²³
 J. D. Ruiz Alvarez²³ D. Giljanovic²⁴ N. Godinovic²⁴ D. Lelas²⁴ I. Puljak²⁴ Z. Antunovic,²⁵ M. Kovac²⁵
 T. Sculac²⁵ P. Bargassa²⁶ V. Brigljevic²⁶ B. K. Chitroda²⁶ D. Ferencek²⁶ S. Mishra²⁶ M. Roguljic²⁶
 A. Starodumov^{26,m} T. Susa²⁶ A. Attikis²⁷ K. Christoforou²⁷ S. Konstantinou²⁷ J. Mousa²⁷ C. Nicolaou,²⁷
 F. Ptochos²⁷ P. A. Razis²⁷ H. Rykaczewski,²⁷ H. Saka²⁷ A. Stepennov²⁷ M. Finger^{28,m} M. Finger Jr.,²⁸
 A. Kveton²⁸ E. Ayala²⁹ E. Carrera Jarrin³⁰ H. Abdalla^{31,n} Y. Assran,^{31,o,p} M. Abdullah Al-Mashad³²
 M. A. Mahmoud³² S. Bhowmik³³ R. K. Dewanjee³³ K. Ehataht³³ M. Kadastik,³³ T. Lange³³ S. Nandan³³
 C. Nielsen³³ J. Pata³³ M. Raidal³³ L. Tani³³ C. Veelken³³ P. Eerola³⁴ H. Kirschenmann³⁴ K. Osterberg³⁴
 M. Voutilainen³⁴ S. Bharthuar³⁵ E. Brückner³⁵ F. Garcia³⁵ J. Havukainen³⁵ M. S. Kim³⁵ R. Kinnunen,³⁵
 T. Lampén³⁵ K. Lassila-Perini³⁵ S. Lehti³⁵ T. Lindén,³⁵ M. Lotti,³⁵ L. Martikainen³⁵ M. Myllymäki³⁵
 M. m. Rantanen³⁵ H. Siikonen³⁵ E. Tuominen³⁵ J. Tuominenemi³⁵ P. Luukka³⁶ H. Petrow³⁶ T. Tuuva,^{36,a}
 C. Amendola³⁷ M. Besancon³⁷ F. Couderc³⁷ M. Dejardin³⁷ D. Denegri,³⁷ J. L. Faure,³⁷ F. Ferri³⁷ S. Ganjour³⁷,
 P. Gras³⁷ G. Hamel de Monchenault³⁷ V. Lohezic³⁷ J. Malcles³⁷ J. Rander,³⁷ A. Rosowsky³⁷ M. Ö. Sahin³⁷
 A. Savoy-Navarro^{37,q} P. Simkina³⁷ M. Titov³⁷ C. Baldenegro Barrera³⁸ F. Beaudette³⁸ A. Buchot Perraguin³⁸,
 P. Busson³⁸ A. Cappati³⁸ C. Charlott³⁸ F. Damas³⁸ O. Davignon³⁸ B. Diab³⁸ G. Falmagne³⁸
 B. A. Fontana Santos Alves³⁸ S. Ghosh³⁸ R. Granier de Cassagnac³⁸ A. Hakimi³⁸ B. Harikrishnan³⁸ G. Liu³⁸
 J. Motta³⁸ M. Nguyen³⁸ C. Ochando³⁸ L. Portales³⁸ R. Salerno³⁸ U. Sarkar³⁸ J. B. Sauvan³⁸ Y. Sirois³⁸
 A. Tarabini³⁸ E. Vernazza³⁸ A. Zabi³⁸ A. Zghiche³⁸ J.-L. Agram^{39,r} J. Andrea³⁹ D. Appar³⁹ D. Bloch³⁹,
 G. Bourgatte³⁹ J.-M. Brom³⁹ E. C. Chabert³⁹ C. Collard³⁹ D. Darej,³⁹ U. Goerlach³⁹ C. Grimault,³⁹
 A.-C. Le Bihan³⁹ P. Van Hove³⁹ S. Beauceron⁴⁰ B. Blançon⁴⁰ G. Boudoul⁴⁰ A. Carle,⁴⁰ N. Chanon⁴⁰
 J. Choi⁴⁰ D. Contardo⁴⁰ P. Depasse⁴⁰ C. Dozen^{40,s} H. El Mamouni,⁴⁰ J. Fay⁴⁰ S. Gascon⁴⁰ M. Gouzevitch⁴⁰,
 G. Grenier⁴⁰ B. Ille⁴⁰ I. B. Laktineh,⁴⁰ M. Lethuillier⁴⁰ L. Mirabito,⁴⁰ S. Perries,⁴⁰ M. Vander Donckt⁴⁰,
 P. Verdier⁴⁰ S. Viret,⁴⁰ I. Bagaturia^{41,t} I. Lomidze⁴¹ Z. Tsamalaidze^{41,m} V. Botta⁴² L. Feld⁴² K. Klein⁴²,
 M. Lipinski⁴² D. Meuser⁴² A. Pauls⁴² N. Röwert⁴² M. Teroerde⁴² S. Diekmann⁴³ A. Dodonova⁴³
 N. Eich⁴³ D. Eliseev⁴³ M. Erdmann⁴³ P. Fackeldey⁴³ B. Fischer⁴³ T. Hebbeker⁴³ K. Hoepfner⁴³ F. Ivone⁴³,
 M. y. Lee⁴³ L. Mastrolorenzo,⁴³ M. Merschmeyer⁴³ A. Meyer⁴³ S. Mondal⁴³ S. Mukherjee⁴³ D. Noll⁴³
 A. Novak⁴³ F. Nowotny,⁴³ A. Pozdnyakov⁴³ Y. Rath,⁴³ W. Redjeb⁴³ F. Rehm,⁴³ H. Reithler⁴³ A. Schmidt⁴³,
 S. C. Schuler,⁴³ A. Sharma⁴³ A. Stein⁴³ F. Torres Da Silva De Araujo^{43,u} L. Vigilante,⁴³ S. Wiedenbeck⁴³,
 S. Zaleski,⁴³ C. Dziwok⁴⁴ G. Flügge⁴⁴ W. Haj Ahmad^{44,v} O. Hlushchenko,⁴⁴ T. Kress⁴⁴ A. Nowack⁴⁴

- O. Pooth^{ID},⁴⁴ A. Stahl^{ID},⁴⁴ T. Ziemons^{ID},⁴⁴ A. Zott^{ID},⁴⁴ H. Aarup Petersen^{ID},⁴⁵ M. Aldaya Martin^{ID},⁴⁵ J. Alimena^{ID},⁴⁵ Y. An^{ID},⁴⁵ P. Asmuss,⁴⁵ S. Baxter^{ID},⁴⁵ M. Bayatmakou^{ID},⁴⁵ H. Becerril Gonzalez^{ID},⁴⁵ O. Behnke^{ID},⁴⁵ S. Bhattacharya^{ID},⁴⁵ F. Blekman^{ID},^{45,w} K. Borras^{ID},^{45,x} D. Brunner^{ID},⁴⁵ A. Campbell^{ID},⁴⁵ A. Cardini^{ID},⁴⁵ C. Cheng,⁴⁵ F. Colombina^{ID},⁴⁵ S. Consuegra Rodríguez^{ID},⁴⁵ G. Correia Silva^{ID},⁴⁵ M. De Silva^{ID},⁴⁵ G. Eckerlin,⁴⁵ D. Eckstein^{ID},⁴⁵ L. I. Estevez Banos^{ID},⁴⁵ O. Filatov^{ID},⁴⁵ E. Gallo^{ID},^{45,w} A. Geiser^{ID},⁴⁵ A. Giraldi^{ID},⁴⁵ G. Greau,⁴⁵ A. Grohsjean^{ID},⁴⁵ V. Guglielmi^{ID},⁴⁵ M. Guthoff^{ID},⁴⁵ A. Jafari^{ID},^{45,y} N. Z. Jomhari^{ID},⁴⁵ B. Kaech^{ID},⁴⁵ M. Kasemann^{ID},⁴⁵ H. Kaveh^{ID},⁴⁵ C. Kleinwort^{ID},⁴⁵ R. Kogler^{ID},⁴⁵ M. Komm^{ID},⁴⁵ D. Krücker^{ID},⁴⁵ W. Lange,⁴⁵ D. Leyva Pernia^{ID},⁴⁵ K. Lipka^{ID},^{45,z} W. Lohmann^{ID},^{45,aa} R. Mankel^{ID},⁴⁵ I.-A. Melzer-Pellmann^{ID},⁴⁵ M. Mendizabal Morentin^{ID},⁴⁵ J. Metwally,⁴⁵ A. B. Meyer^{ID},⁴⁵ G. Milella^{ID},⁴⁵ M. Mormile^{ID},⁴⁵ A. Mussgiller^{ID},⁴⁵ A. Nürnberg^{ID},⁴⁵ Y. Otarid,⁴⁵ D. Pérez Adán^{ID},⁴⁵ E. Ranken^{ID},⁴⁵ A. Raspereza^{ID},⁴⁵ B. Ribeiro Lopes^{ID},⁴⁵ J. Rübenach,⁴⁵ A. Saggio^{ID},⁴⁵ M. Savitskyi^{ID},⁴⁵ M. Scham^{ID},^{45,bb,x} V. Scheurer,⁴⁵ S. Schnake^{ID},^{45,x} P. Schütze^{ID},⁴⁵ C. Schwanenberger^{ID},^{45,w} M. Shchedrolosiev^{ID},⁴⁵ R. E. Sosa Ricardo^{ID},⁴⁵ D. Stafford,⁴⁵ N. Tonon^{ID},^{45,a} F. Vazzoler^{ID},⁴⁵ A. Ventura Barroso^{ID},⁴⁵ R. Walsh^{ID},⁴⁵ Q. Wang^{ID},⁴⁵ Y. Wen^{ID},⁴⁵ K. Wichmann,⁴⁵ L. Wiens^{ID},^{45,x} C. Wissing^{ID},⁴⁵ S. Wuchterl^{ID},⁴⁵ Y. Yang^{ID},⁴⁵ A. Zimmermann Castro Santos^{ID},⁴⁵ A. Albrecht^{ID},⁴⁶ S. Albrecht^{ID},⁴⁶ M. Antonello^{ID},⁴⁶ S. Bein^{ID},⁴⁶ L. Benato^{ID},⁴⁶ M. Bonanomi^{ID},⁴⁶ P. Connor^{ID},⁴⁶ K. De Leo^{ID},⁴⁶ M. Eich,⁴⁶ K. El Morabit^{ID},⁴⁶ A. Fröhlich,⁴⁶ C. Garbers^{ID},⁴⁶ E. Garutti^{ID},⁴⁶ M. Hajheidari,⁴⁶ J. Haller^{ID},⁴⁶ A. Hinzmann^{ID},⁴⁶ H. R. Jabusch^{ID},⁴⁶ G. Kasieczka^{ID},⁴⁶ P. Keicher,⁴⁶ R. Klanner^{ID},⁴⁶ W. Korcari^{ID},⁴⁶ T. Kramer^{ID},⁴⁶ V. Kutzner^{ID},⁴⁶ F. Labe^{ID},⁴⁶ J. Lange^{ID},⁴⁶ A. Lobanov^{ID},⁴⁶ C. Matthies^{ID},⁴⁶ A. Mehta^{ID},⁴⁶ L. Moureaux^{ID},⁴⁶ M. Mrowietz,⁴⁶ A. Nigamova^{ID},⁴⁶ Y. Nissan,⁴⁶ A. Paasch^{ID},⁴⁶ K. J. Pena Rodriguez^{ID},⁴⁶ T. Quadfasel^{ID},⁴⁶ M. Rieger^{ID},⁴⁶ D. Savoii^{ID},⁴⁶ J. Schindler^{ID},⁴⁶ P. Schleper^{ID},⁴⁶ M. Schröder^{ID},⁴⁶ J. Schwandt^{ID},⁴⁶ M. Sommerhalder^{ID},⁴⁶ H. Stadie^{ID},⁴⁶ G. Steinbrück^{ID},⁴⁶ A. Tews,⁴⁶ M. Wolf^{ID},⁴⁶ S. Brommer^{ID},⁴⁷ M. Burkart,⁴⁷ E. Butz^{ID},⁴⁷ T. Chwalek^{ID},⁴⁷ A. Dierlamm^{ID},⁴⁷ A. Droll,⁴⁷ N. Faltermann^{ID},⁴⁷ M. Giffels^{ID},⁴⁷ J. O. Gosewisch,⁴⁷ A. Gottmann^{ID},⁴⁷ F. Hartmann^{ID},^{47,cc} M. Horzela^{ID},⁴⁷ U. Husemann^{ID},⁴⁷ M. Klute^{ID},⁴⁷ R. Koppenhöfer^{ID},⁴⁷ M. Link,⁴⁷ A. Lintuluoto^{ID},⁴⁷ S. Maier^{ID},⁴⁷ S. Mitra^{ID},⁴⁷ Th. Müller^{ID},⁴⁷ M. Neukum,⁴⁷ M. Oh^{ID},⁴⁷ G. Quast^{ID},⁴⁷ K. Rabbertz^{ID},⁴⁷ I. Shvetsov^{ID},⁴⁷ H. J. Simonis^{ID},⁴⁷ N. Trevisani^{ID},⁴⁷ R. Ulrich^{ID},⁴⁷ J. van der Linden^{ID},⁴⁷ R. F. Von Cube^{ID},⁴⁷ M. Wassmer^{ID},⁴⁷ S. Wieland^{ID},⁴⁷ R. Wolf^{ID},⁴⁷ S. Wunsch,⁴⁷ X. Zuo^{ID},⁴⁷ G. Anagnostou,⁴⁸ P. Assiouras^{ID},⁴⁸ G. Daskalakis^{ID},⁴⁸ A. Kyriakis,⁴⁸ A. Stakia^{ID},⁴⁸ M. Diamantopoulou,⁴⁹ D. Karasavvas,⁴⁹ P. Kontaxakis^{ID},⁴⁹ A. Manousakis-Katsikakis^{ID},⁴⁹ G. Melachroinos,⁴⁹ A. Panagiotou,⁴⁹ I. Papavergou^{ID},⁴⁹ N. Saoulidou^{ID},⁴⁹ K. Theofilatos^{ID},⁴⁹ E. Tziaferi^{ID},⁴⁹ K. Vellidis^{ID},⁴⁹ I. Zisopoulos^{ID},⁴⁹ G. Bakas^{ID},⁵⁰ T. Chatzistavrou,⁵⁰ G. Karapostoli^{ID},⁵⁰ K. Kousouris^{ID},⁵⁰ I. Papakrivopoulos^{ID},⁵⁰ G. Tsipolitis,⁵⁰ A. Zacharopoulou,⁵⁰ K. Adamidis,⁵¹ I. Bestintzanos,⁵¹ I. Evangelou^{ID},⁵¹ C. Foudas,⁵¹ P. Gianneios^{ID},⁵¹ C. Kamtsikis,⁵¹ P. Katsoulis,⁵¹ P. Kokkas^{ID},⁵¹ P. G. Kosmoglou Kioseoglou^{ID},⁵¹ N. Manthos^{ID},⁵¹ I. Papadopoulos^{ID},⁵¹ J. Strologas^{ID},⁵¹ M. Bartók^{ID},^{52,dd} C. Hajdu^{ID},⁵² D. Horvath^{ID},^{52,ee,ff} F. Sikler^{ID},⁵² V. Veszpremi^{ID},⁵² M. Csanád^{ID},⁵³ K. Farkas^{ID},⁵³ M. M. A. Gadallah^{ID},^{53,gg} P. Major^{ID},⁵³ K. Mandal^{ID},⁵³ G. Pásztor^{ID},⁵³ A. J. Rádl^{ID},^{53,hh} O. Surányi^{ID},⁵³ G. I. Veres^{ID},⁵³ G. Bencze,⁵⁴ N. Beni^{ID},⁵⁴ S. Czellar,⁵⁴ J. Karancsi^{ID},^{54,dd} J. Molnar,⁵⁴ Z. Szillasi,⁵⁴ D. Teyssier^{ID},⁵⁴ P. Raics,⁵⁵ B. Ujvari^{ID},^{55,ii} G. Zilizi^{ID},⁵⁵ T. Csorgo^{ID},^{56,hh} F. Nemes^{ID},^{56,hh} T. Novak^{ID},⁵⁶ J. Babbar^{ID},⁵⁷ S. Bansal^{ID},⁵⁷ S. B. Beri,⁵⁷ V. Bhatnagar^{ID},⁵⁷ G. Chaudhary^{ID},⁵⁷ S. Chauhan^{ID},⁵⁷ N. Dhingra^{ID},^{57,jj} R. Gupta,⁵⁷ A. Kaur^{ID},⁵⁷ A. Kaur^{ID},⁵⁷ H. Kaur^{ID},⁵⁷ M. Kaur^{ID},⁵⁷ S. Kumar^{ID},⁵⁷ P. Kumari^{ID},⁵⁷ M. Meena^{ID},⁵⁷ K. Sandeep^{ID},⁵⁷ T. Sheokand,⁵⁷ J. B. Singh^{ID},^{57,kk} A. Singla^{ID},⁵⁷ A. Ahmed^{ID},⁵⁸ A. Bhardwaj^{ID},⁵⁸ A. Chhetri^{ID},⁵⁸ B. C. Choudhary^{ID},⁵⁸ A. Kumar^{ID},⁵⁸ M. Naimuddin^{ID},⁵⁸ K. Ranjan^{ID},⁵⁸ S. Saumya^{ID},⁵⁸ S. Baradia^{ID},⁵⁹ S. Barman^{ID},^{59,ll} S. Bhattacharya^{ID},⁵⁹ D. Bhowmik,⁵⁹ S. Dutta^{ID},⁵⁹ S. Dutta,⁵⁹ B. Gomber^{ID},^{59,mm} M. Maity,^{59,ll} P. Palit^{ID},⁵⁹ G. Saha^{ID},⁵⁹ B. Sahu^{ID},^{59,mm} S. Sarkar,⁵⁹ P. K. Behera^{ID},⁶⁰ S. C. Behera^{ID},⁶⁰ S. Chatterjee^{ID},⁶⁰ P. Kalbhor^{ID},⁶⁰ J. R. Komaragiri^{ID},^{60,nn} D. Kumar^{ID},^{60,nn} A. Muhammad^{ID},⁶⁰ L. Panwar^{ID},^{60,nn} R. Pradhan^{ID},⁶⁰ P. R. Pujahari^{ID},⁶⁰ N. R. Saha^{ID},⁶⁰ A. Sharma^{ID},⁶⁰ A. K. Sikdar^{ID},⁶⁰ S. Verma^{ID},⁶⁰ K. Naskar^{ID},^{61,oo} T. Aziz,⁶² I. Das^{ID},⁶² S. Dugad,⁶² M. Kumar^{ID},⁶² G. B. Mohanty^{ID},⁶² P. Suryadevara,⁶² S. Banerjee^{ID},⁶³ M. Guchait^{ID},⁶³ S. Karmakar^{ID},⁶³ S. Kumar^{ID},⁶³ G. Majumder^{ID},⁶³ K. Mazumdar^{ID},⁶³ S. Mukherjee^{ID},⁶³ A. Thachayath^{ID},⁶³ S. Bahinipati^{ID},^{64,pp} A. K. Das,⁶⁴ C. Kar^{ID},⁶⁴ P. Mal^{ID},⁶⁴ T. Mishra^{ID},⁶⁴ V. K. Muraleedharan Nair Bindhu^{ID},^{64,qq} A. Nayak^{ID},^{64,qq} P. Saha^{ID},⁶⁴ S. K. Swain^{ID},⁶⁴ S. Varghese^{ID},⁶⁴ D. Vats^{ID},^{64,qq} A. Alpana^{ID},⁶⁵ S. Dube^{ID},⁶⁵ B. Kansal^{ID},⁶⁵ A. Laha^{ID},⁶⁵ S. Pandey^{ID},⁶⁵ A. Rastogi^{ID},⁶⁵ S. Sharma^{ID},⁶⁵ H. Bakhshiansohi^{ID},^{66,rr,ss} E. Khazaie^{ID},^{66,ss} M. Zeinali^{ID},^{66,tt} S. Chenarani^{ID},^{67,uu} S. M. Etesami^{ID},⁶⁷ M. Khakzad^{ID},⁶⁷ M. Mohammadi Najafabadi^{ID},⁶⁷ M. Grunewald^{ID},⁶⁸ M. Abbrescia^{ID},^{69a,69b} R. Aly^{ID},^{69a,69b,vv} C. Aruta^{ID},^{69a,69b} A. Colaleo^{ID},^{69a} D. Creanza^{ID},^{69a,69c} L. Cristella^{ID},^{69a,69b} B. D'Anzi^{ID},^{69a,69b} N. De Filippis^{ID},^{69a,69c} M. De Palma^{ID},^{69a,69b} A. Di Florio^{ID},^{69a,69b} W. Elmetenawee^{ID},^{69a,69b} F. Errico^{ID},^{69a,69b} L. Fiore^{ID},^{69a} G. Iaselli^{ID},^{69a,69c} G. Maggi^{ID},^{69a,69c}

- M. Maggi^{69a} I. Margjeka^{69a,69b} V. Mastrapasqua^{69a,69b} S. My^{69a,69b} S. Nuzzo^{69a,69b} A. Pellecchia^{69a,69b}
 A. Pompili^{69a,69b} G. Pugliese^{69a,69c} R. Radogna^{69a} D. Ramos^{69a} A. Ranieri^{69a} G. Selvaggi^{69a,69b}
 L. Silvestris^{69a} F. M. Simone^{69a,69b} Ü. Sözbilir^{69a} A. Stamerra^{69a} R. Venditti^{69a} P. Verwilligen^{69a}
 G. Abbiendi^{70a} C. Battilana^{70a,70b} D. Bonacorsi^{70a,70b} L. Borgonovi^{70a} L. Brigliadori^{70a} R. Campanini^{70a,70b}
 P. Capiluppi^{70a,70b} A. Castro^{70a,70b} F. R. Cavallo^{70a} M. Cuffiani^{70a,70b} G. M. Dallavalle^{70a} T. Diotalevi^{70a,70b}
 F. Fabbri^{70a} A. Fanfani^{70a,70b} D. Fasanella^{70a,70b} P. Giacomelli^{70a} L. Giommi^{70a,70b} C. Grandi^{70a}
 L. Guiducci^{70a,70b} S. Lo Meo^{70a,ww} L. Lunerti^{70a,70b} S. Marcellini^{70a} G. Masetti^{70a} F. L. Navarria^{70a,70b}
 A. Perrotta^{70a} F. Primavera^{70a,70b} A. M. Rossi^{70a,70b} T. Rovelli^{70a,70b} G. P. Siroli^{70a,70b} S. Costa^{71a,71b,xx}
 A. Di Mattia^{71a} R. Potenza^{71a,71b} A. Tricomi^{71a,71b,xx} C. Tuve^{71a,71b} G. Barbagli^{72a} G. Bardelli^{72a,72b}
 B. Camaiani^{72a,72b} A. Cassese^{72a} R. Ceccarelli^{72a,72b} V. Ciulli^{72a,72b} C. Civinini^{72a} R. D'Alessandro^{72a,72b}
 E. Focardi^{72a,72b} G. Latino^{72a,72b} P. Lenzi^{72a,72b} M. Lizzo^{72a,72b} M. Meschini^{72a} S. Paoletti^{72a} G. Sguazzoni^{72a}
 L. Viliani^{72a} L. Benussi⁷³ S. Bianco⁷³ S. Meola^{73,yy} D. Piccolo⁷³ M. Bozzo^{74a,74b} P. Chatagnon^{74a}
 F. Ferro^{74a} E. Robutti^{74a} S. Tosi^{74a,74b} A. Benaglia^{75a} G. Boldrini^{75a} F. Brivio^{75a,75b} F. Cetorelli^{75a,75b}
 F. De Guio^{75a,75b} M. E. Dinardo^{75a,75b} P. Dini^{75a} S. Gennai^{75a} A. Ghezzi^{75a,75b} P. Govoni^{75a,75b} L. Guzzi^{75a,75b}
 M. T. Lucchini^{75a,75b} M. Malberti^{75a} S. Malvezzi^{75a} A. Massironi^{75a} D. Menasce^{75a} L. Moroni^{75a}
 M. Paganoni^{75a,75b} D. Pedrini^{75a} B. S. Pinolini^{75a} S. Ragazzi^{75a,75b} N. Redaelli^{75a} T. Tabarelli de Fatis^{75a,75b}
 D. Zuolo^{75a,75b} S. Buontempo^{76a} A. Cagnotta^{76a,76b} F. Carnevali^{76a,76b} N. Cavalllo^{76a,76c} A. De Iorio^{76a,76b}
 F. Fabozzi^{76a,76c} A. O. M. Iorio^{76a,76b} L. Lista^{76a,76b,zz} P. Paolucci^{76a,cc} B. Rossi^{76a} C. Sciacca^{76a,76b}
 R. Ardino^{77a} P. Azzi^{77a} N. Bacchetta^{77a,aaa} M. Biasotto^{77a,bbb} D. Bisello^{77a,77b} P. Bortignon^{77a}
 A. Bragagnolo^{77a,77b} R. Carlin^{77a,77b} P. Checchia^{77a} T. Dorigo^{77a} F. Gasparini^{77a,77b} G. Grossi^{77a} L. Layer^{77a,ccc}
 E. Lusiani^{77a} M. Margoni^{77a,77b} A. T. Meneguzzo^{77a,77b} J. Pazzini^{77a,77b} P. Ronchese^{77a,77b} R. Rossin^{77a,77b}
 F. Simonetto^{77a,77b} G. Strong^{77a} M. Tosi^{77a,77b} H. Yarar^{77a,77b} M. Zanetti^{77a,77b} P. Zotto^{77a,77b}
 A. Zucchetta^{77a,77b} G. Zumerle^{77a,77b} S. Abu Zeid^{78a,ddd} C. Aimè^{78a,78b} A. Braghieri^{78a} S. Calzaferri^{78a,78b}
 D. Fiorina^{78a,78b} P. Montagna^{78a,78b} V. Re^{78a} C. Riccardi^{78a,78b} P. Salvini^{78a} I. Vai^{78a,78b} P. Vitulo^{78a,78b}
 P. Asenov^{79a,eee} G. M. Bilei^{79a} D. Ciangottini^{79a,79b} L. Fanò^{79a,79b} M. Magherini^{79a,79b} G. Mantovani^{79a,79b}
 V. Mariani^{79a,79b} M. Menichelli^{79a} F. Moscatelli^{79a,eee} A. Piccinelli^{79a,79b} M. Presilla^{79a,79b} A. Rossi^{79a,79b}
 A. Santocchia^{79a,79b} D. Spiga^{79a} T. Tedeschi^{79a,79b} P. Azzurri^{80a} G. Bagliesi^{80a} V. Bertacchi^{80a,80c}
 R. Bhattacharya^{80a} L. Bianchini^{80a,80b} T. Boccali^{80a} E. Bossini^{80a,80b} D. Bruschini^{80a,80c} R. Castaldi^{80a}
 M. A. Ciocci^{80a,80b} V. D'Amante^{80a,80d} R. Dell'Orso^{80a} S. Donato^{80a} A. Giassi^{80a} F. Ligabue^{80a,80c}
 D. Matos Figueiredo^{80a} A. Messineo^{80a,80b} M. Musich^{80a,80b} F. Palla^{80a} S. Parolia^{80a} G. Ramirez-Sanchez^{80a,80c}
 A. Rizzi^{80a,80b} G. Rolandi^{80a,80c} S. Roy Chowdhury^{80a} T. Sarkar^{80a} A. Scribano^{80a} P. Spagnolo^{80a}
 R. Tenchini^{80a} G. Tonelli^{80a,80b} N. Turini^{80a,80d} A. Venturi^{80a} P. G. Verdini^{80a} P. Barria^{81a} M. Campana^{81a,81b}
 F. Cavallari^{81a} D. Del Re^{81a,81b} E. Di Marco^{81a} M. Diemoz^{81a} E. Longo^{81a,81b} P. Meridiani^{81a}
 G. Organini^{81a,81b} F. Pandolfi^{81a} R. Paramatti^{81a,81b} C. Quaranta^{81a,81b} S. Rahatlou^{81a,81b} C. Rovelli^{81a}
 F. Santanastasio^{81a,81b} L. Soffi^{81a} R. Tramontano^{81a,81b} N. Amapane^{82a,82b} R. Arcidiacono^{82a,82c} S. Argiro^{82a,82b}
 M. Arneodo^{82a,82c} N. Bartosik^{82a} R. Bellan^{82a,82b} A. Bellora^{82a,82b} C. Biino^{82a} N. Cartiglia^{82a} M. Costa^{82a,82b}
 R. Covarelli^{82a,82b} N. Demaria^{82a} L. Finco^{82a} M. Grippo^{82a,82b} B. Kiani^{82a,82b} F. Legger^{82a} F. Luongo^{82a,82b}
 C. Mariotti^{82a} S. Maselli^{82a} A. Mecca^{82a,82b} E. Migliore^{82a,82b} M. Monteno^{82a} R. Mulargia^{82a}
 M. M. Obertino^{82a,82b} G. Ortona^{82a} L. Pacher^{82a,82b} N. Pastrone^{82a} M. Pelliccioni^{82a} M. Ruspa^{82a,82c}
 K. Shchelina^{82a} F. Siviero^{82a,82b} V. Sola^{82a,82b} A. Solano^{82a,82b} D. Soldi^{82a,82b} A. Staiano^{82a}
 C. Tarricone^{82a,82b} M. Tornago^{82a,82b} D. Trocino^{82a} G. Umoret^{82a,82b} A. Vagnerini^{82a,82b} E. Vlasov^{82a,82b}
 S. Belforte^{83a} V. Candelise^{83a,83b} M. Casarsa^{83a} F. Cossutti^{83a} G. Della Ricca^{83a,83b} G. Sorrentino^{83a,83b}
 S. Dogra⁸⁴ C. Huh⁸⁴ B. Kim⁸⁴ D. H. Kim⁸⁴ G. N. Kim⁸⁴ J. Kim⁸⁴ J. Lee⁸⁴ S. W. Lee⁸⁴ C. S. Moon⁸⁴
 Y. D. Oh⁸⁴ S. I. Pak⁸⁴ M. S. Ryu⁸⁴ S. Sekmen⁸⁴ Y. C. Yang⁸⁴ H. Kim⁸⁵ D. H. Moon⁸⁵ E. Asilar⁸⁶
 T. J. Kim⁸⁶ J. Park⁸⁶ S. Choi⁸⁷ S. Han⁸⁷ B. Hong⁸⁷ K. Lee⁸⁷ K. S. Lee⁸⁷ J. Lim⁸⁷ J. Park⁸⁷ S. K. Park⁸⁷
 J. Yoo⁸⁷ J. Goh⁸⁸ H. S. Kim⁸⁹ Y. Kim⁸⁹ S. Lee⁸⁹ J. Almond⁹⁰ J. H. Bhyun⁹⁰ J. Choi⁹⁰ S. Jeon⁹⁰ J. Kim⁹⁰
 J. S. Kim⁹⁰ S. Ko⁹⁰ H. Kwon⁹⁰ H. Lee⁹⁰ S. Lee⁹⁰ B. H. Oh⁹⁰ S. B. Oh⁹⁰ H. Seo⁹⁰ U.K. Yang⁹⁰ I. Yoon⁹⁰
 W. Jang⁹¹ D. Y. Kang⁹¹ Y. Kang⁹¹ D. Kim⁹¹ S. Kim⁹¹ B. Ko⁹¹ J. S. H. Lee⁹¹ Y. Lee⁹¹ J. A. Merlin⁹¹
 I. C. Park⁹¹ Y. Roh⁹¹ D. Song⁹¹ I. J. Watson⁹¹ S. Yang⁹¹ S. Ha⁹² H. D. Yoo⁹² M. Choi⁹³ M. R. Kim⁹³

- H. Lee,⁹³ Y. Lee,⁹³ I. Yu,⁹³ T. Beyrouthy,⁹⁴ Y. Maghrbi,⁹⁴ K. Dreimanis,⁹⁵ G. Pikurs,⁹⁵ A. Potrebko,⁹⁵ M. Seidel,⁹⁵ V. Veckalns,^{95,fff} M. Ambrozas,⁹⁶ A. Juodagalvis,⁹⁶ A. Rinkevicius,⁹⁶ G. Tamulaitis,⁹⁶ N. Bin Norjoharuddeen,⁹⁷ S. Y. Hoh,^{97,ggg} I. Yusuff,^{97,ggg} Z. Zolkapli,⁹⁷ J. F. Benitez,⁹⁸ A. Castaneda Hernandez,⁹⁸ H. A. Encinas Acosta,
L. G. Gallegos Maríñez,⁹⁸ M. León Coello,⁹⁸ J. A. Murillo Quijada,⁹⁸ A. Sehrawat,⁹⁸ L. Valencia Palomo,⁹⁸
G. Ayala,⁹⁹ H. Castilla-Valdez,⁹⁹ I. Heredia-De La Cruz,^{99,hhh} R. Lopez-Fernandez,⁹⁹ C. A. Mondragon Herrera,⁹⁹
D. A. Perez Navarro,⁹⁹ A. Sánchez Hernández,⁹⁹ C. Oropeza Barrera,¹⁰⁰ F. Vazquez Valencia,¹⁰⁰ I. Pedraza,¹⁰¹
H. A. Salazar Ibarguen,¹⁰¹ C. Uribe Estrada,¹⁰¹ I. Bubanja,¹⁰² J. Mijuskovic,^{102,iii} N. Raicevic,¹⁰² A. Ahmad,¹⁰³
M. I. Asghar,¹⁰³ A. Awais,¹⁰³ M. I. M. Awan,¹⁰³ M. Gul,¹⁰³ H. R. Hoorani,¹⁰³ W. A. Khan,¹⁰³ V. Avati,¹⁰⁴
L. Grzanka,¹⁰⁴ M. Malawski,¹⁰⁴ H. Bialkowska,¹⁰⁵ M. Bluj,¹⁰⁵ B. Boimska,¹⁰⁵ M. Górski,¹⁰⁵ M. Kazana,¹⁰⁵
M. Szleper,¹⁰⁵ P. Zalewski,¹⁰⁵ K. Bunkowski,¹⁰⁶ K. Doroba,¹⁰⁶ A. Kalinowski,¹⁰⁶ M. Konecki,¹⁰⁶
J. Krolikowski,¹⁰⁶ M. Araujo,¹⁰⁷ D. Bastos,¹⁰⁷ A. Boletti,¹⁰⁷ P. Faccioli,¹⁰⁷ M. Gallinaro,¹⁰⁷ J. Hollar,¹⁰⁷
N. Leonardo,¹⁰⁷ T. Niknejad,¹⁰⁷ M. Pisano,¹⁰⁷ J. Seixas,¹⁰⁷ J. Varela,¹⁰⁷ P. Adzic,^{108,iii} P. Milenovic,¹⁰⁸
M. Dordevic,¹⁰⁹ J. Milosevic,¹⁰⁹ M. Aguilar-Benitez,¹¹⁰ J. Alcaraz Maestre,¹¹⁰ M. Barrio Luna,¹¹⁰
Cristina F. Bedoya,¹¹⁰ M. Cepeda,¹¹⁰ M. Cerrada,¹¹⁰ N. Colino,¹¹⁰ B. De La Cruz,¹¹⁰ A. Delgado Peris,¹¹⁰
D. Fernández Del Val,¹¹⁰ J. P. Fernández Ramos,¹¹⁰ J. Flix,¹¹⁰ M. C. Fouz,¹¹⁰ O. Gonzalez Lopez,¹¹⁰
S. Goy Lopez,¹¹⁰ J. M. Hernandez,¹¹⁰ M. I. Josa,¹¹⁰ J. León Holgado,¹¹⁰ D. Moran,¹¹⁰ C. Perez Dengra,¹¹⁰
A. Pérez-Calero Yzquierdo,¹¹⁰ J. Puerta Pelayo,¹¹⁰ I. Redondo,¹¹⁰ D. D. Redondo Ferrero,¹¹⁰ L. Romero,¹¹⁰
S. Sánchez Navas,¹¹⁰ J. Sastre,¹¹⁰ L. Urda Gómez,¹¹⁰ J. Vazquez Escobar,¹¹⁰ C. Willmott,¹¹⁰ J. F. de Trocóniz,¹¹¹
B. Alvarez Gonzalez,¹¹² J. Cuevas,¹¹² J. Fernandez Menendez,¹¹² S. Folgueras,¹¹² I. Gonzalez Caballero,¹¹²
J. R. González Fernández,¹¹² E. Palencia Cortezon,¹¹² C. Ramón Alvarez,¹¹² V. Rodríguez Bouza,¹¹²
A. Soto Rodríguez,¹¹² A. Trapote,¹¹² C. Vico Villalba,¹¹² J. A. Brochero Cifuentes,¹¹³ I. J. Cabrillo,¹¹³
A. Calderon,¹¹³ J. Duarte Campderros,¹¹³ M. Fernandez,¹¹³ C. Fernandez Madrazo,¹¹³ G. Gomez,¹¹³
C. Lasaosa García,¹¹³ C. Martinez Rivero,¹¹³ P. Martinez Ruiz del Arbol,¹¹³ F. Matorras,¹¹³ P. Matorras Cuevas,¹¹³
J. Piedra Gomez,¹¹³ C. Prieels,¹¹³ L. Scodellaro,¹¹³ I. Vila,¹¹³ J. M. Vizan Garcia,¹¹³ M. K. Jayananda,¹¹⁴
B. Kailasapathy,^{114,kkk} D. U. J. Sonnadara,¹¹⁴ D. D. C. Wickramarathna,¹¹⁴ W. G. D. Dharmaratna,^{115,III}
K. Liyanage,¹¹⁵ N. Perera,¹¹⁵ N. Wickramage,¹¹⁵ D. Abbaneo,¹¹⁶ E. Auffray,¹¹⁶ G. Auzinger,¹¹⁶ J. Baechler,¹¹⁶
D. Barney,¹¹⁶ A. Bermúdez Martínez,¹¹⁶ M. Bianco,¹¹⁶ B. Bilin,¹¹⁶ A. A. Bin Anuar,¹¹⁶ A. Bocci,¹¹⁶
E. Brondolin,¹¹⁶ C. Caillol,¹¹⁶ T. Camporesi,¹¹⁶ G. Cerminara,¹¹⁶ N. Chernyavskaya,¹¹⁶ S. S. Chhibra,¹¹⁶
S. Choudhury,¹¹⁶ M. Cipriani,¹¹⁶ D. d'Enterria,¹¹⁶ A. Dabrowski,¹¹⁶ A. David,¹¹⁶ A. De Roeck,¹¹⁶
M. M. Defranchis,¹¹⁶ M. Deile,¹¹⁶ M. Dobson,¹¹⁶ M. Dünser,¹¹⁶ N. Dupont,¹¹⁶ F. Fallavollita,^{116,mmm} A. Florent,¹¹⁶
L. Forthomme,¹¹⁶ G. Franzoni,¹¹⁶ W. Funk,¹¹⁶ S. Ghosh,^{116,nnn} S. Giani,¹¹⁶ D. Gigi,¹¹⁶ K. Gill,¹¹⁶ F. Glege,¹¹⁶
L. Gouskos,¹¹⁶ E. Govorkova,¹¹⁶ M. Haranko,¹¹⁶ J. Hegeman,¹¹⁶ V. Innocente,¹¹⁶ T. James,¹¹⁶ P. Janot,¹¹⁶
J. Kaspar,¹¹⁶ J. Kieseler,¹¹⁶ N. Kratochwil,¹¹⁶ S. Laurila,¹¹⁶ P. Lecoq,¹¹⁶ E. Leutgeb,¹¹⁶ C. Lourenço,¹¹⁶
B. Maier,¹¹⁶ L. Malgeri,¹¹⁶ M. Mannelli,¹¹⁶ A. C. Marini,¹¹⁶ F. Meijers,¹¹⁶ S. Mersi,¹¹⁶ E. Meschi,¹¹⁶
F. Moortgat,¹¹⁶ M. Mulders,¹¹⁶ S. Orfanelli,¹¹⁶ L. Orsini,¹¹⁶ F. Pantaleo,¹¹⁶ E. Perez,¹¹⁶ M. Peruzzi,¹¹⁶ A. Petrilli,¹¹⁶
G. Petrucciani,¹¹⁶ A. Pfeiffer,¹¹⁶ M. Pierini,¹¹⁶ D. Piparo,¹¹⁶ M. Pitt,¹¹⁶ H. Qu,¹¹⁶ T. Quast,¹¹⁶ D. Rabady,¹¹⁶
A. Racz,¹¹⁶ G. Reales Gutierrez,¹¹⁶ M. Rovere,¹¹⁶ H. Sakulin,¹¹⁶ J. Salfeld-Nebgen,¹¹⁶ S. Scarfi,¹¹⁶ M. Selvaggi,¹¹⁶
A. Sharma,¹¹⁶ P. Silva,¹¹⁶ P. Sphicas,^{116,ooo} A. G. Stahl Leiton,¹¹⁶ S. Summers,¹¹⁶ K. Tatar,¹¹⁶ D. Treille,¹¹⁶
P. Tropea,¹¹⁶ A. Tsirou,¹¹⁶ D. Walter,¹¹⁶ J. Wanczyk,^{116,ppp} K. A. Wozniak,¹¹⁶ W. D. Zeuner,¹¹⁶ T. Bevilacqua,^{117,qqq}
L. Caminada,^{117,qqq} A. Ebrahimi,¹¹⁷ W. Erdmann,¹¹⁷ R. Horisberger,¹¹⁷ Q. Ingram,¹¹⁷ H. C. Kaestli,¹¹⁷
D. Kotlinski,¹¹⁷ C. Lange,¹¹⁷ M. Missiroli,^{117,qqq} L. Noehte,^{117,qqq} T. Rohe,¹¹⁷ T. K. Arrestad,¹¹⁸
K. Androsov,^{118,ppp} M. Backhaus,¹¹⁸ A. Calandri,¹¹⁸ K. Datta,¹¹⁸ A. De Cosa,¹¹⁸ G. Dissertori,¹¹⁸ M. Dittmar,¹¹⁸
M. Donegà,¹¹⁸ F. Eble,¹¹⁸ M. Galli,¹¹⁸ K. Gedia,¹¹⁸ F. Glessgen,¹¹⁸ T. A. Gómez Espinosa,¹¹⁸ C. Grab,¹¹⁸
D. Hits,¹¹⁸ W. Lustermann,¹¹⁸ A.-M. Lyon,¹¹⁸ R. A. Manzoni,¹¹⁸ L. Marchese,¹¹⁸ C. Martin Perez,¹¹⁸
A. Mascellani,^{118,ppp} F. Nesi-Tedaldi,¹¹⁸ J. Niedziela,¹¹⁸ F. Pauss,¹¹⁸ V. Perovic,¹¹⁸ S. Pigazzini,¹¹⁸
M. G. Ratti,¹¹⁸ M. Reichmann,¹¹⁸ C. Reissel,¹¹⁸ T. Reitenspiess,¹¹⁸ B. Ristic,¹¹⁸ F. Riti,¹¹⁸ D. Ruini,¹¹⁸
D. A. Sanz Becerra,¹¹⁸ R. Seidita,¹¹⁸ J. Steggemann,^{118,ppp} D. Valsecchi,¹¹⁸ R. Wallny,¹¹⁸ C. Amsler,^{119,rrr}
P. Bärtschi,¹¹⁹ C. Botta,¹¹⁹ D. Brzhechko,¹¹⁹ M. F. Canelli,¹¹⁹ K. Cormier,¹¹⁹ A. De Wit,¹¹⁹ R. Del Burgo,¹¹⁹
J. K. Heikkilä,¹¹⁹ M. Huwiler,¹¹⁹ W. Jin,¹¹⁹ A. Jofrehei,¹¹⁹ B. Kilminster,¹¹⁹ S. Leontsinis,¹¹⁹ S. P. Liechti,¹¹⁹

- A. Macchiolo¹¹⁹, P. Meiring¹¹⁹, V. M. Mikuni¹¹⁹, U. Molinatti¹¹⁹, I. Neutelings¹¹⁹, A. Reimers¹¹⁹, P. Robmann¹¹⁹, S. Sanchez Cruz¹¹⁹, K. Schweiger¹¹⁹, M. Senger¹¹⁹, Y. Takahashi¹¹⁹, C. Adloff^{120,sss}, C. M. Kuo¹²⁰, W. Lin¹²⁰, P. K. Rout¹²⁰, P. C. Tiwari^{120,nn}, S. S. Yu¹²⁰, L. Ceard¹²¹, Y. Chao¹²¹, K. F. Chen¹²¹, P. s. Chen¹²¹, H. Cheng¹²¹, W.-S. Hou¹²¹, R. Khurana¹²¹, G. Kole¹²¹, Y. y. Li¹²¹, R.-S. Lu¹²¹, E. Paganis¹²¹, A. Psallidas¹²¹, A. Steen¹²¹, H. y. Wu¹²¹, E. Yazgan¹²¹, C. Asawatangtrakuldee¹²², N. Srikanthas¹²², V. Wachirapusanand¹²², D. Agyel¹²³, F. Boran¹²³, Z. S. Demiroglu¹²³, F. Dolek¹²³, I. Dumanoglu^{123,ttt}, E. Eskut¹²³, Y. Guler^{123,uuu}, E. Gurpinar Guler^{123,uuu}, C. Isik¹²³, O. Kara¹²³, A. Kayis Topaksu¹²³, U. Kiminsu¹²³, G. Onengut¹²³, K. Ozdemir^{123,vvv}, A. Polatoz¹²³, B. Tali^{123,www}, U. G. Tok¹²³, S. Turkcapar¹²³, E. Uslan¹²³, I. S. Zorbakir¹²³, G. Karapinar^{124,xxx}, K. Ocalan^{124,yyy}, M. Yalvac^{124,zzz}, B. Akgun¹²⁵, I. O. Atakisi¹²⁵, E. Gürmez¹²⁵, M. Kaya^{125,aaaa}, O. Kaya^{125,bbbb}, S. Tekten^{125,cccc}, A. Cakir¹²⁶, K. Cankocak^{126,ttt}, Y. Komurcu¹²⁶, S. Sen^{126,dddd}, O. Aydilek¹²⁷, S. Cerci^{127,www}, V. Epshteyn¹²⁷, B. Hacisahinoglu¹²⁷, I. Hos^{127,eeee}, B. Isildak^{127,ffff}, B. Kaynak¹²⁷, S. Ozkorucuklu¹²⁷, C. Simsek¹²⁷, D. Sunar Cerci^{127,www}, B. Grynyov¹²⁸, L. Levchuk¹²⁹, D. Anthony¹³⁰, J. J. Brooke¹³⁰, A. Bundock¹³⁰, E. Clement¹³⁰, D. Cussans¹³⁰, H. Flacher¹³⁰, M. Glowacki¹³⁰, J. Goldstein¹³⁰, H. F. Heath¹³⁰, L. Kreczko¹³⁰, B. Krikler¹³⁰, S. Paramesvaran¹³⁰, S. Seif El Nasr-Storey¹³⁰, V. J. Smith¹³⁰, N. Stylianou^{130,gggg}, K. Walkingshaw Pass¹³⁰, R. White¹³⁰, A. H. Ball¹³¹, K. W. Bell¹³¹, A. Belyaev^{131,hhhh}, C. Brew¹³¹, R. M. Brown¹³¹, D. J. A. Cockerill¹³¹, C. Cooke¹³¹, K. V. Ellis¹³¹, K. Harder¹³¹, S. Harper¹³¹, M.-L. Holmberg^{131,iiii}, Sh. Jain¹³¹, J. Linacre¹³¹, K. Manolopoulos¹³¹, D. M. Newbold¹³¹, E. Olaiya¹³¹, D. Petyt¹³¹, T. Reis¹³¹, G. Salvi¹³¹, T. Schuh¹³¹, C. H. Shepherd-Themistocleous¹³¹, I. R. Tomalin¹³¹, T. Williams¹³¹, R. Bainbridge¹³², P. Bloch¹³², S. Bonomally¹³², J. Borg¹³², C. E. Brown¹³², O. Buchmuller¹³², V. Cacchio¹³², C. A. Carrillo Montoya¹³², V. Cepaitis¹³², G. S. Chahal^{132,iiii}, D. Colling¹³², J. S. Danca¹³², P. Dauncey¹³², G. Davies¹³², J. Davies¹³², M. Della Negra¹³², S. Fayer¹³², G. Fedi¹³², G. Hall¹³², M. H. Hassanshahi¹³², A. Howard¹³², G. Iles¹³², J. Langford¹³², L. Lyons¹³², A.-M. Magnan¹³², S. Malik¹³², A. Martelli¹³², M. Mieskolainen¹³², D. G. Monk¹³², J. Nash^{132,kkkk}, M. Pesaresi¹³², B. C. Radburn-Smith¹³², A. Richards¹³², A. Rose¹³², E. Scott¹³², C. Seez¹³², R. Shukla¹³², A. Tapper¹³², K. Uchida¹³², G. P. Uttley¹³², L. H. Vage¹³², T. Virdee^{132,cc}, M. Vojinovic¹³², N. Wardle¹³², S. N. Webb¹³², D. Winterbottom¹³², K. Coldham¹³³, J. E. Cole¹³³, A. Khan¹³³, P. Kyberd¹³³, I. D. Reid¹³³, S. Abdullin¹³⁴, A. Brinkerhoff¹³⁴, B. Caraway¹³⁴, J. Dittmann¹³⁴, K. Hatakeyama¹³⁴, J. Hiltbrand¹³⁴, A. R. Kanuganti¹³⁴, B. McMaster¹³⁴, M. Saunders¹³⁴, S. Sawant¹³⁴, C. Sutantawibul¹³⁴, M. Toms¹³⁴, J. Wilson¹³⁴, R. Bartek¹³⁵, A. Dominguez¹³⁵, C. Huerta Escamilla¹³⁵, A. E. Simsek¹³⁵, R. Uniyal¹³⁵, A. M. Vargas Hernandez¹³⁵, R. Chudasama¹³⁶, S. I. Cooper¹³⁶, D. Di Croce¹³⁶, S. V. Gleyzer¹³⁶, C. U. Perez¹³⁶, P. Rumerio^{136,III}, E. Usai¹³⁶, C. West¹³⁶, A. Akpinar¹³⁷, A. Albert¹³⁷, D. Arcaro¹³⁷, C. Cosby¹³⁷, Z. Demiragli¹³⁷, C. Erice¹³⁷, E. Fontanesi¹³⁷, D. Gastler¹³⁷, S. May¹³⁷, J. Rohlf¹³⁷, K. Salyer¹³⁷, D. Sperka¹³⁷, D. Spitzbart¹³⁷, I. Suarez¹³⁷, A. Tsatsos¹³⁷, S. Yuan¹³⁷, G. Benelli¹³⁸, X. Coubez^{138,x}, D. Cutts¹³⁸, M. Hadley¹³⁸, U. Heintz¹³⁸, J. M. Hogan^{138,mmmm}, T. Kwon¹³⁸, G. Landsberg¹³⁸, K. T. Lau¹³⁸, D. Li¹³⁸, J. Luo¹³⁸, M. Narain¹³⁸, N. Pervan¹³⁸, S. Sagir^{138,nnnn}, F. Simpson¹³⁸, W. Y. Wong¹³⁸, X. Yan¹³⁸, D. Yu¹³⁸, W. Zhang¹³⁸, S. Abbott¹³⁹, J. Bonilla¹³⁹, C. Brainerd¹³⁹, R. Breedon¹³⁹, M. Calderon De La Barca Sanchez¹³⁹, M. Chertok¹³⁹, J. Conway¹³⁹, P. T. Cox¹³⁹, R. Erbacher¹³⁹, G. Haza¹³⁹, F. Jensen¹³⁹, O. Kukral¹³⁹, G. Mocellin¹³⁹, M. Mulhearn¹³⁹, D. Pellett¹³⁹, B. Regnery¹³⁹, W. Wei¹³⁹, Y. Yao¹³⁹, F. Zhang¹³⁹, M. Bachtis¹⁴⁰, R. Cousins¹⁴⁰, A. Datta¹⁴⁰, J. Hauser¹⁴⁰, M. Ignatenko¹⁴⁰, M. A. Iqbal¹⁴⁰, T. Lam¹⁴⁰, E. Manca¹⁴⁰, W. A. Nash¹⁴⁰, D. Saltzberg¹⁴⁰, B. Stone¹⁴⁰, V. Valuev¹⁴⁰, R. Clare¹⁴¹, J. W. Gary¹⁴¹, M. Gordon¹⁴¹, G. Hanson¹⁴¹, O. R. Long¹⁴¹, N. Manganelli¹⁴¹, W. Si¹⁴¹, S. Wimpenny¹⁴¹, J. G. Branson¹⁴², S. Cittolin¹⁴², S. Cooperstein¹⁴², D. Diaz¹⁴², J. Duarte¹⁴², R. Gerosa¹⁴², L. Giannini¹⁴², J. Guiang¹⁴², R. Kansal¹⁴², V. Krutelyov¹⁴², R. Lee¹⁴², J. Letts¹⁴², M. Masciovecchio¹⁴², F. Mokhtar¹⁴², M. Pieri¹⁴², M. Quinnan¹⁴², B. V. Sathia Narayanan¹⁴², V. Sharma¹⁴², M. Tadel¹⁴², E. Vourliotis¹⁴², F. Würthwein¹⁴², Y. Xiang¹⁴², A. Yagil¹⁴², L. Brennan¹⁴³, C. Campagnari¹⁴³, M. Citron¹⁴³, G. Collura¹⁴³, A. Dorsett¹⁴³, J. Incandela¹⁴³, M. Kilpatrick¹⁴³, J. Kim¹⁴³, A. J. Li¹⁴³, P. Masterson¹⁴³, H. Mei¹⁴³, M. Oshiro¹⁴³, J. Richman¹⁴³, U. Sarica¹⁴³, R. Schmitz¹⁴³, F. Setti¹⁴³, J. Sheplock¹⁴³, P. Siddireddy¹⁴³, D. Stuart¹⁴³, S. Wang¹⁴³, A. Bornheim¹⁴⁴, O. Cerri¹⁴⁴, A. Latorre¹⁴⁴, J. M. Lawhorn¹⁴⁴, J. Mao¹⁴⁴, H. B. Newman¹⁴⁴, T. Q. Nguyen¹⁴⁴, M. Spiropulu¹⁴⁴, J. R. Vlimant¹⁴⁴, C. Wang¹⁴⁴, S. Xie¹⁴⁴, R. Y. Zhu¹⁴⁴, J. Alison¹⁴⁵, S. An¹⁴⁵, M. B. Andrews¹⁴⁵, P. Bryant¹⁴⁵, V. Dutta¹⁴⁵, T. Ferguson¹⁴⁵, A. Harilal¹⁴⁵, C. Liu¹⁴⁵

- T. Mudholkar¹⁴⁵ S. Murthy¹⁴⁵ M. Paulini¹⁴⁵ A. Roberts¹⁴⁵ A. Sanchez¹⁴⁵ W. Terrill¹⁴⁵ J. P. Cumalat¹⁴⁶
 W. T. Ford¹⁴⁶ A. Hassani¹⁴⁶ G. Karathanasis¹⁴⁶ E. MacDonald¹⁴⁶ F. Marini¹⁴⁶ A. Perloff¹⁴⁶ C. Savard¹⁴⁶
 N. Schonbeck¹⁴⁶ K. Stenson¹⁴⁶ K. A. Ulmer¹⁴⁶ S. R. Wagner¹⁴⁶ N. Zipper¹⁴⁶ J. Alexander¹⁴⁷
 S. Bright-Thonney¹⁴⁷ X. Chen¹⁴⁷ D. J. Cranshaw¹⁴⁷ J. Fan¹⁴⁷ X. Fan¹⁴⁷ D. Gadkari¹⁴⁷ S. Hogan¹⁴⁷
 J. Monroy¹⁴⁷ J. R. Patterson¹⁴⁷ J. Reichert¹⁴⁷ M. Reid¹⁴⁷ A. Ryd¹⁴⁷ J. Thom¹⁴⁷ P. Wittich¹⁴⁷ R. Zou¹⁴⁷
 M. Albrow¹⁴⁸ M. Alyari¹⁴⁸ O. Amram¹⁴⁸ G. Apollinari¹⁴⁸ A. Apresyan¹⁴⁸ L. A. T. Bauerdick¹⁴⁸ D. Berry¹⁴⁸
 J. Berryhill¹⁴⁸ P. C. Bhat¹⁴⁸ K. Burkett¹⁴⁸ J. N. Butler¹⁴⁸ A. Canepa¹⁴⁸ G. B. Cerati¹⁴⁸ H. W. K. Cheung¹⁴⁸
 F. Chlebana¹⁴⁸ K. F. Di Petrillo¹⁴⁸ J. Dickinson¹⁴⁸ I. Dutta¹⁴⁸ V. D. Elvira¹⁴⁸ Y. Feng¹⁴⁸ J. Freeman¹⁴⁸
 A. Gandrakota¹⁴⁸ Z. Gecse¹⁴⁸ L. Gray¹⁴⁸ D. Green¹⁴⁸ S. Grünendahl¹⁴⁸ D. Guerrero¹⁴⁸ O. Gutsche¹⁴⁸
 R. M. Harris¹⁴⁸ R. Heller¹⁴⁸ T. C. Herwig¹⁴⁸ J. Hirschauer¹⁴⁸ L. Horyn¹⁴⁸ B. Jayatilaka¹⁴⁸ S. Jindariani¹⁴⁸
 M. Johnson¹⁴⁸ U. Joshi¹⁴⁸ T. Klijnsma¹⁴⁸ B. Klima¹⁴⁸ K. H. M. Kwok¹⁴⁸ S. Lammel¹⁴⁸ D. Lincoln¹⁴⁸
 R. Lipton¹⁴⁸ T. Liu¹⁴⁸ C. Madrid¹⁴⁸ K. Maeshima¹⁴⁸ C. Mantilla¹⁴⁸ D. Mason¹⁴⁸ P. McBride¹⁴⁸
 P. Merkel¹⁴⁸ S. Mrenna¹⁴⁸ S. Nahm¹⁴⁸ J. Ngadiuba¹⁴⁸ D. Noonan¹⁴⁸ S. Norberg¹⁴⁸ V. Papadimitriou¹⁴⁸
 N. Pastika¹⁴⁸ K. Pedro¹⁴⁸ C. Pena^{148,0000} F. Ravera¹⁴⁸ A. Reinsvold Hall^{148,pppp} L. Ristori¹⁴⁸
 E. Sexton-Kennedy¹⁴⁸ N. Smith¹⁴⁸ A. Soha¹⁴⁸ L. Spiegel¹⁴⁸ S. Stoynev¹⁴⁸ J. Strait¹⁴⁸ L. Taylor¹⁴⁸
 S. Tkaczyk¹⁴⁸ N. V. Tran¹⁴⁸ L. Uplegger¹⁴⁸ E. W. Vaandering¹⁴⁸ I. Zoi¹⁴⁸ P. Avery¹⁴⁹ D. Bourilkov¹⁴⁹
 L. Cadamuro¹⁴⁹ P. Chang¹⁴⁹ V. Cherepanov¹⁴⁹ R. D. Field¹⁴⁹ E. Koenig¹⁴⁹ M. Kolosova¹⁴⁹ J. Konigsberg¹⁴⁹
 A. Korytov¹⁴⁹ E. Kuznetsova^{149,qqqq} K. H. Lo¹⁴⁹ K. Matchev¹⁴⁹ N. Menendez¹⁴⁹ G. Mitselmakher¹⁴⁹
 A. Muthirakalayil Madhu¹⁴⁹ N. Rawal¹⁴⁹ D. Rosenzweig¹⁴⁹ S. Rosenzweig¹⁴⁹ K. Shi¹⁴⁹ J. Wang¹⁴⁹
 Z. Wu¹⁴⁹ T. Adams¹⁵⁰ A. Askew¹⁵⁰ N. Bower¹⁵⁰ R. Habibullah¹⁵⁰ V. Hagopian¹⁵⁰ T. Kolberg¹⁵⁰
 G. Martinez¹⁵⁰ H. Prosper¹⁵⁰ O. Viazlo¹⁵⁰ M. Wulansatiti¹⁵⁰ R. Yohay¹⁵⁰ J. Zhang¹⁵⁰ M. M. Baarmand¹⁵¹
 S. Butalla¹⁵¹ T. Elkafrawy^{151,ddd} M. Hohlmann¹⁵¹ R. Kumar Verma¹⁵¹ M. Rahmani¹⁵¹ F. Yumiceva¹⁵¹
 M. R. Adams¹⁵² R. Cavanaugh¹⁵² S. Dittmer¹⁵² O. Evdokimov¹⁵² C. E. Gerber¹⁵² D. J. Hofman¹⁵²
 D. S. Lemos¹⁵² A. H. Merrit¹⁵² C. Mills¹⁵² G. Oh¹⁵² T. Roy¹⁵² S. Rudrabhatla¹⁵² M. B. Tonjes¹⁵²
 N. Varelas¹⁵² X. Wang¹⁵² Z. Ye¹⁵² J. Yoo¹⁵² M. Alhusseini¹⁵³ K. Dilsiz^{153,mrr} L. Emediato¹⁵³
 G. Karaman¹⁵³ O. K. Köseyan¹⁵³ J.-P. Merlo¹⁵³ A. Mestvirishvili^{153,ssss} J. Nachtman¹⁵³ O. Neogi¹⁵³
 H. Ogul^{153,ttt} Y. Onel¹⁵³ A. Penzo¹⁵³ C. Snyder¹⁵³ E. Tiras^{153,uuu} B. Blumenfeld¹⁵⁴ L. Corcodilos¹⁵⁴
 J. Davis¹⁵⁴ A. V. Gritsan¹⁵⁴ S. Kyriacou¹⁵⁴ P. Maksimovic¹⁵⁴ J. Roskes¹⁵⁴ S. Sekhar¹⁵⁴ M. Swartz¹⁵⁴
 T. Á. Vámi¹⁵⁴ A. Abreu¹⁵⁵ L. F. Alcerro Alcerro¹⁵⁵ J. Anguiano¹⁵⁵ P. Baringer¹⁵⁵ A. Bean¹⁵⁵ Z. Flowers¹⁵⁵
 J. King¹⁵⁵ G. Krintiras¹⁵⁵ M. Lazarovits¹⁵⁵ C. Le Mahieu¹⁵⁵ C. Lindsey¹⁵⁵ J. Marquez¹⁵⁵ N. Minafra¹⁵⁵
 M. Murray¹⁵⁵ M. Nickel¹⁵⁵ C. Rogan¹⁵⁵ C. Royon¹⁵⁵ R. Salvatico¹⁵⁵ S. Sanders¹⁵⁵ C. Smith¹⁵⁵
 Q. Wang¹⁵⁵ G. Wilson¹⁵⁵ B. Allmond¹⁵⁶ S. Duric¹⁵⁶ A. Ivanov¹⁵⁶ K. Kaadze¹⁵⁶ A. Kalogeropoulos¹⁵⁶
 D. Kim¹⁵⁶ Y. Maravin¹⁵⁶ T. Mitchell¹⁵⁶ A. Modak¹⁵⁶ K. Nam¹⁵⁶ D. Roy¹⁵⁶ F. Rebassoo¹⁵⁷ D. Wright¹⁵⁷
 E. Adams¹⁵⁸ A. Baden¹⁵⁸ O. Baron¹⁵⁸ A. Belloni¹⁵⁸ A. Bethani¹⁵⁸ Y. m. Chen¹⁵⁸ S. C. Eno¹⁵⁸
 N. J. Hadley¹⁵⁸ S. Jabeen¹⁵⁸ R. G. Kellogg¹⁵⁸ T. Koeth¹⁵⁸ Y. Lai¹⁵⁸ S. Lascio¹⁵⁸ A. C. Mignerey¹⁵⁸
 S. Nabili¹⁵⁸ C. Palmer¹⁵⁸ C. Papageorgakis¹⁵⁸ L. Wang¹⁵⁸ K. Wong¹⁵⁸ J. Bendavid¹⁵⁹ W. Busza¹⁵⁹
 I. A. Cali¹⁵⁹ Y. Chen¹⁵⁹ M. D'Alfonso¹⁵⁹ J. Eysermans¹⁵⁹ C. Freer¹⁵⁹ G. Gomez-Ceballos¹⁵⁹
 M. Goncharov¹⁵⁹ P. Harris¹⁵⁹ D. Kovalskyi¹⁵⁹ J. Krupa¹⁵⁹ Y.-J. Lee¹⁵⁹ K. Long¹⁵⁹ C. Mironov¹⁵⁹ C. Paus¹⁵⁹
 D. Rankin¹⁵⁹ C. Roland¹⁵⁹ G. Roland¹⁵⁹ Z. Shi¹⁵⁹ G. S. F. Stephans¹⁵⁹ J. Wang¹⁵⁹ Z. Wang¹⁵⁹
 B. Wyslouch¹⁵⁹ T. J. Yang¹⁵⁹ R. M. Chatterjee¹⁶⁰ B. Crossman¹⁶⁰ B. M. Joshi¹⁶⁰ C. Kapsiak¹⁶⁰ M. Krohn¹⁶⁰
 Y. Kubota¹⁶⁰ D. Mahon¹⁶⁰ J. Mans¹⁶⁰ M. Revering¹⁶⁰ R. Rusack¹⁶⁰ R. Saradhy¹⁶⁰ N. Schroeder¹⁶⁰
 N. Strobbe¹⁶⁰ M. A. Wadud¹⁶⁰ L. M. Cremaldi¹⁶¹ K. Bloom¹⁶² M. Bryson¹⁶² D. R. Claes¹⁶² C. Fangmeier¹⁶²
 F. Golf¹⁶² C. Joo¹⁶² I. Kravchenko¹⁶² I. Reed¹⁶² J. E. Siado¹⁶² G. R. Snow^{162,a} W. Tabb¹⁶² A. Wightman¹⁶²
 F. Yan¹⁶² A. G. Zecchinelli¹⁶² G. Agarwal¹⁶³ H. Bandyopadhyay¹⁶³ L. Hay¹⁶³ I. Iashvili¹⁶³
 A. Kharchilava¹⁶³ C. McLean¹⁶³ M. Morris¹⁶³ D. Nguyen¹⁶³ J. Pekkanen¹⁶³ S. Rappoccio¹⁶³ H. Rejeb Sfar¹⁶³
 A. Williams¹⁶³ G. Alverson¹⁶⁴ E. Barberis¹⁶⁴ Y. Haddad¹⁶⁴ Y. Han¹⁶⁴ A. Krishna¹⁶⁴ J. Li¹⁶⁴ J. Lidrych¹⁶⁴
 G. Madigan¹⁶⁴ B. Marzocchi¹⁶⁴ D. M. Morse¹⁶⁴ V. Nguyen¹⁶⁴ T. Oriimoto¹⁶⁴ A. Parker¹⁶⁴ L. Skinnari¹⁶⁴
 A. Tishelman-Charny¹⁶⁴ T. Wamorkar¹⁶⁴ B. Wang¹⁶⁴ A. Wisecarver¹⁶⁴ D. Wood¹⁶⁴ S. Bhattacharya¹⁶⁵
 J. Bueghly¹⁶⁵ Z. Chen¹⁶⁵ A. Gilbert¹⁶⁵ K. A. Hahn¹⁶⁵ Y. Liu¹⁶⁵ N. Odell¹⁶⁵ M. H. Schmitt¹⁶⁵ M. Velasco¹⁶⁵

- R. Band¹⁶⁶ R. Bucci,¹⁶⁶ M. Cremonesi,¹⁶⁶ A. Das¹⁶⁶ R. Goldouzian¹⁶⁶ M. Hildreth¹⁶⁶ K. Hurtado Anampa¹⁶⁶ C. Jessop¹⁶⁶ K. Lannon¹⁶⁶ J. Lawrence¹⁶⁶ N. Loukas¹⁶⁶ L. Lutton¹⁶⁶ J. Mariano,¹⁶⁶ N. Marinelli,¹⁶⁶ I. Mcalister,¹⁶⁶ T. McCauley¹⁶⁶ C. McGrady¹⁶⁶ K. Mohrman¹⁶⁶ C. Moore¹⁶⁶ Y. Musienko^{166,m} R. Ruchti¹⁶⁶ A. Townsend¹⁶⁶ M. Wayne¹⁶⁶ H. Yockey,¹⁶⁶ M. Zarucki¹⁶⁶ L. Zygalas¹⁶⁶ B. Bylsma,¹⁶⁷ M. Carrigan¹⁶⁷ L. S. Durkin¹⁶⁷ C. Hill¹⁶⁷ M. Joyce¹⁶⁷ A. Lesauvage¹⁶⁷ M. Nunez Ornelas¹⁶⁷ K. Wei,¹⁶⁷ B. L. Winer¹⁶⁷ B. R. Yates¹⁶⁷ F. M. Addesa¹⁶⁸ H. Bouchamaoui¹⁶⁸ P. Das¹⁶⁸ G. Dezoort¹⁶⁸ P. Elmer¹⁶⁸ A. Frankenthal¹⁶⁸ B. Greenberg¹⁶⁸ N. Haubrich¹⁶⁸ S. Higginbotham¹⁶⁸ G. Kopp¹⁶⁸ S. Kwan¹⁶⁸ D. Lange¹⁶⁸ A. Loeliger¹⁶⁸ D. Marlow¹⁶⁸ I. Ojalvo¹⁶⁸ J. Olsen¹⁶⁸ D. Stickland¹⁶⁸ C. Tully¹⁶⁸ S. Malik¹⁶⁹ A. S. Bakshi¹⁷⁰ V. E. Barnes¹⁷⁰ S. Chandra¹⁷⁰ R. Chawla¹⁷⁰ S. Das¹⁷⁰ A. Gu¹⁷⁰ L. Gutay,¹⁷⁰ M. Jones¹⁷⁰ A. W. Jung¹⁷⁰ D. Kondratyev¹⁷⁰ A. M. Koshy,¹⁷⁰ M. Liu¹⁷⁰ G. Negro¹⁷⁰ N. Neumeister¹⁷⁰ G. Paspalaki¹⁷⁰ S. Piperov¹⁷⁰ A. Purohit¹⁷⁰ J. F. Schulte¹⁷⁰ M. Stojanovic^{170,q} J. Thieman¹⁷⁰ A. K. Virdi¹⁷⁰ F. Wang¹⁷⁰ R. Xiao¹⁷⁰ W. Xie¹⁷⁰ J. Dolen¹⁷¹ N. Parashari¹⁷¹ D. Acosta¹⁷² A. Baty¹⁷² T. Carnahan¹⁷² S. Dildick¹⁷² K. M. Ecklund¹⁷² P. J. Fernández Manteca¹⁷² S. Freed,¹⁷² P. Gardner,¹⁷² F. J. M. Geurts¹⁷² A. Kumar¹⁷² W. Li¹⁷² O. Miguel Colin¹⁷² B. P. Padley¹⁷² R. Redjimi,¹⁷² J. Rotter¹⁷² S. Yang¹⁷² E. Yigitbasi¹⁷² Y. Zhang¹⁷² A. Bodek¹⁷³ P. de Barbaro¹⁷³ R. Demina¹⁷³ J. L. Dulemba¹⁷³ C. Fallon,¹⁷³ A. Garcia-Bellido¹⁷³ O. Hindrichs¹⁷³ A. Khukhunaishvili¹⁷³ P. Parygin¹⁷³ E. Popova¹⁷³ R. Taus¹⁷³ G. P. Van Onsem¹⁷³ K. Goulianios¹⁷⁴ B. Chiarito,¹⁷⁵ J. P. Chou¹⁷⁵ Y. Gershtein¹⁷⁵ E. Halkiadakis¹⁷⁵ A. Hart¹⁷⁵ M. Heindl¹⁷⁵ D. Jaroslawski¹⁷⁵ O. Karacheban^{175,aa} I. Laflotte¹⁷⁵ P. Meltzer,¹⁷⁵ R. Montalvo,¹⁷⁵ K. Nash,¹⁷⁵ M. Osherson¹⁷⁵ B. Rand,¹⁷⁵ H. Routray¹⁷⁵ S. Salur¹⁷⁵ S. Somalwar¹⁷⁵ R. Stone¹⁷⁵ S. A. Thayil¹⁷⁵ S. Thomas,¹⁷⁵ J. Vora¹⁷⁵ H. Wang¹⁷⁵ H. Acharya,¹⁷⁶ A. G. Delannoy¹⁷⁶ S. Fiorendi¹⁷⁶ T. Holmes¹⁷⁶ E. Nibigira¹⁷⁶ S. Spanier¹⁷⁶ M. Ahmad¹⁷⁷ O. Bouhalil^{177,vvvv} M. Dalchenko¹⁷⁷ A. Delgado¹⁷⁷ R. Eusebi¹⁷⁷ J. Gilmore¹⁷⁷ T. Huang¹⁷⁷ T. Kamon^{177,wwww} H. Kim¹⁷⁷ S. Luo¹⁷⁷ S. Malhotra,¹⁷⁷ R. Mueller¹⁷⁷ D. Overton¹⁷⁷ D. Rathjens¹⁷⁷ A. Safonov¹⁷⁷ N. Akchurin¹⁷⁸ J. Damgov¹⁷⁸ V. Hegde¹⁷⁸ K. Lamichhane¹⁷⁸ S. W. Lee¹⁷⁸ T. Mengke,¹⁷⁸ S. Muthumuni¹⁷⁸ T. Peltola¹⁷⁸ I. Volobouev¹⁷⁸ A. Whitbeck¹⁷⁸ E. Appelt¹⁷⁹ S. Greene,¹⁷⁹ A. Gurrola¹⁷⁹ W. Johns¹⁷⁹ R. Kunnawalkam Elayavalli¹⁷⁹ A. Melo¹⁷⁹ F. Romeo¹⁷⁹ P. Sheldon¹⁷⁹ S. Tuo¹⁷⁹ J. Velkovska¹⁷⁹ J. Viinikainen¹⁷⁹ B. Cardwell¹⁸⁰ B. Cox¹⁸⁰ G. Cummings¹⁸⁰ J. Hakala¹⁸⁰ R. Hirosky¹⁸⁰ A. Ledovskoy¹⁸⁰ A. Li¹⁸⁰ C. Neu¹⁸⁰ C. E. Perez Lara¹⁸⁰ P. E. Karchin¹⁸¹ A. Aravind,¹⁸² S. Banerjee¹⁸² K. Black¹⁸² T. Bose¹⁸² S. Dasu¹⁸² I. De Bruyn¹⁸² P. Everaerts¹⁸² C. Galloni,¹⁸² H. He¹⁸² M. Herndon¹⁸² A. Herve¹⁸² C. K. Koraka¹⁸² A. Lanaro,¹⁸² R. Loveless¹⁸² J. Madhusudanan Sreekala¹⁸² A. Mallampalli¹⁸² A. Mohammadi¹⁸² S. Mondal,¹⁸² G. Parida¹⁸² D. Pinna,¹⁸² A. Savin,¹⁸² V. Shang¹⁸² V. Sharma¹⁸² W. H. Smith¹⁸² D. Teague,¹⁸² H. F. Tsoi¹⁸² W. Vetens¹⁸² A. Warden¹⁸² S. Afanasiev¹⁸³ V. Andreev¹⁸³ Yu. Andreev¹⁸³ T. Aushev¹⁸³ M. Azarkin¹⁸³ A. Babaev¹⁸³ A. Belyaev¹⁸³ V. Blinov,^{183,m} E. Boos¹⁸³ V. Borshch¹⁸³ D. Budkouski¹⁸³ V. Bunichev¹⁸³ M. Chadeeva^{183,m} V. Chekhovsky,¹⁸³ R. Chistov^{183,m} A. Dermenev¹⁸³ T. Dimova^{183,m} I. Dremin¹⁸³ M. Dubinin^{183,0000} L. Dudko¹⁸³ G. Gavrilov¹⁸³ V. Gavrilov¹⁸³ S. Gninenko¹⁸³ V. Golovtcov¹⁸³ N. Golubev¹⁸³ I. Golutvin¹⁸³ I. Gorbunov¹⁸³ A. Gribushin¹⁸³ Y. Ivanov¹⁸³ V. Kachanov¹⁸³ L. Kardapoltsev^{183,m} V. Karjavine¹⁸³ A. Karneyeu¹⁸³ V. Kim^{183,m} M. Kirakosyan,¹⁸³ D. Kirpichnikov¹⁸³ M. Kirsanov¹⁸³ V. Klyukhin¹⁸³ O. Kodolova^{183,xxxx} D. Konstantinov¹⁸³ V. Korenkov¹⁸³ A. Kozyrev^{183,m} N. Krasnikov¹⁸³ A. Lanev¹⁸³ P. Levchenko^{183,yyyy} A. Litomin,¹⁸³ N. Lychkovskaya¹⁸³ V. Makarenko¹⁸³ A. Malakhov¹⁸³ V. Matveev^{183,m,m} V. Murzin¹⁸³ A. Nikitenko^{183,zzzz,xxxx} S. Obraztsov¹⁸³ A. Oskin,¹⁸³ I. Ovtin^{183,m} V. Palichik¹⁸³ V. Perelygin¹⁸³ M. Perfilov,¹⁸³ S. Polikarpov^{183,m} V. Popov¹⁸³ O. Radchenko^{183,m} M. Savina¹⁸³ V. Savrin¹⁸³ V. Shalaev¹⁸³ S. Shmatov¹⁸³ S. Shulha¹⁸³ Y. Skovpen^{183,m} S. Slabospitskii¹⁸³ V. Smirnov¹⁸³ A. Snigirev¹⁸³ D. Sosnov¹⁸³ V. Sulimov¹⁸³ E. Tcherniaev¹⁸³ A. Terkulov¹⁸³ O. Teryaev¹⁸³ I. Tlisova¹⁸³ A. Toropin¹⁸³ L. Uvarov¹⁸³ A. Uzunian¹⁸³ A. Vorobyev,^{183,a} N. Voityshin¹⁸³ B. S. Yuldashev,^{183,aaaaa} A. Zarubin¹⁸³ I. Zhizhin¹⁸³ and A. Zhokin¹⁸³

(CMS Collaboration)

¹*Yerevan Physics Institute, Yerevan, Armenia*²*Institut für Hochenergiephysik, Vienna, Austria*³*Universiteit Antwerpen, Antwerpen, Belgium*

- ⁴Vrije Universiteit Brussel, Brussel, Belgium
⁵Université Libre de Bruxelles, Bruxelles, Belgium
⁶Ghent University, Ghent, Belgium
⁷Université Catholique de Louvain, Louvain-la-Neuve, Belgium
⁸Centro Brasileiro de Pesquisas Fisicas, Rio de Janeiro, Brazil
⁹Universidade do Estado do Rio de Janeiro, Rio de Janeiro, Brazil
¹⁰Universidade Estadual Paulista, Universidade Federal do ABC, São Paulo, Brazil
¹¹Institute for Nuclear Research and Nuclear Energy, Bulgarian Academy of Sciences, Sofia, Bulgaria
¹²University of Sofia, Sofia, Bulgaria
¹³Instituto De Alta Investigación, Universidad de Tarapacá, Casilla 7 D, Arica, Chile
¹⁴Beihang University, Beijing, China
¹⁵Department of Physics, Tsinghua University, Beijing, China
¹⁶Institute of High Energy Physics, Beijing, China
¹⁷State Key Laboratory of Nuclear Physics and Technology, Peking University, Beijing, China
¹⁸Sun Yat-Sen University, Guangzhou, China
¹⁹University of Science and Technology of China, Hefei, China
²⁰Institute of Modern Physics and Key Laboratory of Nuclear Physics and Ion-beam Application (MOE)—Fudan University, Shanghai, China
²¹Zhejiang University, Hangzhou, Zhejiang, China
²²Universidad de Los Andes, Bogota, Colombia
²³Universidad de Antioquia, Medellin, Colombia
²⁴University of Split, Faculty of Electrical Engineering, Mechanical Engineering and Naval Architecture, Split, Croatia
²⁵University of Split, Faculty of Science, Split, Croatia
²⁶Institute Rudjer Boskovic, Zagreb, Croatia
²⁷University of Cyprus, Nicosia, Cyprus
²⁸Charles University, Prague, Czech Republic
²⁹Escuela Politecnica Nacional, Quito, Ecuador
³⁰Universidad San Francisco de Quito, Quito, Ecuador
³¹Academy of Scientific Research and Technology of the Arab Republic of Egypt, Egyptian Network of High Energy Physics, Cairo, Egypt
³²Center for High Energy Physics (CHEP-FU), Fayoum University, El-Fayoum, Egypt
³³National Institute of Chemical Physics and Biophysics, Tallinn, Estonia
³⁴Department of Physics, University of Helsinki, Helsinki, Finland
³⁵Helsinki Institute of Physics, Helsinki, Finland
³⁶Lappeenranta-Lahti University of Technology, Lappeenranta, Finland
³⁷IRFU, CEA, Université Paris-Saclay, Gif-sur-Yvette, France
³⁸Laboratoire Leprince-Ringuet, CNRS/IN2P3, Ecole Polytechnique, Institut Polytechnique de Paris, Palaiseau, France
³⁹Université de Strasbourg, CNRS, IPHC UMR 7178, Strasbourg, France
⁴⁰Institut de Physique des 2 Infinis de Lyon (IP2I), Villeurbanne, France
⁴¹Georgian Technical University, Tbilisi, Georgia
⁴²RWTH Aachen University, I. Physikalisches Institut, Aachen, Germany
⁴³RWTH Aachen University, III. Physikalisches Institut A, Aachen, Germany
⁴⁴RWTH Aachen University, III. Physikalisches Institut B, Aachen, Germany
⁴⁵Deutsches Elektronen-Synchrotron, Hamburg, Germany
⁴⁶University of Hamburg, Hamburg, Germany
⁴⁷Karlsruhe Institut fuer Technologie, Karlsruhe, Germany
⁴⁸Institute of Nuclear and Particle Physics (INPP), NCSR Demokritos, Aghia Paraskevi, Greece
⁴⁹National and Kapodistrian University of Athens, Athens, Greece
⁵⁰National Technical University of Athens, Athens, Greece
⁵¹University of Ioánnina, Ioánnina, Greece
⁵²HUN-REN Wigner Research Centre for Physics, Budapest, Hungary
⁵³MTA-ELTE Lendület CMS Particle and Nuclear Physics Group, Eötvös Loránd University, Budapest, Hungary
⁵⁴Institute of Nuclear Research ATOMKI, Debrecen, Hungary
⁵⁵Institute of Physics, University of Debrecen, Debrecen, Hungary
⁵⁶Karoly Robert Campus, MATE Institute of Technology, Gyongyos, Hungary
⁵⁷Panjab University, Chandigarh, India
⁵⁸University of Delhi, Delhi, India

- ⁵⁹Saha Institute of Nuclear Physics, HBNI, Kolkata, India
⁶⁰Indian Institute of Technology Madras, Madras, India
⁶¹Bhabha Atomic Research Centre, Mumbai, India
⁶²Tata Institute of Fundamental Research-A, Mumbai, India
⁶³Tata Institute of Fundamental Research-B, Mumbai, India
⁶⁴National Institute of Science Education and Research,
An OCC of Homi Bhabha National Institute, Bhubaneswar, Odisha, India
⁶⁵Indian Institute of Science Education and Research (IISER), Pune, India
⁶⁶Isfahan University of Technology, Isfahan, Iran
⁶⁷Institute for Research in Fundamental Sciences (IPM), Tehran, Iran
⁶⁸University College Dublin, Dublin, Ireland
^{69a}INFN Sezione di Bari, Bari, Italy
^{69b}Università di Bari, Bari, Italy
^{69c}Politecnico di Bari, Bari, Italy
^{70a}INFN Sezione di Bologna, Bologna, Italy
^{70b}Università di Bologna, Bologna, Italy
^{71a}INFN Sezione di Catania, Catania, Italy
^{71b}Università di Catania, Catania, Italy
^{72a}INFN Sezione di Firenze, Firenze, Italy
^{72b}Università di Firenze, Firenze, Italy
⁷³INFN Laboratori Nazionali di Frascati, Frascati, Italy
^{74a}INFN Sezione di Genova, Genova, Italy
^{74b}Università di Genova, Genova, Italy
^{75a}INFN Sezione di Milano-Bicocca, Milano, Italy
^{75b}Università di Milano-Bicocca, Milano, Italy
^{76a}INFN Sezione di Napoli, Napoli, Italy
^{76b}Università di Napoli 'Federico II', Napoli, Italy
^{76c}Università della Basilicata, Potenza, Italy
^{76d}Scuola Superiore Meridionale (SSM), Napoli, Italy
^{77a}INFN Sezione di Padova, Padova, Italy
^{77b}Università di Padova, Padova, Italy
^{77c}Università di Trento, Trento, Italy
^{78a}INFN Sezione di Pavia, Pavia, Italy
^{78b}Università di Pavia, Pavia, Italy
^{79a}INFN Sezione di Perugia, Perugia, Italy
^{79b}Università di Perugia, Perugia, Italy
^{80a}INFN Sezione di Pisa, Pisa, Italy
^{80b}Università di Pisa, Pisa, Italy
^{80c}Scuola Normale Superiore di Pisa, Pisa, Italy
^{80d}Università di Siena, Siena, Italy
^{81a}INFN Sezione di Roma, Roma, Italy
^{81b}Sapienza Università di Roma, Roma, Italy
^{82a}INFN Sezione di Torino, Torino, Italy
^{82b}Università di Torino, Torino, Italy
^{82c}Università del Piemonte Orientale, Novara, Italy
^{83a}INFN Sezione di Trieste, Trieste, Italy
^{83b}Università di Trieste, Trieste, Italy
⁸⁴Kyungpook National University, Daegu, Korea
⁸⁵Chonnam National University, Institute for Universe and Elementary Particles, Kwangju, Korea
⁸⁶Hanyang University, Seoul, Korea
⁸⁷Korea University, Seoul, Korea
⁸⁸Kyung Hee University, Department of Physics, Seoul, Korea
⁸⁹Sejong University, Seoul, Korea
⁹⁰Seoul National University, Seoul, Korea
⁹¹University of Seoul, Seoul, Korea
⁹²Yonsei University, Department of Physics, Seoul, Korea
⁹³Sungkyunkwan University, Suwon, Korea
⁹⁴College of Engineering and Technology, American University of the Middle East (AUM),
Dasman, Kuwait
⁹⁵Riga Technical University, Riga, Latvia

- ⁹⁶Vilnius University, Vilnius, Lithuania
⁹⁷National Centre for Particle Physics, Universiti Malaya, Kuala Lumpur, Malaysia
⁹⁸Universidad de Sonora (UNISON), Hermosillo, Mexico
⁹⁹Centro de Investigacion y de Estudios Avanzados del IPN, Mexico City, Mexico
¹⁰⁰Universidad Iberoamericana, Mexico City, Mexico
¹⁰¹Benemerita Universidad Autonoma de Puebla, Puebla, Mexico
¹⁰²University of Montenegro, Podgorica, Montenegro
¹⁰³National Centre for Physics, Quaid-I-Azam University, Islamabad, Pakistan
¹⁰⁴AGH University of Krakow, Faculty of Computer Science,
Electronics and Telecommunications, Krakow, Poland
¹⁰⁵National Centre for Nuclear Research, Swierk, Poland
¹⁰⁶Institute of Experimental Physics, Faculty of Physics, University of Warsaw, Warsaw, Poland
¹⁰⁷Laboratório de Instrumentação e Física Experimental de Partículas, Lisboa, Portugal
¹⁰⁸Faculty of Physics, University of Belgrade, Belgrade, Serbia
¹⁰⁹VINCA Institute of Nuclear Sciences, University of Belgrade, Belgrade, Serbia
¹¹⁰Centro de Investigaciones Energéticas Medioambientales y Tecnológicas (CIEMAT), Madrid, Spain
¹¹¹Universidad Autónoma de Madrid, Madrid, Spain
¹¹²Universidad de Oviedo, Instituto Universitario de Ciencias y Tecnologías Espaciales de Asturias
(ICTEA), Oviedo, Spain
¹¹³Instituto de Física de Cantabria (IFCA), CSIC-Universidad de Cantabria, Santander, Spain
¹¹⁴University of Colombo, Colombo, Sri Lanka
¹¹⁵University of Ruhuna, Department of Physics, Matara, Sri Lanka
¹¹⁶CERN, European Organization for Nuclear Research, Geneva, Switzerland
¹¹⁷Paul Scherrer Institut, Villigen, Switzerland
¹¹⁸ETH Zurich—Institute for Particle Physics and Astrophysics (IPA), Zurich, Switzerland
¹¹⁹Universität Zürich, Zurich, Switzerland
¹²⁰National Central University, Chung-Li, Taiwan
¹²¹National Taiwan University (NTU), Taipei, Taiwan
¹²²High Energy Physics Research Unit, Department of Physics, Faculty of Science,
Chulalongkorn University, Bangkok, Thailand
¹²³Çukurova University, Physics Department, Science and Art Faculty, Adana, Turkey
¹²⁴Middle East Technical University, Physics Department, Ankara, Turkey
¹²⁵Bogazici University, Istanbul, Turkey
¹²⁶Istanbul Technical University, Istanbul, Turkey
¹²⁷Istanbul University, Istanbul, Turkey
¹²⁸Institute for Scintillation Materials of National Academy of Science of Ukraine, Kharkiv, Ukraine
¹²⁹National Science Centre, Kharkiv Institute of Physics and Technology, Kharkiv, Ukraine
¹³⁰University of Bristol, Bristol, United Kingdom
¹³¹Rutherford Appleton Laboratory, Didcot, United Kingdom
¹³²Imperial College, London, United Kingdom
¹³³Brunel University, Uxbridge, United Kingdom
¹³⁴Baylor University, Waco, Texas, USA
¹³⁵Catholic University of America, Washington, DC, USA
¹³⁶The University of Alabama, Tuscaloosa, Alabama, USA
¹³⁷Boston University, Boston, Massachusetts, USA
¹³⁸Brown University, Providence, Rhode Island, USA
¹³⁹University of California, Davis, Davis, California, USA
¹⁴⁰University of California, Los Angeles, California, USA
¹⁴¹University of California, Riverside, Riverside, California, USA
¹⁴²University of California, San Diego, La Jolla, California, USA
¹⁴³University of California, Santa Barbara—Department of Physics, Santa Barbara, California, USA
¹⁴⁴California Institute of Technology, Pasadena, California, USA
¹⁴⁵Carnegie Mellon University, Pittsburgh, Pennsylvania, USA
¹⁴⁶University of Colorado Boulder, Boulder, Colorado, USA
¹⁴⁷Cornell University, Ithaca, New York, USA
¹⁴⁸Fermi National Accelerator Laboratory, Batavia, Illinois, USA
¹⁴⁹University of Florida, Gainesville, Florida, USA
¹⁵⁰Florida State University, Tallahassee, Florida, USA
¹⁵¹Florida Institute of Technology, Melbourne, Florida, USA
¹⁵²University of Illinois Chicago, Chicago, USA, Chicago, USA

¹⁵³*The University of Iowa, Iowa City, Iowa, USA*¹⁵⁴*Johns Hopkins University, Baltimore, Maryland, USA*¹⁵⁵*The University of Kansas, Lawrence, Kansas, USA*¹⁵⁶*Kansas State University, Manhattan, Kansas, USA*¹⁵⁷*Lawrence Livermore National Laboratory, Livermore, California, USA*¹⁵⁸*University of Maryland, College Park, Maryland, USA*¹⁵⁹*Massachusetts Institute of Technology, Cambridge, Massachusetts, USA*¹⁶⁰*University of Minnesota, Minneapolis, Minnesota, USA*¹⁶¹*University of Mississippi, Oxford, Mississippi, USA*¹⁶²*University of Nebraska-Lincoln, Lincoln, Nebraska, USA*¹⁶³*State University of New York at Buffalo, Buffalo, New York, USA*¹⁶⁴*Northeastern University, Boston, Massachusetts, USA*¹⁶⁵*Northwestern University, Evanston, Illinois, USA*¹⁶⁶*University of Notre Dame, Notre Dame, Indiana, USA*¹⁶⁷*The Ohio State University, Columbus, Ohio, USA*¹⁶⁸*Princeton University, Princeton, New Jersey, USA*¹⁶⁹*University of Puerto Rico, Mayaguez, Puerto Rico, USA*¹⁷⁰*Purdue University, West Lafayette, Indiana, USA*¹⁷¹*Purdue University Northwest, Hammond, Indiana, USA*¹⁷²*Rice University, Houston, Texas, USA*¹⁷³*University of Rochester, Rochester, New York, USA*¹⁷⁴*The Rockefeller University, New York, New York, USA*¹⁷⁵*Rutgers, The State University of New Jersey, Piscataway, New Jersey, USA*¹⁷⁶*University of Tennessee, Knoxville, Tennessee, USA*¹⁷⁷*Texas A&M University, College Station, Texas, USA*¹⁷⁸*Texas Tech University, Lubbock, Texas, USA*¹⁷⁹*Vanderbilt University, Nashville, Tennessee, USA*¹⁸⁰*University of Virginia, Charlottesville, Virginia, USA*¹⁸¹*Wayne State University, Detroit, Michigan, USA*¹⁸²*University of Wisconsin—Madison, Madison, Wisconsin, USA*¹⁸³*An institute or international laboratory covered by a cooperation agreement with CERN*^aDeceased.^bAlso at Yerevan State University, Yerevan, Armenia.^cAlso at TU Wien, Vienna, Austria.^dAlso at Institute of Basic and Applied Sciences, Faculty of Engineering, Arab Academy for Science, Technology and Maritime Transport, Alexandria, Egypt.^eAlso at Université Libre de Bruxelles, Bruxelles, Belgium.^fAlso at Universidade Estadual de Campinas, Campinas, Brazil.^gAlso at Federal University of Rio Grande do Sul, Porto Alegre, Brazil.^hAlso at UFMS, Nova Andradina, Brazil.ⁱAlso at University of Chinese Academy of Sciences, Beijing, China.^jAlso at Nanjing Normal University, Nanjing, China.^kAlso at The University of Iowa, Iowa City, Iowa, USA.^lAlso at University of Chinese Academy of Sciences, Beijing, China.^mAlso at Another institute or international laboratory covered by a cooperation agreement with CERN.ⁿAlso at Cairo University, Cairo, Egypt.^oAlso at Suez University, Suez, Egypt.^pAlso at British University in Egypt, Cairo, Egypt.^qAlso at Purdue University, West Lafayette, Indiana, USA.^rAlso at Université de Haute Alsace, Mulhouse, France.^sAlso at Department of Physics, Tsinghua University, Beijing, China.^tAlso at Ilia State University, Tbilisi, Georgia.^uAlso at The University of the State of Amazonas, Manaus, Brazil.^vAlso at Erzincan Binali Yildirim University, Erzincan, Turkey.^wAlso at University of Hamburg, Hamburg, Germany.^xAlso at RWTH Aachen University, III. Physikalisches Institut A, Aachen, Germany.^yAlso at Isfahan University of Technology, Isfahan, Iran.^zAlso at Bergische University Wuppertal (BUW), Wuppertal, Germany.^{aa}Also at Brandenburg University of Technology, Cottbus, Germany.

- ^{bb} Also at Forschungszentrum Jülich, Juelich, Germany.
^{cc} Also at CERN, European Organization for Nuclear Research, Geneva, Switzerland.
^{dd} Also at Institute of Physics, University of Debrecen, Debrecen, Hungary.
^{ee} Also at Institute of Nuclear Research ATOMKI, Debrecen, Hungary.
^{ff} Also at Universitatea Babes-Bolyai—Facultatea de Fizica, Cluj-Napoca, Romania.
^{gg} Also at Physics Department, Faculty of Science, Assiut University, Assiut, Egypt.
^{hh} Also at HUN-REN Wigner Research Centre for Physics, Budapest, Hungary.
ⁱⁱ Also at Faculty of Informatics, University of Debrecen, Debrecen, Hungary.
^{jj} Also at Punjab Agricultural University, Ludhiana, India.
^{kk} Also at UPES—University of Petroleum and Energy Studies, Dehradun, India.
^{ll} Also at University of Visva-Bharati, Santiniketan, India.
^{mm} Also at University of Hyderabad, Hyderabad, India.
ⁿⁿ Also at Indian Institute of Science (IISc), Bangalore, India.
^{oo} Also at Indian Institute of Technology (IIT), Mumbai, India.
^{pp} Also at IIT Bhubaneswar, Bhubaneswar, India.
^{qq} Also at Institute of Physics, Bhubaneswar, India.
^{rr} Also at Deutsches Elektronen-Synchrotron, Hamburg, Germany.
^{ss} Also at Department of Physics, Isfahan University of Technology, Isfahan, Iran.
^{tt} Also at Sharif University of Technology, Tehran, Iran.
^{uu} Also at Department of Physics, University of Science and Technology of Mazandaran, Behshahr, Iran.
^{vv} Also at Helwan University, Cairo, Egypt.
^{ww} Also at Italian National Agency for New Technologies, Energy and Sustainable Economic Development, Bologna, Italy.
^{xx} Also at Centro Siciliano di Fisica Nucleare e di Struttura Della Materia, Catania, Italy.
^{yy} Also at Università degli Studi Guglielmo Marconi, Roma, Italy.
^{zz} Also at Scuola Superiore Meridionale, Università di Napoli 'Federico II', Napoli, Italy.
^{aaa} Also at Fermi National Accelerator Laboratory, Batavia, Illinois, USA.
^{bbb} Also at Laboratori Nazionali di Legnaro dell'INFN, Legnaro, Italy.
^{ccc} Also at Università di Napoli 'Federico II', Napoli, Italy.
^{ddd} Also at Ain Shams University, Cairo, Egypt.
^{eee} Also at Consiglio Nazionale delle Ricerche—Istituto Officina dei Materiali, Perugia, Italy.
^{fff} Also at Riga Technical University, Riga, Latvia.
^{ggg} Also at Department of Applied Physics, Faculty of Science and Technology, Universiti Kebangsaan Malaysia, Bangi, Malaysia.
^{hhh} Also at Consejo Nacional de Ciencia y Tecnología, Mexico City, Mexico.
ⁱⁱⁱ Also at IRFU, CEA, Université Paris-Saclay, Gif-sur-Yvette, France.
^{jjj} Also at Faculty of Physics, University of Belgrade, Belgrade, Serbia.
^{kkk} Also at Trincomalee Campus, Eastern University, Sri Lanka, Nilaveli, Sri Lanka.
^{lll} Also at Saegis Campus, Nugegoda, Sri Lanka.
^{mmm} Also at INFN Sezione di Pavia, Università di Pavia, Pavia, Italy.
ⁿⁿⁿ Also at Indian Institute of Technology Hyderabad, Hyderabad, India.
^{ooo} Also at National and Kapodistrian University of Athens, Athens, Greece.
^{ppp} Also at Ecole Polytechnique Fédérale Lausanne, Lausanne, Switzerland.
^{qqq} Also at Universität Zürich, Zurich, Switzerland.
^{rrr} Also at Stefan Meyer Institute for Subatomic Physics, Vienna, Austria.
 Also at Laboratoire d'Annecy-le-Vieux de Physique des Particules, IN2P3-CNRS, Annecy-le-Vieux, France.
^{ttt} Also at Near East University, Research Center of Experimental Health Science, Mersin, Turkey.
^{uuu} Also at Konya Technical University, Konya, Turkey.
^{vvv} Also at Izmir Bakircay University, Izmir, Turkey.
^{www} Also at Adiyaman University, Adiyaman, Turkey.
^{xxx} Also at Istanbul Gedik University, Istanbul, Turkey.
^{yyy} Also at Necmettin Erbakan University, Konya, Turkey.
^{zzz} Also at Bozok Üniversitesi Rektörlüğü, Yozgat, Turkey.
^{aaaa} Also at Marmara University, Istanbul, Turkey.
^{bbbb} Also at Milli Savunma University, Istanbul, Turkey.
^{cccc} Also at Kafkas University, Kars, Turkey.
^{dddd} Also at Hacettepe University, Ankara, Turkey.
^{eeee} Also at Istanbul University—Cerrahpasa, Faculty of Engineering, Istanbul, Turkey.
^{ffff} Also at Ozyegin University, Istanbul, Turkey.
^{gggg} Also at Vrije Universiteit Brussel, Brussel, Belgium.
^{hhhh} Also at School of Physics and Astronomy, University of Southampton, Southampton, United Kingdom.
ⁱⁱⁱⁱ Also at University of Bristol, Bristol, United Kingdom.

- ^{jjjj} Also at IPPP Durham University, Durham, United Kingdom.
^{kkkk} Also at Monash University, Faculty of Science, Clayton, Australia.
^{llll} Also at Università di Torino, Torino, Italy.
^{mmmm} Also at Bethel University, St. Paul, Minnesota, USA.
ⁿⁿⁿⁿ Also at Karamanoğlu Mehmetbey University, Karaman, Turkey.
^{oooo} Also at California Institute of Technology, Pasadena, California, USA.
^{pppp} Also at United States Naval Academy, Annapolis, Maryland, USA.
^{qqqq} Also at University of Florida, Gainesville, Florida, USA.
^{rrrr} Also at Bingol University, Bingol, Turkey.
^{ssss} Also at Georgian Technical University, Tbilisi, Georgia.
^{tttt} Also at Sinop University, Sinop, Turkey.
^{uuuu} Also at Erciyes University, Kayseri, Turkey.
^{vvvv} Also at Texas A&M University at Qatar, Doha, Qatar.
^{wwww} Also at Kyungpook National University, Daegu, Korea.
^{xxxx} Also at Yerevan Physics Institute, Yerevan, Armenia.
^{yyyy} Also at Northeastern University, Boston, Massachusetts, USA.
^{zzzz} Also at Imperial College, London, United Kingdom.
^{aaaa} Also at Institute of Nuclear Physics of the Uzbekistan Academy of Sciences, Tashkent, Uzbekistan.